UNDERSTANDING AND IMPROVING REPRESENTATIONS OF PROCESSES DETERMINING HIGH-LATITUDE MIXED-PHASE CLOUD PROPERTIES IN GCMS

A Dissertation

by

MENG ZHANG

Submitted to the Office of Graduate and Professional Studies of
Texas A&M University
in partial fulfillment of the requirements for the degree of

DOCTOR OF PHILOSOPHY

Chair of Committee,	Xiaohong Liu
Committee Members,	Ramalingam Saravanan
	Ping Chang
	Qi Ying
Head of Department,	Ramalingam Saravanan

May 2021

Major Subject: Atmospheric Sciences

ABSTRACT

Mixed-phase clouds, which are composed of both supercooled liquid droplets and ice crystals, are ubiquitous over high-latitude regions. The crude representation of cloud processes generally leads to large uncertainties in modeled mixed-phase cloud properties in General Circulation Models (GCMs). In this dissertation, we aim to examine the sensitivity of modeled high-latitude mixed-phase cloud properties to different representations of cloud microphysical processes. Model results are validated against the U.S. Department of Energy (DOE) Atmospheric Radiation Measurement (ARM) observations and satellite retrievals. First, improved representation of heterogeneous distribution between cloud liquid and ice through modifying the Wegener-Bergeron-Findeisen (WBF) process is investigated in the Community Atmosphere Model version 5 (CAM5). Model results indicate that accounting for this heterogeneous distribution can significantly improve simulated Arctic mixed-phase cloud properties. Biases in underestimated cloud liquid water mass are largely alleviated. Second, sensitivity of simulated Arctic mixed-phase clouds to introductions of the Classical Nucleation Theory (CNT) ice nucleation scheme, the Cloud Layers Unified By Binormals (CLUBB) parameterization, and the updated Morrison and Gettelman microphysics scheme (MG2) during the development of the DOE Energy Exascale Earth System Model (E3SM) Atmosphere Model version 1 (EAMv1) is examined. Results suggest that EAMv1 simulated Arctic mixed-phase clouds are overly dominated by supercooled liquid water and cloud ice water is largely underestimated, which is in

dramatic contrast to CAM5. The underestimated ice crystal production from CNT heterogeneous ice nucleation and the missing ice condensate from CLUBB are primarily responsible for the underestimation of cloud ice water content. Last, hemispheric differences in mixed-phase cloud properties are examined between Utqiaġvik and McMurdo using ground-based remote sensing measurements and EAMv1 simulations. The impact of thermodynamics and aerosol on high-latitude mixed-phase cloud difference between two hemispheres is investigated.

ACKNOWLEDGMENTS

First, I would like to express my greatest appreciation to my advisor Dr. Xiaohong Liu for his incredible support and patient guidance on my research during my Ph.D. study. In addition, I would like to thank Dr. Ramalingam Saravanan, Dr. Ping Chang, and Dr. Qi Ying for their serving on my committee. I also would like to thank Dr. Shaocheng Xie at Lawrence Livermore National Laboratory for his support and guidance on my research during my two terms of summer internship at the laboratory. Moreover, I would like to thank my colleagues: research scientists from Lawrence Livermore National Laboratory and Drs. Wuyin Lin, Zhien Wang, Damao Zhang, Minghui Diao, Yong Wang, Zheng Lu, Chenglai Wu, Ziming Ke, Xi Zhao, Mingxuan Wu, Yang Shi, Lin Lin, Hunter Brown, Stefan Rihimi, Kai Lyu, Hua Xie. Finally, Thank my family and all my friends for their encouragement and support.

This dissertation work is supported by the U.S. Department of Energy (DOE)'s Atmospheric System Research Program (grants DE-SC0014239, DE-SC0018926, and DE-SC0020510) and the Energy Exascale Earth System Model (E3SM) project. Work at Lawrence Livermore national Laboratory was performed under the auspices of the U.S. DOE by Lawrence Livermore National Laboratory under contract No.DE-AC52-07NA27344. We also would like to acknowledge the use of computational resources (doi:10.5065/D6RX99HX) at the NCAR-Wyoming Supercomputing Center provided by the National Science Foundation and the State of Wyoming and supported by NCAR's Computational and Information Systems Laboratory.

CONTRIBUTORS AND FUNDING SOURCES

Contributors

This work was supervised by a dissertation committee consisting of Professors Xiaohong Liu (advisor) and Ramalingam Saravanan and Ping Chang of the Department of Atmospheric Sciences and Professor Qi Ying of the Department of Civil & Environmental Engineering.

The HIPPO observational data analyzed for Chapter III was provided by John J. D'Alessandro and Professor Minghui Diao from Department of Meteorology and Climate Science at San José State University and were published in 2019 in an article listed in the REFERENCE. The observational data analyzed in Chapter V were conducted by Damao Zhang from the Pacific Northwest National Laboratory and were published in 2019 in an article listed in the REFERENCE.

All other work conducted for the dissertation was completed by the student independently.

Funding sources

This work was supported by the U.S. Department of Energy (DOE)'s Atmospheric System Research Program (grants DE-SC0014239, DE-SC0018926, and DE-SC0020510) and the Energy Exascale Earth System Model (E3SM) project. Work at Lawrence Livermore national Laboratory was performed under the auspices of the U.S.

DOE by Lawrence Livermore National Laboratory under contract No.DE-AC52-07NA27344.

TABLE OF CONTENTS

Page

Page

Page

LIST OF FIGURES

Page

Page

Page

Page

LIST OF TABLES

Page

CHAPTER I

INTRODUCTION

1.1. Importance of mixed-phase cloud in climate system

Since the mid-20th century, global mean surface air temperature has increased by ~0.6℃ amid the global warming environment. Observations indicate that the warming over the Arctic region is nearly twice as fast as the rest of the globe, which is known as the "Arctic amplification" (Cohen et al., 2020; Screen & Simmonds, 2010). Several feedback mechanisms have been found to play important roles modulating the Arctic amplification. The positive surface albedo feedback, resulted from changes in sea ice and snow cover extent, is one of the well-known mechanisms (Deser et al., 2000; Pistone et al., 2019). The appearance of darker surface due to melting of sea ice and snow cover can decrease surface albedo in high latitude regions. Reduced surface albedo then tends to absorb more solar radiation and leads to a stronger warming in the Arctic. Aerosols are also believed to have substantial impact on the Arctic climate change. For example, black carbon and dust can deposit onto the bright ground surface to decrease the high surface albedo through snow darkening effect (Rahimi et al., 2019, 2020; Yasunari et al., 2015). These absorbing aerosols tend to absorb stronger radiative fluxes and further influence surface energy budget in the climate system. On the other hand, aerosol can impact high-latitude climate change via its indirect effect on clouds. Changes in cloud properties such as cloud water content and cloud lifetime have been recognized to play

an important role in regulating not only the water cycle and energy budget but also atmospheric feedback loops in the earth system (He et al., 2019).

Over high-latitude regions, mixed-phase clouds, composed of a mixture of supercooled liquid droplets and ice crystals at subfreezing temperatures (-40℃ – 0℃), are ubiquitous all year round. These mixed-phase clouds have been observed with frequency of occurrence larger than 30% annually (Khanal & Wang, 2018). Higher frequency of occurrence has been found during spring and early autumn seasons in the Arctic (de Boer et al., 2009; Shupe, 2011; Shupe et al., 2006, 2011; Zhang, Vogelmann, et al., 2019). Such high cloud frequency of occurrence can be partially explained by the long lifetime of single-layer stratiform mixed-phase clouds which is contrary to the unstable thermodynamic nature of mixed-phase clouds. The complex coupling between cloud microphysics, radiation, dynamics, and surface properties is largely responsible for the prolonged characteristics of Arctic mixed-phase clouds (Morrison et al., 2012).

Due to the distinct optical properties between supercooled liquid droplets and ice particles, the relative abundance of these two hydrometeors, which is defined as the mixed-phase cloud phase partitioning, is one of the most important properties regulating mixed-phase cloud radiative forcing (Vergara-Temprado et al., 2018). For example, when clouds are dominated by small-size supercooled liquid droplets, a large portion of incident shortwave solar radiation will be scattered back to the top of atmosphere (TOA) due to the large cloud reflectivity. On the other hand, when ice particles are emerged inside clouds, the relatively large size of ice particles can decrease cloud optical thickness, which then will allow more solar radiation reaching the surface. Therefore, the

phase partitioning between liquid and ice can exert a large impact on the surface energy budget (Bennartz et al., 2013; Hofer et al., 2019; Nicolas et al., 2017) and influence regional and global climate changes (Lawson & Gettelman, 2014; Lohmann & Neubauer, 2018; Tan & Storelvmo, 2019). For example, Bennartz et al. (2013) showed that the amount of liquid water in low-level mixed-phase clouds substantially controls the downwelling radiative flux at the surface. Extensive surface melting across the Greenland ice sheet occurred when clouds were optically thick enough and low enough to exert a longwave radiative warming, while shortwave radiation could still reach surface and raise the surface temperature. Hofer et al., (2019) also concluded that longwave cloud radiative effect is strongly sensitive to the amounts of liquid water. The uncertain liquid water path (LWP) simulated from models will contribute to large uncertainties in the prediction of future surface ice melting events over the Greenland Ice Sheet.

Mixed-phase cloud phase partitioning is also important for future climate predictions in general circulation models (GCMs), in terms of climate sensitivity. By constraining simulated phase partitioning with satellite observations, the equilibrium climate sensitivity (ECS) — which is the equilibrated global surface temperature change in response to a doubling of atmospheric CO_2 concentration — has been found to increase by up to 1.3℃ (Tan et al., 2016). The higher ECS is the result of weakened negative cloud phase feedback. According to Tan et al. (2016), with a double CO_2 concentration forcing, the entire troposphere will become deepened. Isotherms throughout the troposphere will then move toward higher altitudes compared to their

initial states. As a result, at any given altitude, the ice water in initial mixed-phase clouds is more likely to appear in liquid phase in the warmed atmosphere. Because mixed-phase clouds with larger amounts of liquid water are more reflective of shortwave radiation, the enhanced cooling due to stronger reflection can counteract the warming induced by a doubling of CO_2 concentration. Therefore, changes in the amount of cloud liquid water in model simulated initial mixed-phase clouds can substantially impact the strength of negative cloud phase feedback and therefore influence the intensity of future climate warming. Meanwhile, ECS simulated in recent Coupled Model Intercomparison Project phase 6 (CMIP6) models has increased substantially compared to previous models in the Coupled Model Intercomparison Project phase 5 (CMIP5). ECS values from CMIP6 models vary between 1.8 and 5.6 K, which exceed the best estimate range of 1.5 – 4.5 K (Bodas-Salcedo et al., 2019; Gettelman et al., 2019; Zelinka et al., 2020). Among a few GCMs that have large ECS values, it has been found that improvements in the phase partitioning of mixed-phase clouds mostly attribute to the increased ECS. Compared to CMIP5 model participants, increases in CMIP6 model simulated liquid water mass mixing ratio weaken the response of cloud ice water to the future warming; and this weaker negative cloud phase feedback induces stronger positive net cloud feedbacks and the higher ECS. Therefore, it is critical for GCMs to capture a reasonable phase partitioning of mixed-phase clouds, which will merit a solid future climate projection.

1.2. Important microphysical processes regulating mixed-phase cloud properties

There are a number of essential physical processes controlling the microphysical properties (e.g., phase partitioning) of mixed-phase clouds. Heterogeneous ice nucleation is one of the most important processes. When ice nucleating particles (INPs), such as dust particles, are immersed inside supercooled liquid droplets, heterogeneous ice nucleation can be initiated by these INPs to freeze droplets as temperature decreases. This is known as the immersion ice nucleation. Besides that, heterogenous freezing can also take place in the condensation mode, contact mode, and deposition mode. Condensation freezing occurs when liquid water is condensed on INPs, and nearly at the same time these INPs initiate the freezing of liquid droplets to form ice particles. Contact freezing refers to the freezing of liquid droplets as an INP particle collides with supercooled liquid droplets; and deposition freezing represents the direct deposition of water vapor onto dry INPs. It has been found that immersion/condensation nucleation is the dominant process in heterogeneous freezing to generate ice particles in the Arctic mixed-phase clouds (Fridlind et al., 2007; Prenni et al., 2007). In spite of the role as INP, aerosols can also modulate mixed-phase cloud properties through their influence on liquid droplet formation and droplet size distribution as cloud condensation nuclei (CCN). The competition between INP and CCN for available water vapor was found to suppress cloud ice formation if CCN coexists with INP in the atmosphere (Simpson et al., 2018). Meanwhile, Lance et al. (2011) suggested that even though larger droplet size was found to correlate well with ice precipitating particles, the narrower droplet size

distribution under polluted environment can lead to fewer precipitating ice particles in mixed-phase clouds than those in clean conditions at the same temperature.

Because the equilibrium vapor pressure with respect to ice is lower than that to liquid, once ice particles are spawned, they can grow via the Wegener-Bergeron-Findeisen (WBF) process (Bergeron, 1935; Findeisen, 1938; Wegener, 1911) at the expense of surrounding liquid droplets. The depositional mass growth of ice particles can substantially influence the efficiency of precipitation formation as well as mixed-phase cloud glaciation, which will further change cloud longevity, emissivity, and cloud organizations.

Secondary ice production is another important process modulating ice crystal number concentrations in mixed-phase clouds (Field et al., 2017; O'Shea et al., 2017). Although a comprehensive understanding of secondary ice production is still limited nowadays, a few mechanisms such as droplet fragmentation during freezing, splintering during ice particle riming, and collision between ice particles are found important (Field et al., 2017; Morrison et al., 2020; Phillips et al., 2018).

Many other factors can affect aforementioned microphysical processes. For instance, using a single ice approach to prognostically represent ice particle properties, Zhao et al. (2017) found that the better parametrization of particle shape in GCM yields a promising simulation of mixed-phase clouds. The flexibility of their parameterization to simulate ice properties (e.g., shape, mass, area) based on meteorological conditions shows a significant impact on ice terminal velocity and sedimentation, as well as ice deposition process. Orographic lifting also plays a role in the maintenance of cloud

liquid water by changing the saturation environment required for cloud formation (Lohmann et al., 2016).

1.3. Large uncertainties in simulated mixed-phase cloud properties in GCMs

Large uncertainties remain in representations of mixed-phase cloud phase partitioning in GCMs. For example, when simulated liquid water mass mixing ratio is equally abundant compared to cloud ice water, temperature of simulated mixed-phase clouds can vary by 40℃ among different CMIP5 models over the Southern Ocean (McCoy et al., 2015, 2016). Such a large model discrepancy contributes to large uncertainties in simulated cloud feedback and climate sensitivity, which makes GCMs challenging to have a convergent future climate projection (Bodas-Salcedo et al., 2019; Gettelman et al., 2019; Tan et al., 2016; Zelinka et al., 2020).

One source of uncertainties in mixed-phase cloud simulations comes from the crude representation of formation and growth processes of cloud hydrometeors, and interactions between different types of hydrometeors. For example, heterogeneous ice nucleation parameterizations implemented in most GCMs are based on measurements from field campaigns (DeMott et al., 2010), laboratory experiments (DeMott et al., 2015; Niemand et al., 2012), or the Classical Nucleation Theory (CNT) (Hoose et al., 2010; Wang et al., 2014). Although considerable progresses have been made in the understanding of heterogeneous ice production process, there is still a lack of reliable representations of atmospheric processes of INPs and aerosol-cloud interactions in mixed-phase clouds (Hartmann et al., 2020; Shi & Liu, 2019; Tobo et al., 2019; Wilson

et al, 2015). Another poorly understood cloud process lies in the fact that observed INP concentration cannot explain the observed number concentration of ice crystals in the Arctic mixed-phase clouds. Such a bias implies the treatment of secondary ice production is not well parameterized in GCMs (Field et al., 2017). Moreover, simulated mixed-phase cloud phase partitioning is found to be sensitive to the treatment of WBF process (Storelvmo et al., 2008; Tan & Storelvmo, 2016). However, because of the coarse model resolution, subgrid heterogeneous distribution of cloud liquid and ice in mixed-phase clouds is generally not considered in GCMs, which can significantly affect the WBF process rate (Tan & Storelvmo, 2016). Additionally, it is known that the interaction between cloud microphysics and other cloud physics (e.g., shallow convection) is also important for modeled mixed-phase cloud properties. By allowing more liquid water detrained from shallow convection to stratiform clouds, the amount of simulated mixed-phase cloud liquid water is largely increased over the Southern Ocean. The high bias in surface shortwave radiative flux is then reduced in the Community Atmosphere Model version 5 (CAM5) simulations (Kay et al., 2016; Wang et al., 2018).

1.4. Research objectives

In this study, we aim to address the following objectives regarding mixed-phase clouds in GCMs. We will

- Evaluate model simulated high-latitude mixed-phase cloud properties with observations. Both satellite and ground-based remote-sensing measurements will be utilized in model validations. We will pay a special attention to single-layer

stratiform mixed-phase clouds, in which complicated interactions between multiple overlapped cloud layers are excluded.

- Understand the sensitivity of simulated mixed-phase clouds to ice related microphysical processes. Processes including heterogeneous ice nucleation and WBF process will be examined using different treatments in GCMs. Their impacts on simulated high-latitude mixed-phase cloud properties will be investigated. We will also understand the effect of thermodynamics and aerosols on the hemispheric differences in mixed-phase cloud properties between the Arctic and Antarctic.
- Improve the representation of microphysical processes in GCMs to better capture observed mixed-phase clouds. The heterogenous distribution between cloud liquid and ice will be implemented in CAM5 to better represent the WBF process in cloud microphysics. Meanwhile, an improved treatment for detrained cloud water from shallow convection and deep convection will also be tested.

CHAPTER II

MODELS AND OBSERVATIONAL DATA

2.1. Model description

2.1.1. CESM

Community Earth System Model (CESM), one of the most comprehensive earth system models (ESM) from National Center for Atmospheric Research (NCAR), is developed to represent principal components of the earth system for climate system research. CESM includes models of atmosphere, land surface, ocean, and sea ice. The atmosphere component of CESM — CAM version 5.3 — is used in this dissertation (Neale et al., 2010).

The standard CAM5 is run on the 1.9° × 2.5° horizontal resolution; and it has 30 vertical layers with 8 layers within the planetary boundary layer (PBL). A two-moment cloud microphysics scheme (Morrison & Gettelman 2008, hereafter MG1) is included in CAM5, in which cloud liquid and cloud ice mass mixing ratios and number concentrations are prognostically determined, while rain and snow are treated diagnostically. Cloud condensation and cloud fraction are calculated in cloud macrophysics following Park et al. (2014). Other physical parameterizations in CAM5 include Zhang and McFarlane (1995) scheme for deep convections, Park and Bretherton (2009) for shallow convections, and Bretherton and Park (2009) scheme for PBL turbulence processes. Aerosol processes are treated using the three-mode version of

modal aerosol module (MAM3) (Liu et al., 2012). The Rapid Radiative Transfer Model for GCMs (RRTMG) (Iacono et al., 2008) is applied in the aerosol and cloud radiative transfer calculations.

Used as the default heterogeneous ice nucleation parameterization for mixed-phase clouds in CAM5, the scheme of Meyers et al. (1992) is not related to aerosol properties. Instead, the Meyers scheme determines the INP number concentration from immersion/condensation and deposition freezing only based on ambient temperatures. Earlier studies found that this scheme tends to overestimate INP number concentration in the Arctic mixed-phase clouds (DeMott et al., 2010, 2015; Prenni et al., 2007). Different from the deterministic Meyers parameterization, the CNT ice nucleation scheme uses the stochastic hypothesis to represent ice nucleation as a function of time (Chen et al., 2008; Hoose et al., 2010). The CNT ice nucleation scheme links the heterogeneous ice nucleation rate to aerosol properties such as their composition, number concentration, and size. Immersion/condensation, deposition, and contact nucleation are all included in the CNT. To consider the heterogeneity in nucleation ability of individual aerosol particles (e.g., dust and black carbon), a log-normal probability distribution function (PDF) is used in the representation of contact angle, which is the angle that aerosol surface meets the interface between ice germs and liquid and water vapor (Wang et al., 2014). In this dissertation study, we replace the Meyer scheme with CNT in all our CAM5 simulations.

2.1.2. E3SM

The U.S. Department of Energy (DOE) Energy Exascale Earth System Model version 1 (E3SMv1) (Golaz et al. 2019) is one of the state-of-the-art ESMs available for the community. Its atmosphere component, E3SM Atmosphere Model (i.e., EAMv1) is developed from CAM5 with substantial changes in model dynamic core, vertical and horizontal resolution, and physics parameterizations (Rasch et al., 2019; Xie et al., 2018). Instead of the finite-volume (FV) dynamic core in CAM5, EAMv1 is now run on the spectral element (SE) dynamic core. The model can be run on either 1-degree or 0.25-degree horizontal resolutions, and we use the lower resolution model version in our dissertation study. EAMv1 has 72 vertical layers and there are 17 layers within the PBL, with vertical resolution ranging between 20 m and 200 m.

There are a few new parameterizations implemented in EAMv1 during the model development. One new feature in EAMv1 is the use of Cloud Layers Unified By Binormals (CLUBB) parameterization to unify the treatments of PBL turbulence, shallow convection, and cloud macrophysics. CLUBB utilizes the triple joint PDF of vertical velocity (w), liquid water potential temperature (θ_l), and total specific water content (q_t) to achieve the high-order turbulence closure. Variances and correlations between θ_l, q_t, and w and the third-order moment w'^3 are predicted by CLUBB equations, and these parameters are used to determine the trivariate PDF function which follows a double Gaussian distribution. Momentum terms such as $\overline{u'^2}$, $\overline{v'^2}$ are prognosed by CLUBB. Other momentum terms such as $\overline{u'w'}$, $\overline{v'w'}$ are diagnosed and closed with a down-gradient approach (Golaz et al., 2002; Larson, 2017). Other higher-order moments

(e.g., $\overline{w'^2 q_t'}$, $\overline{w' q_t'^2}$, $\overline{w' \theta_l'^2}$) are closed via the integration of CLUBB assumed PDF function. Moreover, cloud fraction and cloud condensation are determined through the integral of saturated portion of CLUBB's joint PDF (Larson et al., 2002). Note that the current CLUBB only accounts for liquid phase processes. Ice phase processes are not explicitly defined in CLUBB's assumed PDF approach, but a turbulence eddy diffusion scheme is used to calculate the transport of cloud ice mass when CLUBB is implemented (Bogenschutz et al., 2013). Ice cloud fraction, on the other hand, is calculated based on relative humidity (Gettelman et al., 2010).

For cloud microphysics, EAMv1 utilizes the second version of two-moment Morrison and Gettelman scheme (hereafter MG2; Gettelman & Morrison, 2015) for stratiform clouds. The scheme prognostically calculates the mass and number concentrations of liquid droplets, ice crystals and precipitation hydrometeors (rain and snow). Meanwhile, MG2 changes the sequence of updating cloud droplet number concentration due to aerosol activation. In EAMv1, this calculation has been moved to the beginning of the cloud microphysics scheme, which is at the same location where cloud condensate is determined from cloud macrophysics. A 5-minute sub-time step is also used in MG2 in order to better couple with the CLUBB. We note that there is an artificial tuning parameter of 0.1 to the WBF process in the released version of EAMv1. This tuning parameter uniformly slows down the WBF process by a factor of 10 over the entire globe. For mixed-phase cloud regime, EAMv1 uses the CNT scheme to consider aerosol properties in heterogenous ice nucleation process, so that aerosol-cloud interactions can be better represented in mixed-phase clouds.

Other physics parameterizations incorporated in EAMv1 include the new 4-mode version of Modal Aerosol Module (MAM4) (Liu et al., 2016), the unified treatment for aerosol convective transport and scavenging (Wang, Easter et al., 2013), the release of resuspended aerosol particles due to raindrop evaporation to the coarse mode, the treatment of marine organic aerosols, and a linearized ozone chemistry (Linoz2) for stratospheric ozone (Hsu & Prather, 2009; McLinden et al., 2000). The same deep convection scheme (Zhang & McFarlane, 1995) is used in EAMv1 as CAM5.

2.2. Observations

2.2.1. M-PACE field campaign

Mixed-Phase Arctic Cloud Experiment (M-PACE) field campaign was conducted in October 2004 at the DOE Atmospheric Radiation Measurement (ARM) North Slope of Alaska (NSA) site. The campaign was designed to understand key microphysical processes regulating properties of Arctic mixed-phase clouds.

Large-scale synoptic circulation played an important role in the formation and maintenance of clouds during the M-PACE field campaign (Verlinde et al., 2007; Xie et al., 2006). A high-pressure system was developed to the northeast of the Alaska coast in the early period of the experiment (5 - 14 October). The east-northeasterly flow prevailed over the NSA site in the lower troposphere. Cold air associated with the cold pack ice to the north of Alaska reached the NSA. Together with a weak trough in the upper level, surface temperature dropped considerably below -10℃ by 8 October. From 9 to 14 October, resilient single-layer boundary layer mixed-phase clouds were formed

over the open ocean and were advected to the NSA site. After 14 October, the surface high-pressure system slowly propagated southeastward, and a strong low-pressure center that formed near Kamchatka began to influence Alaskan coasts, which brought southerly and southwesterly flow to the NSA. Deep clouds were frequently observed during this time period, associated with frontal systems generated by this low-pressure system.

Table 2.1. *Summary of M-PACE Observations (Reprinted from Zhang et al., (2020))*

Observation	Quantity	Source and reference
ACRED	LWC/LWP and IWC/IWP	ARM cloud retrieval ensemble dataset (ACRED; Zhao et al., 2012)
ARSCL	Cloud fraction	Active Remotely Sensed Clouds Locations (ARSCL) algorithm (Clothiaux et al., 2000)
UND Citation	LWC and IWC	University of North Dakota (UND) Citation aircraft (McFarquhar et al., 2007)

Table 2.1 summarizes the observational dataset we used for model evaluation. During the M-PACE, ground-based remote sensing instruments such as Millimeter Wavelength Cloud Radar (MMCR), Micropulse Lidar (MPL), and Microwave Radiometer (MWR) were deployed to measure macrophysical and microphysical properties of high-latitude mixed-phase clouds. Based on the ARM cloud radar, lidar, and laser ceilometer measurements, the frequency of occurrence of observed clouds was determined using Active Remotely Sensed Clouds Locations (ARSCL) algorithm

(Clothiaux et al., 2000). ARM cloud retrieval ensemble dataset (ACRED) is also used in this dissertation (Zhao et al., 2012). ACRED dataset provides an estimate of uncertainties embedded in retrieval algorithms for mixed-phase cloud microphysical properties. Five different products are included for M-PACE field campaign, and we use four of them for single-layer mixed-phase cloud study. Details about individual product can be found in Zhao et al. (2012). Here, we only briefly introduce key characteristics for each data. For example, MICROBASE dataset, which is the ARM baseline retrieval, provides cloud liquid water content (LWC) (Frisch et al., 1995; Liao & Sassen, 1994) and ice water content (IWC) (Ivanova et al., 2001; Liu & Illingworth, 2000) based on empirical parameterizations. Retrievals from SHUPE_TURNER adopt both empirically and physically based assumptions. Turner (2005) and Frisch et al. (1995) are used for liquid phase cloud water, and the method of Shupe et al. (2005) is used for ice phase properties. Algorithm of WANG product is emphasized specifically for mixed-phase clouds. Ground-based radar and lidar measurements are combined to obtain the LWC and IWC (Wang et al., 2004; Wang & Sassen, 2002). Last but not the least, DONG product only contains liquid water retrievals. Data from MWR and MMCR are used to derive LWP following Dong and Mace (2003). The hourly ACRED data during October 2004 is used in our model evaluation.

Aerosol and cloud properties were also measured onboard the University of North Dakota (UND) Citation aircraft. In-situ measurements of microphysical properties of single-layer boundary layer mixed-phase clouds were obtained between 9-12 October

2004 following McFarquhar et al. (2007). During this period, four flight experiments were performed; and each flight lasted for 1-2 hours with cloud data collected every 10s.

2.2.2. Long-term ground-based measurements

Besides the M-PACE field campaign, long-term ground-based measurements in the Arctic and Antarctic from Zhang, Vogelmann et al. (2019) are also obtained. The seasonality of simulated microphysical properties of single-layer stratiform mixed-phase clouds over high latitudes are validated with these data in both hemispheres.

In the remote Antarctic, the ARM West Antarctic Radiation Experiment (AWARE) field campaign was conducted at the McMurdo station (77.9°S, 166.7°E) from December 2015 to January 2017, aimed to collect comprehensive data of West Antarctic clouds to understand their role in the Antarctic climate change (Lubin et al., 2020). Extensive ground-based remote sensing instruments (e.g., Ka-band ARM zenith radar (KAZR), high spectral resolution lidar (HSRL), and MWR were deployed during the field campaign. In the Arctic, similar sets of instruments were deployed at the NSA Utqiaġvik site (71.3°N, 156.6°W) from October 2013 to February 2017. With complimentary detection capabilities of cloud radar and lidar, single-layer stratiform mixed-phase clouds can be detected and their properties (e.g., LWP, IWP (ice water path), and number concentrations of liquid droplets and ice crystals) can be determined at both locations. Multi-year observations at the Utqiaġvik site provide a reliable statistical analysis of Arctic cloud microphysical properties. Meanwhile, Silber et al. (2019) suggested that cloud statistics from the AWARE field campaign is generally

representative for long-term characteristics of mixed-phase cloud properties over the Antarctic coastal regions.

During the AWARE field campaign at McMurdo station and at Utqiaġvik site from 2008 to 2010, measurements of aerosol composition and mass concentration were performed. Aerosol dataset were processed by Dr. Lynn Russell's group at Scripps Institution of Oceanography. Organic matter (OM) aerosols were collected with Fourier transform infrared (FTIR) filter. The sum of five groups of species (alkane, amine, alcohol, carbonyl and carboxylic acid) is quantified as OM. X-ray fluorescence (XRF) spectroscopy was used to analyze element mass for aerosol particles. Above the detection threshold, mass of element composition of S, Na, Cl, Si, Al, Fe, Ti, Ca, Mg, K, V, Zn, and Br is quantified at both Utqiaġvik and McMurdo. More detailed information about aerosol measurements can be found in Liu et al. (2018) for the AWARE field campaign and in Frossard et al. (2020) for Utqiaġvik site. Note that due to the availability of online dataset (https://doi.org/10.6075/J01N7ZN2), only aerosol data from 2008 in the Arctic is used here.

To understand the aerosol effect on mixed-phase clouds, observational dataset of total aerosol optical depth (AOD) and number concentrations of cloud condensate nuclei (CCN) are also obtained from ARM products. AOD were measured with the Cimel sunphotometer (CSPHOT, https://www.arm.gov/capabilities/instruments/csphot) at Utqiaġvik and McMurdo. Climatology data from 1997 to 2018 were collected for the Arctic while only data during the AWARE field campaign were available for the Antarctic region. Cloud condensation nuclei counter is used to measure the

concentration of activated aerosol particles under supersaturated conditions provided by the instrument. CCN number concentration is then calculated as a function of supersaturation in the observation (https://www.arm.gov/capabilities/instruments/ccn). With the deployment of this instrument at the Oliktok Point from 2017 to 2019, which is an adjacent observational site southeastward to the Utqiaġvik, we adopt the CCN measurements at Oliktok Point to represent ambient CCN concentrations in the Arctic. Over the Antarctic, measurements of CCN during the AWARE field campaign is also used for model evaluation.

Furthermore, measurements of atmospheric environmental states, such as temperature and moisture, are collected from the ARM Best Estimate (ARMBE) products (Xie et al., 2010). To investigate the role of large-scale atmospheric states on high-latitude mixed-phase clouds, data from the year of 2016 at Uqtiagvik site and data during the AWARE field campaign at McMurdo are used in this dissertation.

2.2.3. Satellite retrievals

In this dissertation, 2B-CLDCLASS-LIDAR products (Sassen et al., 2008; Wang, Vane et al., 2013) derived from CloudSat and CALIPSO onboard A-Train satellites are used to evaluate EAMv1 simulated mixed-phase clouds. Compared to the ground-based measurements at ARM sites, satellite remote sensing data provides mixed-phase cloud properties over a broader coverage in polar regions, which benefits the evaluation of simulated clouds in aeras beyond specific locations of ARM sites. Another important advantage of this sophisticated multi-sensor retrieval algorithm is that it

combines the complementary sensitivities of cloud radar and lidar to classify cloud phase and cloud type. For instance, due to the large sensitivity of lidar measurements to small particles, liquid droplets as well as high- and mid-level clouds that are associated with relatively low optical thickness can be detected. Meanwhile, the short wavelength limits the lidar signals to penetrate optically thick clouds in multilayer cloud systems due to strong attenuation. On the other hand, longer wavelength of cloud radar enables the detection of optically thick multilayer clouds, but it has limited detection for small droplets and cold ice clouds with low number concentrationsof cloud particles. Therefore, combining radar and lidar observations provides a reliable cloud classification and detection because of their complimentary capabilities. Combined with MODIS data, CloudSat and CALIPSO measurements classify detected clouds into 8 types (i.e., St, Sc, Cu, Nb, Ac, As, deep convective, or high cloud) based on cloud vertical profiles, horizontal extent, precipitation occurrence, and cloud temperature. Cloud phase is also determined using observed cloud properties. More details can be found at http://www.cloudsat.cira.colostate.edu/sites/default/files/products/files/2B-CLDCLASS-LIDAR_PDICD.P1_R05.rev0_.pdf. For our purpose, single-layer low-level stratiform mixed-phase clouds are sampled from the 2B-CLDCLASS-LIDAR product. Cloud properties such as frequency of occurrence during the year of 2007 are used for model validation.

2.3. Model approach

To achieve our goals of obtaining a process-level understanding about the sensitivity of model simulated mixed-phase clouds to a few ice-related microphysical processes, we perform model simulations with the following approaches to evaluate model results with multiplatform observations.

2.3.1. Single column model

Single column models (SCMs) have been widely used in developing and testing physical parameterizations in GCMs (Klein et al., 2009; Liu et al., 2007, 2011; Morrison et al., 2009; Xie et al., 2005; Yuan et al., 2006). SCM is a simplified GCM that has one model column. It shares the same vertical resolution and same suite of physics parameterizations as standard GCM. With constrained large-scale circulations, advections of water vapor and temperature, and surface fluxes, SCM facilitates the direct comparison to field campaign observations to diagnose deficiencies in model physics parameterizations.

In this dissertation, we utilize the SCM version of CAM5 (SCAM5) which is run under the Eulerian dynamic core with 20-minute time step. SCAM5 experiments are run for the M-PACE field campaign at NSA Utqiaġvik site. Forcing data that drives the SCM simulation, such as advections and divergences of temperature (T) and moisture (Q) and surface fluxes, are derived using sounding measurements and reanalysis data following Xie et al. (2006). To obtain a realistic aerosol background for the M-PACE field campaign, aerosol size distribution and number mixing ratios are prescribed using

observations following Liu et al. (2011). Sulfate, primary organic matter (POM), sea salt, and mineral dust are categorized in the corresponding MAM modes. The mass fraction for each aerosol species in each mode is prescribed as: 70% POM and 30% sulfate in the accumulation mode, and 85% sea salt, 10% sulfate and 5% mineral dust in the coarse mode.

2.3.2. CAPT hindcast

In this dissertation study, we also use the short-term hindcast framework based on the DOE Cloud-Associated Parameterizations Testbed (CAPT) to have a process-level analysis (Ma et al., 2015; Phillips et al., 2004). CAPT simulations are initialized with realistic atmosphere conditions that are constrained by the Numerical Weather Prediction (NWP) Centers' reanalysis data. Simulations are run for a short time period, similar to the weather forecasts. The most important advantage of short-term hindcast approach is that deficiencies in model physics parameterizations can be isolated from biases developed during the evolution of large-scale atmospheric states. This is, on one hand, because large-scale states (e.g., temperature, wind, moisture) are expected to remain close to the reality prescribed by the reanalysis. On the other hand, feedbacks between these large-scale components normally require a longer time scale (~days) to develop in the atmosphere, but physical processes, such as cloud formation and cloud microphysical processes, are much faster to adjust their states (~hours).

It has been found that there is a strong correspondence between short- and long-term systematic errors in GCM simulations (Ma et al., 2014; Williams & Brooks, 2008;

Xie et al., 2012). Errors associated with fast cloud physical processes are readily apparent in day 2 hindcast results; and errors then gradually grow with simulation time and tend to saturate after 5 days with magnitude comparable to climate errors. Short-term hindcasts allow a direct evaluation of the origin of model errors (e.g., errors in cloud parameterizations) by comparing numerical results to observational data obtained from field campaigns. In this dissertation, CAPT approach is used in EAMv1 to evaluate simulated mixed-phase cloud properties with observations collected during the M-PACE field campaign.

2.3.3. Nudging simulation

Nudging is a method to constrain the evolution of selected meteorological states and to ensure them to stay realism. It has been widely used in atmospheric modeling when evaluating simulated results with observational datasets for a given temporal coverage with specific atmospheric conditions (Sun et al., 2019; Zhang et al., 2014). When running nudging simulations, forcing terms are introduced to the prognostic equations that govern the tendencies of certain meteorological variables (e.g., horizontal winds (U, V), temperature (T), and moisture (Q)). These forcing terms are sufficient enough so that they can constrain simulation results toward prescribed states from reanalysis data. The advantage of nudging technique over using SCM and CAPT is that the model still has interactions between simulated large-scale dynamics and parameterized physical processes over the long-term numerical integration. Therefore, the simulation can respond to the state evolution caused by dynamical and physical

processes. In this dissertation, nudging simulations are run in both CAM5 and EAMv1 to compare with long-term data other than M-PACE field campaign.

CHAPTER III

UNDERSTANDING THE IMPACT OF REPRESENTING HETEROGENEOUS DISTRIBUTION OF CLOUD LIQUID AND ICE ON PHASE PARTITIONING OF ARCTIC MIXED-PHASE CLOUDS WITH NCAR CAM5*

3.1. Background

As discussed in Chapter I, WBF process plays an important role in mixed-phase cloud properties by converting cloud liquid water into ice phase. Previous studies found that CAM5 simulated mixed-phase cloud phase partitioning is substantially biased, with cloud liquid water mass mixing ratio underestimated compared to observations (Liu et al., 2011; Xie et al., 2008). An overestimated WBF process rate in cloud microphysics scheme is believed to be mostly responsible for such a low bias in modeled liquid water (Barrett et al., 2017a; Xie et al., 2008). As the occurrence of WBF process depends on ambient supersaturations, local in-cloud dynamics influences the location and frequency of occurrence of WBF process inside mixed-phase clouds (Fan et al., 2011; Korolev, 2007, 2008; Korolev & Field, 2008). For instance, cloud resolving model simulations showed that ice particle growth at the expense of liquid droplets occurs only in ~50% of the cloud volume. Local downdrafts explain most of those limited cloud volumes,

*Reprinted with permission from "Impacts of Representing Heterogeneous Distribution of Cloud Liquid and Ice on Phase Partitioning of Arctic Mixed-Phase Clouds with NCAR CAM5" by Meng Zhang, 2019. *Journal of Geophysical Research: Atmospheres*, 124, 13071–13090, Copyright 2019 by AGU.

because they provide a supersaturated environment with respect to ice while it is still subsaturated with respect to liquid (Fan et al., 2011). In strong updrafts, supersaturation is available for both liquid and ice, and liquid droplets and ice crystals then grow simultaneously. On the other hand, simultaneous evaporation of liquid droplets and ice crystals occurs in strong downdrafts, which are usually associated with deep convective systems or near cloud boundaries. By introducing subgrid variability of vertical velocity to the calculation of WBF process, less frequent WBF process was triggered in Storelvmo et al. (2008), and the transformation of liquid to ice became more comparable to observed clouds. Moreover, the subgrid heterogenous distribution of liquid droplets and ice crystals contributes to another source of uncertainties to the WBF process. In GCMs, the assumption that liquid droplets and ice crystals homogeneously mixed in the whole grid box is commonly applied in cloud microphysics. However, in-situ observations suggested that liquid and ice may not uniformly distribute throughout mixed-phase clouds all the time. Pure liquid and pure ice pockets on the scale of 10^2-10^3 meters were observed (D'Alessandro et al., 2019; Korolev et al., 2003, 2017; Korolev & Isaac, 2006). Thus, the mixing volume between liquid and ice is reduced due to the heterogeneous distribution, resulting in a reduced WBF process rate (Tan & Storelvmo, 2016).

In the following sections of this chapter, we will examine the impact of heterogenous distribution between cloud liquid and cloud ice on the WBF process. By representing such heterogenous structures via modified WBF process in CAM5 using

different assumptions, the influence of mixed-phase cloud heterogeneity on simulated mixed-phase cloud properties will be investigated.

3.2. Methodology

In this section, we propose three approaches to represent the heterogeneous distribution between liquid and ice to modify the WBF process in CAM5's cloud microphysics scheme.

3.2.1. Default WBF process treatment

We start from introducing the default treatment of WBF process in the MG1 cloud microphysics in CAM5. The cloud ice depositional growth rate is determined through Equation (1):

$$A = \frac{q_v^* - q_{vi}^*}{\Gamma_p \tau_i} \tag{1}$$

where q_v^* is the saturated in-cloud water vapor mass mixing ratio with respect to liquid, and q_{vi}^* is the saturated in-cloud water vapor mass mixing ratio with respect to ice. The release of latent heat is accounted for in the psychrometric correction term $\Gamma_p = 1 + (L_s/c_p)(dq_{vi}/dT)$, where L_s is the latent heat of sublimation, c_p is the specific heat at constant pressure, and (dq_{vi}/dT) is the change of ice saturation vapor pressure with

temperature. Note that τ_i is the supersaturation relaxation time scale with respect to cloud ice. It is described as

$$\tau_i = (2\pi N_{0i}\rho_\alpha D_v \lambda_i^{-2})^{-1} \quad (2)$$

The diffusivity of water vapor is given by D_v, and the size distribution of ice crystals is reflected by N_{0i} and λ_i, which are the intercept and slope of ice particle size distribution, respectively, represented by a gamma function.

In CAM5, the calculation of WBF process is activated when temperature is colder than 0℃ and liquid and ice exist at the same time in the same model grid. The WBF process with respect to snow water is determined similarly as Equation (1). We note that cloud liquid and cloud ice are assumed to be homogeneously distributed in MG1 cloud microphysics. One potential issue associated with this assumption is that the WBF process could be too efficient, and all available liquid water within the same model grid would be consumed by ice crystals within one model time step (30 min).

3.2.2. Idealized heterogeneous mixing structure (TS16)

The first assumption representing the heterogeneous distribution in mixed-phase clouds follows an idealized pocket structure proposed by Tan and Storelvmo (2016, hereafter TS16). In their study, pure liquid and pure ice pockets on the size of 100 m are assumed to uniformly distribute on all sides of individual grid box in an alternating sequence. The liquid and ice mixing volume is then changed from a 100 km × 100 km

grid (homogenous mixing, $O(10^3)$ m (vertically) × $O(10^5)$ m (horizontally) × $O(10^5)$ m (horizontally) = $O(10^{13})$ m^3) to a limited volume on the magnitude of $O(10)$ m (vertically) × $O(10^3)$ m (horizontally) × $O(10^3)$ m (horizontally) = $O(10^7)$ m^3. Therefore, the mixing volume is reduced by six orders of magnitude in TS16 compared to the default one. As shown in Equation 1, liquid and ice mixing volume is assumed to inversely correlate to the supersaturation relaxation time scale (τ_i). According to TS16, six orders of magnitude change in the mixing volume can therefore be reflected in the WBF process rate (A) due to the inverse relationship between A and τ_i. WBF process rate is thus reduced by six orders of magnitude.

Following this assumption, the first sensitivity experiment is designed using a perturbation factor of 10^6 to τ_i to test the impact of TS16 assumption on modeled mixed-phase cloud properties. This experiment is referred to as WBF_TS16.

3.2.3. HIPPO observed heterogeneous mixing (HIPPO)

In the second approach, we propose a treatment based on aircraft measurements of cloud particles to represent the heterogeneous structure of mixed-phase clouds. In-situ data from the High-performance Instrumented Airborne Platform for Environmental Research (HIAPER) Pole-to-Pole Observation (HIPPO) Global campaign (Wofsy et al., 2011) are utilized. There were five pole-to-pole research flight deployments (HIPPO#1-5) during the HIPPO field campaign. Two research flights were performed over the Arctic in each deployment, covering areas from 60°N to 87°N and 135°W to 165°W. In this study, we use 1-Hz data obtained in HIPPO#2-5 campaigns during 2009-2011 to

sample the heterogeneous structure of high-latitude mixed-phase clouds. In total, ~65 hours of measurements of temperature, mass and number concentrations of cloud hydrometeors, and particle size distributions are used in our analysis.

Onboard the aircraft, temperature was measured by the Rosemount temperature probe. The accuracy and precision in temperature measurements are 0.5 K and 0.01 K, respectively. Data between temperatures -40℃ and 0℃ are sampled for mixed-phase clouds. Cloud particles were observed by the cloud droplet probe (CDP) and fast two-dimensional cloud probe (2-DC). Particles with sizes between 2-50 μm were measured by the CDP, and the 2-DC probe measured particles ranging from 62.5 to 1600 μm. For particles on the size between 1600 μm and 3200 μm, a mathematic reconstruction is conducted to obtain their size distribution. The mass concentration of particles measured by 2-DC are derived based on Brown and Francis (1995).

According to the method of D'Alessandro et al. (2019), in-cloud environment is defined as: (1) the CDP measured number concentration > 0.03 cm^{-3} and mass concentration > 3.98×10^{-4} g m^{-3}; or (2) at least one particle is detected by the 2-DC and its derived mass concentration is greater than 4.68×10^{-5} g m^{-3}. To further distinguish the phase of measured cloud particles, algorithm shown in Figure 1 of D'Alessandro et al. (2019) is used. Based on the ratio of LWC to total water content (TWC, sum of LWC and IWC), clouds are determined as liquid phase when LWC/TWC$\geq$ 0.9, and as ice phase when LWC/TWC $\leq$ 0.1. Clouds are defined as mixed phase when 0.1 < LWC/TWC < 0.9. Such a phase determination method is consistent to Korolev et al. (2003). Moreover, a "moving average" is conducted on the scale of 10 s and 100 s,

respectively, to investigate the impact of spatial scale change on sampled mixed-phase cloud heterogeneity.

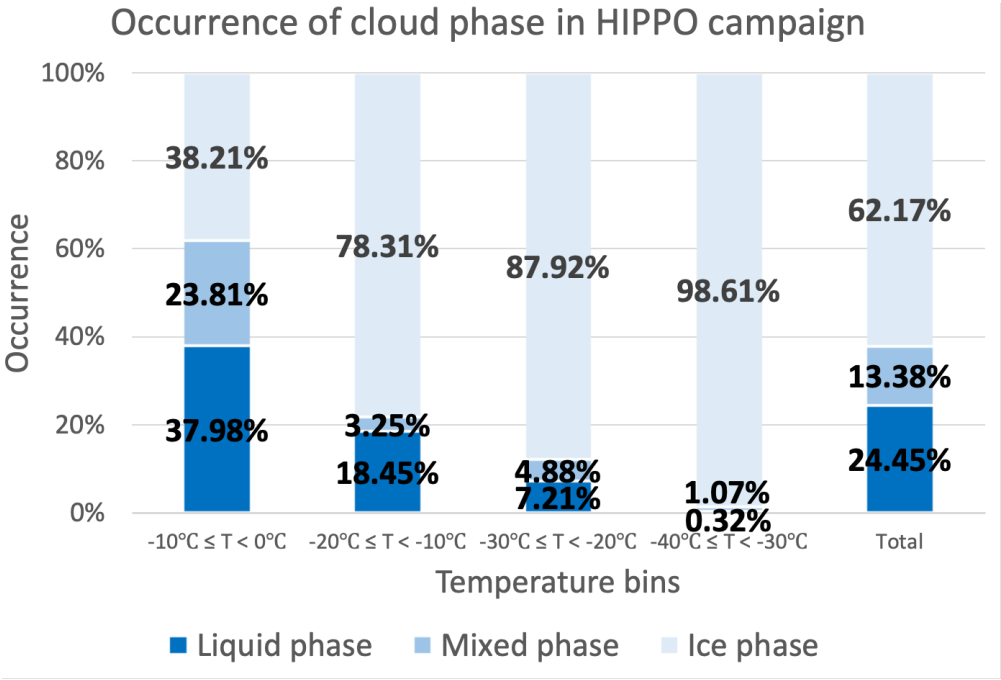

Figure 3.1. Frequency of occurrence of liquid phase (dark blue), mixed phase (light blue), and ice phase (light gray) calculated based on the 1-Hz HIPPO observations. Averaged frequency of occurrence for each phase at four temperature bins and the average over all temperatures (rightmost column) are shown.

Figure 3.1 shows the result of calculated frequency of occurrence of three cloud phases in HIPPO measured clouds. Note that cloud phase data shown here is further sampled to satisfy in-cloud conditions with TWC $\geq$ 0.01 g m^{-3}, and these data are categorized for temperature bins of -10°C – 0°C, -20°C – -10°C, -30°C – -20°C, and -40°C

– -30℃, respectively. It is shown in Figure 3.1 that mixed phase region only occupies a limited fraction of clouds. The frequency of occurrence is ~13.4% when averaging over the 1-Hz measurements among temperature bins. Mixed phase region tends to become more dominant at warmer temperatures and pure ice clouds become more frequent with decreasing temperatures. By considering frequency of occurrence of mixed phase regions at different spatial scales, we propose that 15% of the cloud volume would be mixed phase, and the remaining cloud volume would be in either pure liquid phase or pure ice phase. Therefore, the WBF process will only be active in 15% of Arctic mixed-phase cloud volume, because this process is expected in the mixed phase portion of mixed-phase clouds.

To account for such a mixed phase pattern based on the HIPPO data, we apply a perturbation factor of 0.15 to Equation 1 to examine its effect on simulated mixed-phase cloud properties. This sensitivity experiment is denoted as WBF_HIPPO.

3.2.4. Mass-weighted treatment from observed heterogeneous structure (MSWT)

In the third assumption, we follow the method of Fu and Hollars (2004) to represent the heterogeneous distribution in mixed-phase clouds. Several earlier studies showed that relative humidity inside mixed-phase clouds is close to liquid saturation due to the fast evaporation of liquid droplets and a relatively slower ice deposition rate (D'Alessandro et al., 2019; Korolev & Isaac, 2006; Korolev & Mazin, 2003). Such a liquid saturation assumption has been widely adopted for cloud parameterizations in mixed-phase clouds. MG1 cloud microphysics scheme is one of them. However, by

analyzing in-situ measurements of in-cloud relative humidity during the Surface Heat Budget of the Arctic Ocean (SHEBA)/First International Satellite Cloud Climatology Project (ISCCP) Regional Experiment–Arctic Cloud Experiment (FIRE-ACE) field campaign, Fu and Hollars (2004) found that this liquid saturation assumption is not always accurate in real cloud environment. They reported a large portion of subsaturated cloud data in measured mixed-phase clouds, and they attributed these subsaturations to pure ice areas. Moreover, Fu and Hollars (2004) further showed that a mass-weighted interpolation (MSWT) of relative humidity better agrees with the PDF of observed relative humidity in the Arctic, which implies that a mass-weighted representation can capture the correct physics in mixed-phase clouds. This is true because in-cloud relative humidity is closer to liquid saturation when liquid water mass is dominant in total cloud mass, while in-cloud relative humidity is closer to ice saturation when ice water dominates.

Thus, we apply a mass-weighted treatment (Equation 3) to replace the liquid saturated water vapor mass mixing ratio used in Equation 1.

$$q_v = q_{vl} \times \frac{LWC}{TWC} + q_{vi} \times \frac{IWC}{TWC} \tag{3}$$

In Equation 3, q_{vl} is the saturated water vapor mixing ratio with respect to liquid, and q_{vi} is the saturated water vapor mixing ratio with respect to ice. LWC and IWC are total

in-cloud liquid water mass mixing ratio (liquid plus rain) and total in-cloud ice water mass mixing ratio (ice plus snow), respectively. TWC is summation of LWC and IWC.

As the calculation of WBF process rate is now related to the mass partitioning of condensed cloud water, the impact of heterogeneous distribution such as pure liquid or pure ice on the WBF process can be represented in this mass-weighted treatment. We refer this experiment as WBF_MSWT.

3.3. Model experiments

3.3.1. Single column model simulations

Table 3.1 summarizes the experiments performed with SCAM5. One control experiment and three sensitivity experiments including aforementioned assumptions of modified WBF process are conducted. Details for each model experiment can be found in Table 3.1.

3.3.2. Global simulations

In addition to SCM simulations of M-PACE, CAM5 is also run in the global mode on the 1.9° × 2.5° horizontal resolution. Horizontal wind (U, V) and temperature (T) fields are nudged towards the ERA-Interim reanalysis data from the European Center for Medium-Range Weather Forecasts (ECMWF) in global simulations. 3-year simulations are run from November 2005 to December 2008 and the first two-month results are used for model spin-up. Same experiments as SCM runs (listed in Table 3.1) are conducted to examine the impact of modified WBF treatments on mixed-phase cloud

properties in terms of their seasonal variability. 3-hourly high frequency outputs are used to sample low-level stratiform mixed-phase clouds. Modeled clouds are validated against ARM long-term ground-based measurements. The land grid closest to the NSA Utqiaġvik site is selected for model evaluation.

Table 3.1. *Model Experiments in M-PACE Case Study and Global Simulations (Reprinted from Zhang, Liu et al., (2019))*

Experiments	Simulation type	Model description
CTL	SCM/Nudging	Default model configuration but with CNT ice nucleation scheme. Nudging U, V (horizontal winds), and T (temperature) to the ERA-Interim reanalysis data when running the nudging simulation.
WBF_TS16	SCM/Nudging	Apply a constant perturbation value of 10^6 to the WBF process supersaturation relaxation time scale. Assume pockets with 100 m size uniformly distributed in grid cells as proposed by Tan and Storelvmo (2016).
WBF_HIPPO	SCM/Nudging	Apply a constant perturbation value of 0.15 to the WBF process. Assume mixed-phase region occupies 15% fractional volume of mixed-phase clouds. Derived from HIPPO campaign.
WBF_MSWT	SCM/Nudging	Replace liquid saturated water vapor mixing ratio with mass-weighted water vapor mixing ratio in the WBF process calculation, following Fu and Hollars (2004).
WBF_TS16_ ACC	SCM	Same as the WBF_TS16, but the constant perturbation factor is applied to accretion of liquid droplets and rain drops by snow. Heterogeneous distribution is consistently considered in cloud microphysics.
WBF_TS16_ ACC_L60	SCM	Same as the WBF_TS16_ACC but utilizes 60 vertical layers.
WBF_TS16_ ACC_L120	SCM	Same as the WBF_TS16_ACC but utilizes 120 vertical layers.

Note that sensitivity experiments share the same model configuration as CTL except for the designed modifications for sensitivity tests.

3.4. Results

3.4.1. SCM results in M-PACE

SCAM5 simulated Arctic cloud properties are evaluated against ground-based observations during the M-PACE field campaign. Figure 3.2 compares model simulated cloud fraction to observed cloud frequency of occurrence. The ARSCL retrieved clouds, collected at 10-s and 45-m intervals, are averaged to 3-hour and 25-hPa intervals to better compare with clouds outputted from model simulations.

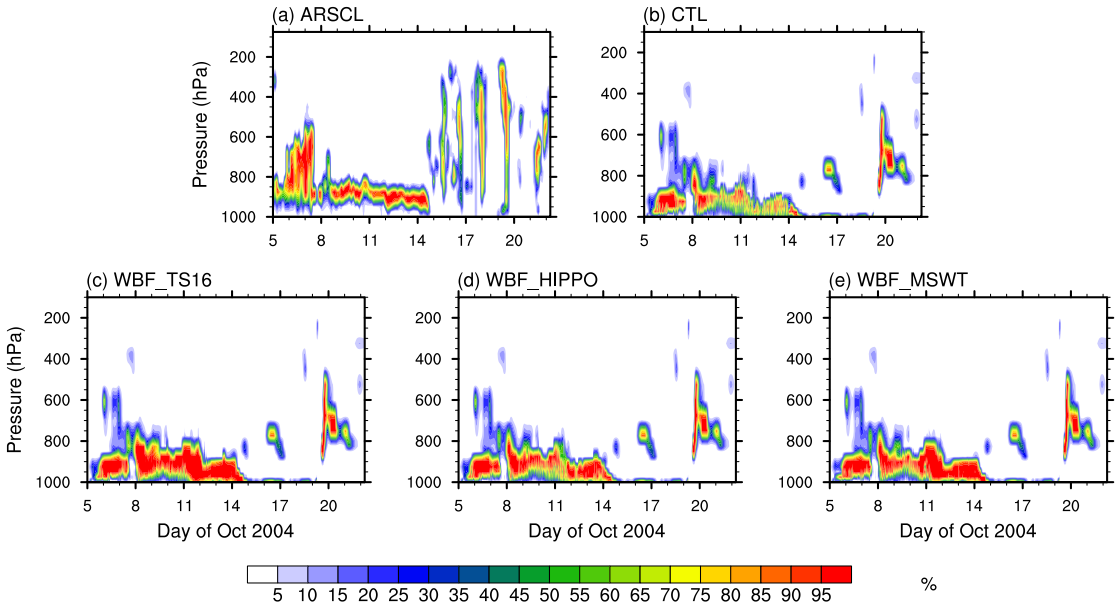

Figure 3.2. Time-pressure cross sections of modeled and observed cloud fraction at the Utqiaġvik site during the M-PACE filed campaign. (a) observed frequency of occurrence of clouds from the ARSCL algorithm. (b) to (e) SCM simulations. CTL is the default experiment assuming homogeneous distribution; WBF_TS16 is the experiment with constant WBF perturbation scale of 10^6; WBF_HIPPO assumes that 15% volume in mixed-phase clouds is homogeneously mixed, where a perturbation of 0.15 is applied to WBF process; WBF_MSWT uses a mass-weighted water vapor mixing ratio in the WBF process calculation. (Reprinted from Zhang, Liu et al., (2019).)

Figure 3.2a shows that multilayer clouds were observed at the NSA Utqiaġvik site during 5-8 October 2004, which were associated with east-northeasterly flow of cold air passing over the cold pack ice. During 9-14 October, resilient single-layer boundary-layer mixed-phase clouds were formed over the open ocean and were advected to the Utqiaġvik. Deep clouds related to frontal systems dominated the last period of M-PACE field campaign. Compared to observations, Figure 3.2b shows that although CTL well simulates the temporal evolution of single-layer mixed-phase clouds, cloud fractions are

substantially underestimated. Multilayer clouds and deep clouds are also poorly reproduced in the default SCAM5. By introducing the heterogeneous distribution of liquid and ice to the WBF process, simulated amounts of cloud fraction are increased and become more comparable to the ARSCL products (Figures 3.2c-3.2e). However, improvements in three sensitivity experiments are mainly identified in single-layer boundary-layer cloud periods, with negligible changes for multilayer and deep clouds. Note that cloud fractions formed from WBF_TS16 and WBF_MSWT are slightly larger than WBF_HIPPO, which indicates different impacts of different assumptions applied to the WBF process. Improvements in cloud fraction can be explained by the increase of relative humidity in the lower troposphere after modifying the WBF process (Figure 3.3f). Moreover, there are large low biases in simulated cloud base height in all four SCM experiments when compared to observations. Such biases are associated with the overestimated specific humidity (Figure 3.3b) and relative humidity (Figure 3.3c) near the surface, which are prescribed in forcing data.

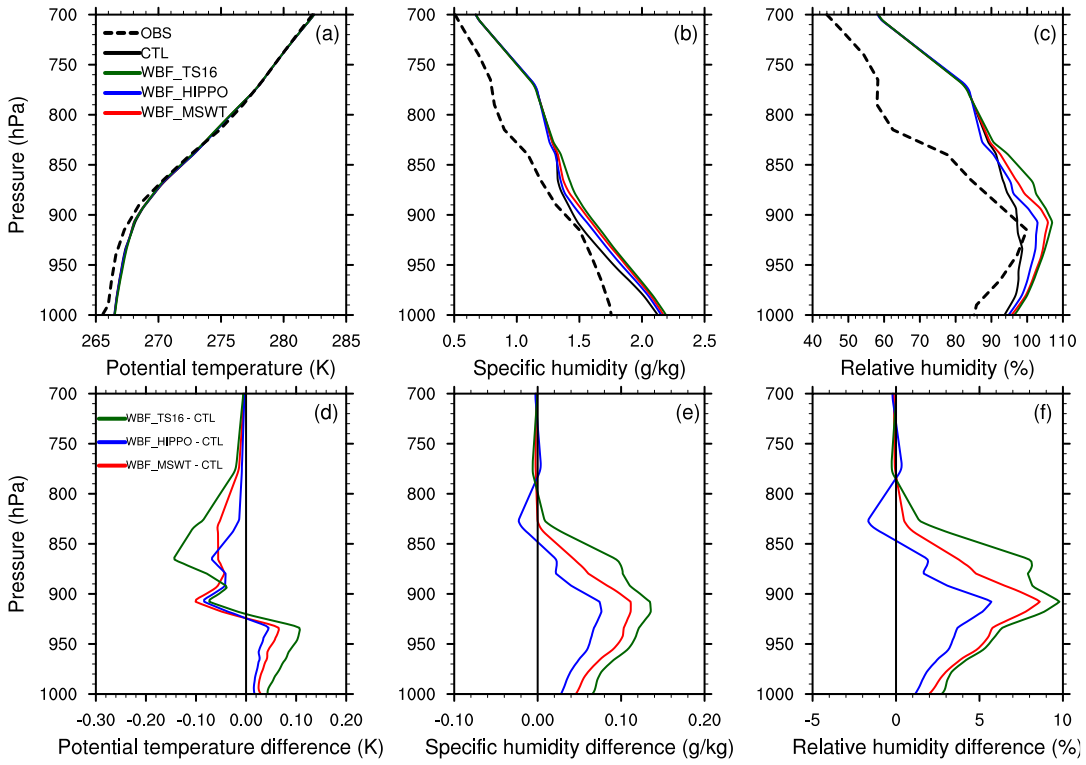

Figure 3.3. Vertical profiles of (a) potential temperature in the unit of K, (b) specific humidity in the unit of g kg^{-1}, and (c) relative humidity in the unit of % for single-layer low-level mixed-phase clouds during the M-PACE field campaign. Profiles are averaged between 9-13 October for both observations and SCM results. (d)-(f) show differences between sensitivity experiments and CTL of potential temperature, specific humidity, and relative humidity, respectively. Observations are from the M-PACE Intensive Operation Period (IOP) forcing data (Xie et al., 2006). (Reprinted from Zhang, Liu et al., (2019).)

Figure 3.4 presents time-pressure cross sections of simulated total LWC (sum of liquid and rain) and total IWC (sum of ice and snow) in CTL and the differences between three sensitivity experiments and CTL. It is shown in Figure 3.4a that minimal LWC is generated in CTL except between 6-9 October. IWC, particularly snow water, dominates the simulated cloud condensate (Figure 3.4e). This is the result of fast

autoconversion process which will be discussed in section 3.4.3. We also note that cloud fraction determined by cloud macrophysics scheme is inconsistent with cloud liquid water amount calculated in cloud microphysics in SCAM5. Such an inconsistency is caused by separate parameterizations used for different properties.

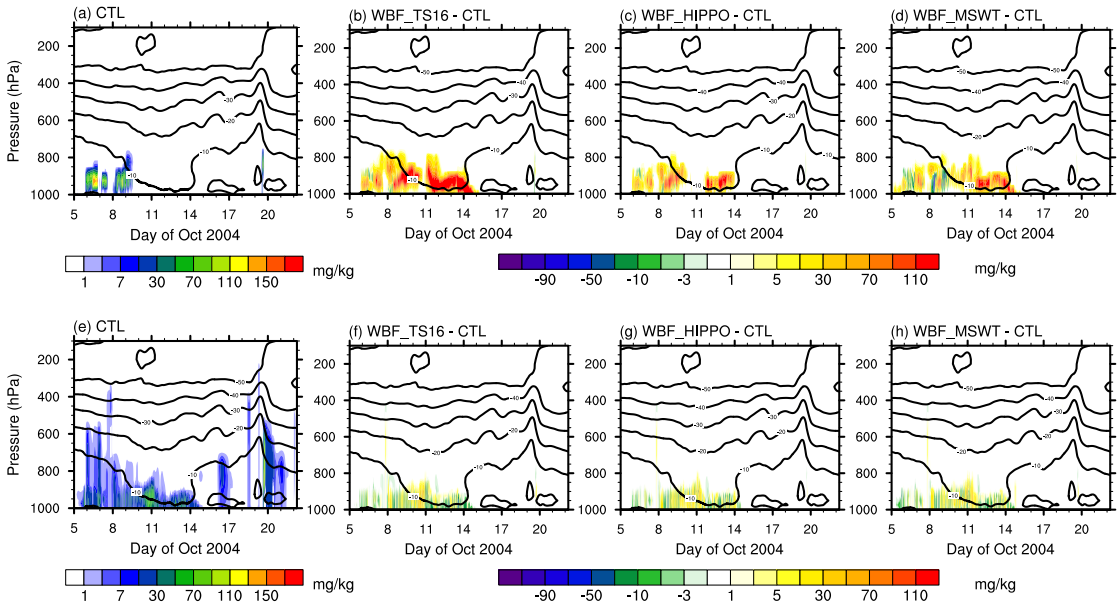

Figure 3.4. Time-pressure cross sections of modeled cloud liquid water (including rain; a-d) and cloud ice water (including snow; e-h) mass mixing ratios at the Utqiaġvik site during the M-PACE filed campaign. Results from CTL and the differences between three sensitivity experiments (WBF_TS16, WBF_HIPPO, and WBF_MSWT; from left to right) and CTL are shown. (Reprinted from Zhang, Liu et al., (2019).)

By comparing three sensitivity experiments to CTL, it is obvious that WBF_TS16, WBF_HIPPO, and WBF_MSWT all increase simulated LWC in single-layer boundary-layer mixed-phase clouds. The LWC enhancement in WBF_TS16 is the

largest while it is the least in WBF_HIPPO. This corresponds well to the perturbation factors in modified WBF process treatment, where a factor of 10^{-6} is used in WBF_TS16 and a factor of 0.15 is in WBF_HIPPO. It is interesting to notice that WBF_MSWT produces LWC in the middle between WBF_TS16 and WBF_HIPPO. This implies that a mass-weighted water vapor mixing ratio in Equation 3 represents an intermediate and varying condition between the extreme pocket structure proposed by Tan and Storelvmo (2016) and the partial homogeneous structure found in HIPPO observations. Figure 3.5 shows the normalized PDF of equivalent perturbing factors used to slow down WBF process in WBF_MSWT. The equivalent slow-down magnitude is defined as the ratio of perturbed WBF process rate using mass-weighted assumption over the default WBF process rate. It is demonstrated that WBF process rate in WBF_MSWT is reduced by factors ranging nine orders of magnitude compared to CTL. The change of WBF process rate depends on the phase partitioning of simulated mixed-phase cloud condensates. One interesting feature is that the perturbation factor has two peaks around 10^{-1} and 10^{-5}-10^{-6}, respectively, coincidentally corresponding to perturbations in WBF_HIPPO and WBF_TS16. Figure 3.6 indicates the distribution of perturbed factors with mass-weighted assumption in simulated clouds. It is shown that the peak of frequency of occurrence at 10^{-1} is mainly result from liquid dominant cloudy area, and ice dominant area is responsible for the peak between 10^{-5} and 10^{-6}.

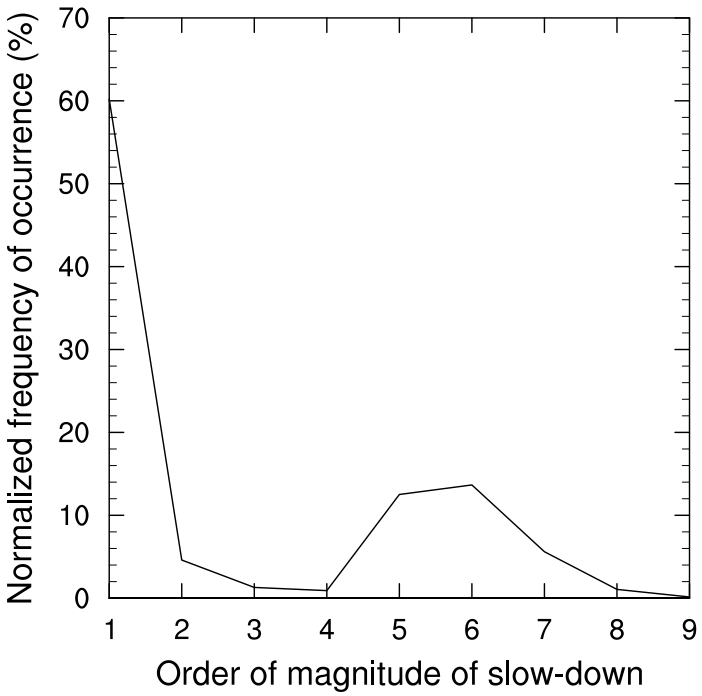

Figure 3.5. Frequency of occurrence of the slow-down magnitude on the WBF process as a result of using mass-weighted water vapor mixing ratio. The WBF process slow-down magnitude is calculated as the ratio of perturbed WBF process rate from mass-weighted treatment to the default WBF process rate. The ratio includes SCM results from 5 October to 22 October. The order of slow-down magnitude from 1-9 is equivalent to a tuning factor between 10^{-1} and 10^{-9} in cloud microphysics. (Reprinted from Zhang, Liu et al., (2019).)

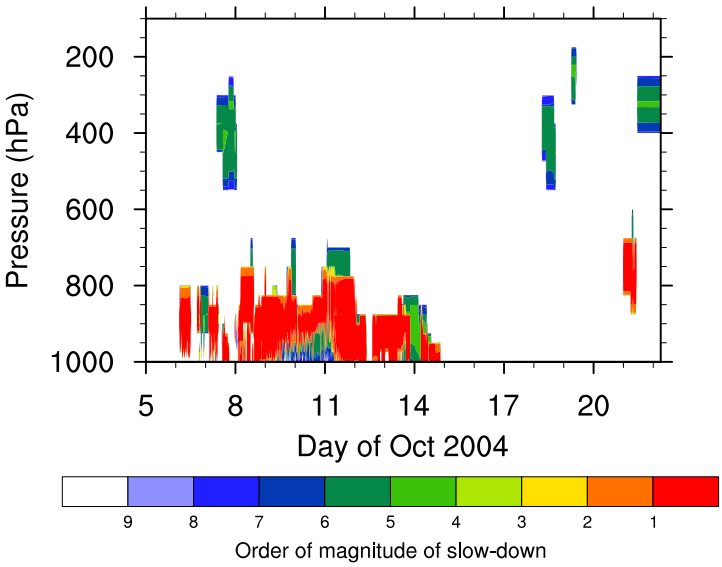

Figure 3.6. Distribution of the slow-down magnitude in WBF process rate in WBF_MSWT simulated clouds. (Reprinted from Zhang, Liu et al., (2019).)

The response of total IWC to modified WBF process is shown in Figures 3.4f-3.4h. In general, changes in IWC are less significant compared to LWC. Despite the expected IWC reduction after modifying WBF process, all three sensitivity experiments exhibit slightly larger IWC than CTL in part of simulated mixed-phase clouds. The increase of both LWC and IWC implies the larger total cloud water condensation in model simulations with modified WBF process. As greater LWC is simulated in mixed-phase clouds when comparing three sensitivity experiments to CTL, the stronger cloud top radiative cooling (shown in Figure 3.3d) induces larger condensation of cloud water.

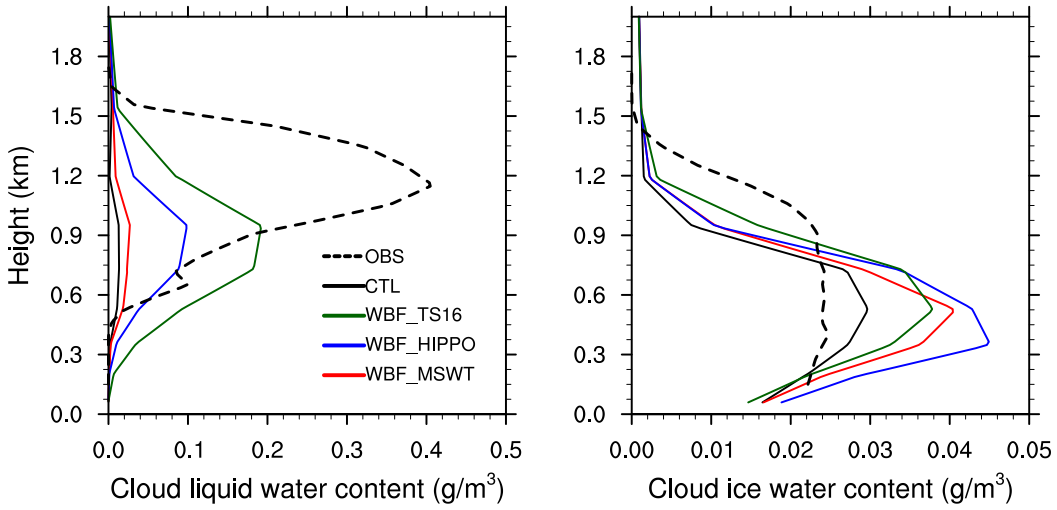

Figure 3.7. Vertical profiles of cloud LWC (left) and cloud IWC (right), averaged between 1200 UTC 9 October and 1200 UTC 10 October during M-PACE. Black dash lines are retrieved liquid and ice water contents from Shupe et al. (2008). Solid black lines represent the SCM CTL. Solid green lines represent WBF_TS16, and solid blue lines are WBF_HIPPO. WBF_MSWT is shown with solid red lines. (Reprinted from Zhang, Liu et al., (2019).)

Figure 3.7 compares vertical profiles of simulated total LWC and IWC with remote sensing retrievals based on Shupe et al. (2008). Both modeled and observed clouds are averaged between 1200 UTC 9 October and 1200 UTC 10 October. It is shown that CTL substantially underestimates LWC but well simulates vertical profiles of IWC. Similar LWC and IWC responses to modified WBF process are found in cloud water vertical profiles as aforementioned, with both increasing compared to CTL. Among three assumptions used in WBF process to represent heterogeneous distributions between liquid and ice, WBF_TS16 has the largest improvement in LWC profiles, albeit with a remaining underestimation of a factor of 2. Meanwhile, simulated IWC using modified WBF process becomes 25-50% larger than CTL. Note that SCM simulated

cloud liquid layers tend to peak 0.6 km lower than observations and cloud base is simulated only ~0.1 km above the surface in all experiments. Such low biases in cloud boundaries are likely due to the biased forcing used to drive the SCM simulation.

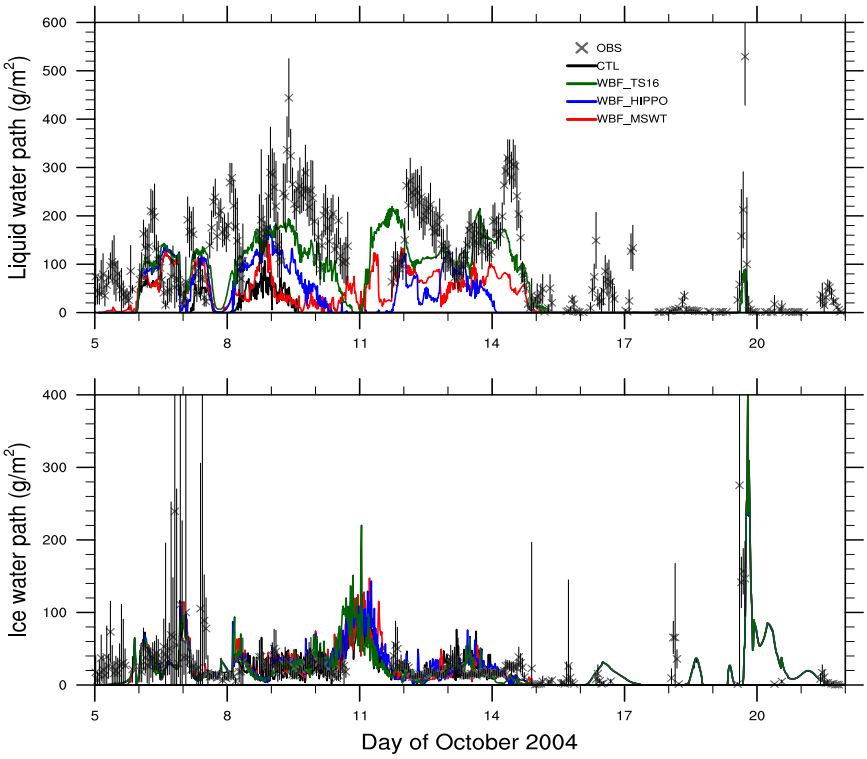

Figure 3.8. Time series of LWP (upper panel) and IWP (lower panel) simulated by SCM and retrieved from ground-based measurements at the NSA Utqiaġvik site during M-PACE. Grey crosses represent remote sensing retrievals and the overlaid grey straight lines indicate one standard deviation. Black lines represent CTL simulation while green lines represent WBF_TS16. WBF_HIPPO is shown in blue, and WBF_MSWT is in red. (Reprinted from Zhang, Liu et al., (2019).)

Figure 3.8 shows the comparison between SCM simulated LWP and IWP and ground-based remote sensing retrievals. Observed LWP is based on the ARM MWR measurements (Wang, 2007), and IWP is retrieved using combined MMCR and MPL data (Wang & Sassen, 2002). It is shown in Figure 3.8 that time series of observed LWP is larger than 100 g m^{-2} throughout the early M-PACE campaign period (6-14 October 2004). However, CTL simulated LWP is substantially underestimated. LWP on the magnitude of 50-100 g m^{-2} are produced before 10 October, and LWP remains close to 0 during the rest time period. Simulations with modified treatments of WBF process are found to improve not only LWP amounts but also temporal persistence of liquid water. The improvement in LWP is different among three sensitivity experiments. For example, the WBF_TS16 experiment indicates the most comparable LWP temporal evolution to observations, and the improvement in WBF_HIPPO experiment is the smallest while WBF_MSWT is in the middle. Such pattern is consistent to previous discussion. Compared to observations, comparable IWP is simulated in the Arctic mixed-phase clouds by SCM. It is also shown that simulated IWP has little sensitivity to modified WBF process. Budget analysis of process tendencies shows that compensating sources for IWC from accretion of liquid droplets and raindrops by snow particles explain the little sensitivity of IWP to WBF modifications (will be discussed in section 3.4.3).

3.4.2. Global simulation results

In the following section, we will focus on the impact of WBF process perturbations on the seasonal variability of Arctic mixed-phase clouds. Macrophysical

and microphysical properties of low-level mixed-phase clouds are sampled in model simulations and are evaluated against long-term ground-based observational data.

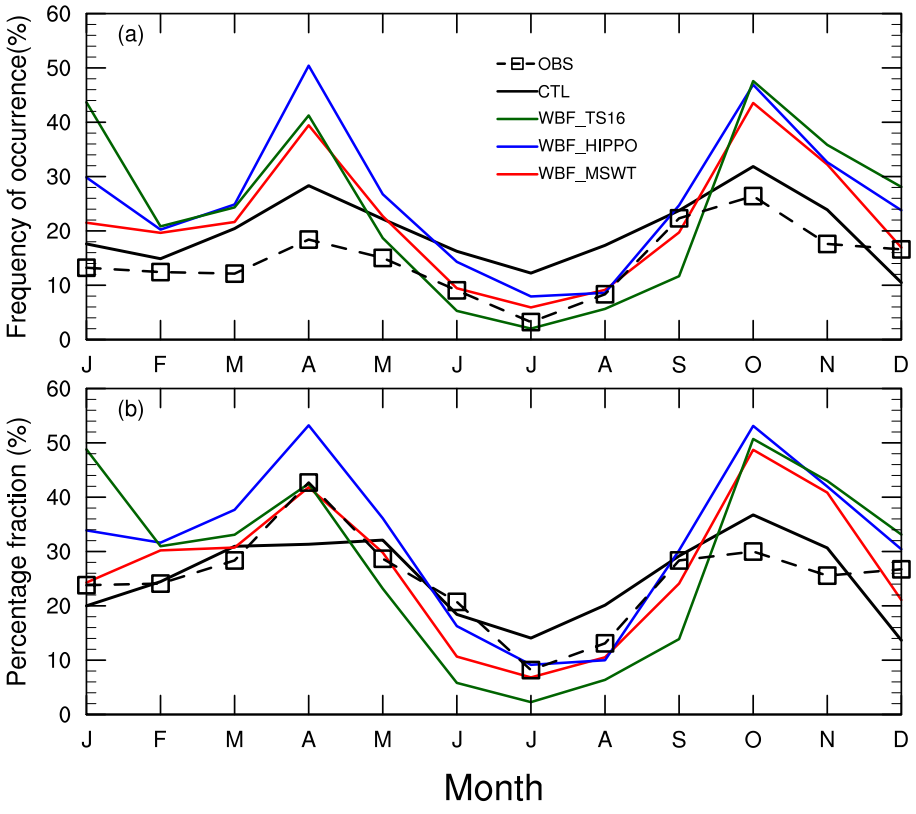

Figure 3.9. Comparison of (a) frequency of occurrence of observed single-layer stratiform mixed-phase clouds and modeled low-level mixed-phase clouds and (b) fractional percentage relative to all clouds at the NSA Utqiaġvik. Frequency of occurrence of mixed-phase clouds is the ratio of profiles of single-layer mixed-phase clouds to all profiles including both cloudy and clear skies, while fractional percentage is the ratio to cloudy-sky profiles. (Reprinted from Zhang, Liu et al., (2019).)

In 3-year nudging simulations, low-level mixed-phase clouds are sampled using 3-hourly outputs. Target clouds are defined as (1) temperature is between 0℃ and -40℃; (2) total LWC and total IWC are larger than 0.001 g kg^{-1} at the same time; (3) cloud top height is below 700 hPa altitude. Similar sensitivity experiments as in SCM (Table 3.1) are performed in the global version of CAM5, but horizontal wind and temperature fields are nudged to ERA-Interim reanalysis data. As mentioned in section 3.3.2, results of global simulations between 2008 and 2010 are evaluated against ground-based remote sensing data between 2014 and 2017 at the NSA Utqiaġvik site (Zhang et al., 2014; Zhang, Vogelmann, et al., 2019). Although there is a time deviation between model simulations and observations, we note the annual statistics of cloud properties should not differ significantly. Therefore, we qualitatively investigate how the perturbation of WBF process would influence seasonal variations of mixed-phase cloud properties.

Figure 3.9 shows the comparison of monthly frequency of occurrence of low-level mixed-phase clouds and the percentage fraction of low-level mixed-phase clouds to all clouds. Frequency of occurrence of observed clouds is determined by the ratio of single-layer stratiform mixed-phase cloud profiles to all-sky profiles, and the percentage fraction is the ratio to only cloudy-sky profiles. For modeled clouds, frequency of occurrence and percentage fraction are defined similarly but for sampled low-level mixed-phase clouds. As single-layer stratiform mixed-phase clouds are dominated by low-level clouds in the Arctic, the evaluation of low-level mixed-phase clouds from model results are statistically abundant. In Figure 3.9, observed single-layer stratiform mixed-phase clouds indicate a strong seasonal variability at the NSA Utqiaġvik site.

Higher frequency of occurrence is observed in boreal spring and fall, and there is a minimum during summertime. Compared to observations, CTL simulates the general seasonal pattern of cloud frequency of occurrence. However, simulated low-level mixed-phase clouds are too frequent throughout the years. By assuming heterogeneous distributions between liquid and ice in WBF process, simulated low-level mixed-phase clouds become more (less) frequent for spring and fall (summer), exhibiting a stronger seasonal variation than CTL. The better maintenance of mixed-phase clouds due to reduced WBF process explains the enhancement of cloud occurrence (spring and fall); and the higher cloud top height is responsible for the reduced occurrence of low-level mixed-phase clouds in the Arctic (summer). Moreover, insignificant sensitivity of frequency of occurrence of low-level mixed-phase clouds is found to different perturbating factors on the WBF process.

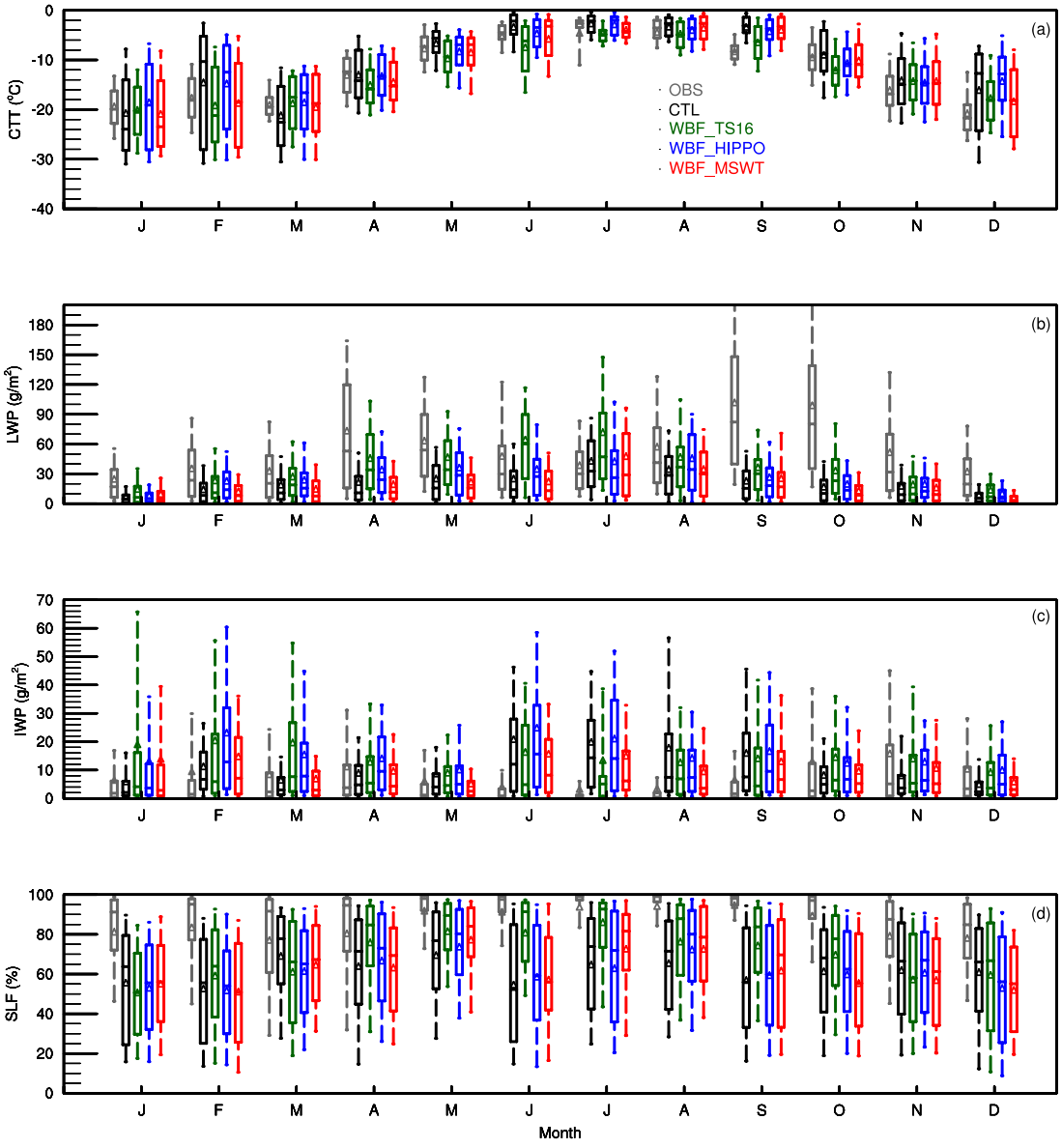

Figure 3.10. Monthly statistics of observed stratiform mixed-phase clouds and modeled low-level mixed-phase clouds at Utqiaġvik: (a) CTT, (b) LWP, (c) IWP, and (d) SLF. The box-and-whisker plots provide 10th, 25th, 50th, 75th, and 90th percentiles of the monthly statistics, and the means are indicated by triangles. Grey color represents the observation, while black for CTL, green for WBF_TS16, blue for WBF_HIPPO, and red for WBF_MSWT. (Reprinted from Zhang, Liu et al., (2019).)

Figure 3.10 shows seasonal variations of observed and modeled cloud properties. Monthly LWP and IWP were derived using Wang and Sassen (2002) for single-layer stratiform mixed-phase clouds. As shown in Figure 3.10a, observed cloud top temperature (CTT) has a strong seasonal variation with warmer CTTs during warm seasons (i.e., JJA). In general, CTL well captures the observed CTT, although there is a slight overestimation during the boreal fall season. With perturbations to the WBF process, all three sensitivity simulations alleviate the overestimation of CTT. The CTT decreasing extent tends to linearly correlate to perturbation factors, as WBF_TS16 shows the largest decrease while WBF_HIPPO is the least and WBF_MSWT in the middle.

For LWP, observations exhibit a local maximum in early fall. All four model simulations underestimate the observed LWP throughout years and misrepresent the maximum LWP in boreal summertime. Consistent to SCM results, WBF_TS16 indicates the largest increase in simulated LWP of low-level mixed-phase clouds. We note that the underestimated LWP can be explained by the underestimation in occurrence of large LWP. Figure 3.11 shows that the probability of small LWP is largely overestimated by the model compared to observations. This difference remains in three sensitivity experiments. The remaining discrepancy from observations is also partially attributed to the compensating loss of liquid water via accretion by snow hydrometeors (will show later).

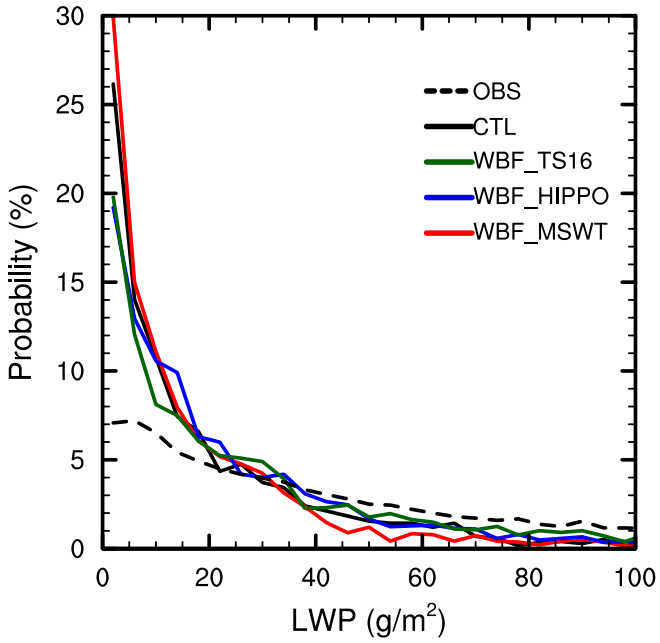

Figure 3.11. Comparison of LWP probability distributions of observed single-layer stratiform mixed-phase clouds and modeled low-level mixed-phase clouds. (Reprinted from Zhang, Liu et al., (2019).)

In terms of IWP, an opposite seasonality of IWP in low-level mixed-phase clouds is simulated in CAM5 compared to observations. For example, a minimum IWP is observed in boreal summer but the model generates an IWP peak at the same time period. Compared to CTL, WBF_TS16 and WBF_MSWT slightly reduce the IWP seasonal difference between summer and winter but the IWP bias in wintertime is moderately enhanced. Besides the compensating snow processes, the cold bias in simulated cloud temperature is also partially responsible for overestimated IWP during the summertime. Moreover, Figure 3.10 shows that supercooled liquid water dominates the observed mixed-phase clouds throughout the years, during which supercooled liquid

fraction (SLF) is higher than 80%. Compared to the observation, simulated SLF in low-level mixed-phase clouds is largely underestimated in CTL. Slight improvements are shown in modeled SLF seasonality in WBF_TS16 and WBF_MSWT, especially for boreal summer due to the reduced high bias in IWP and enhanced LWP in these two experiments.

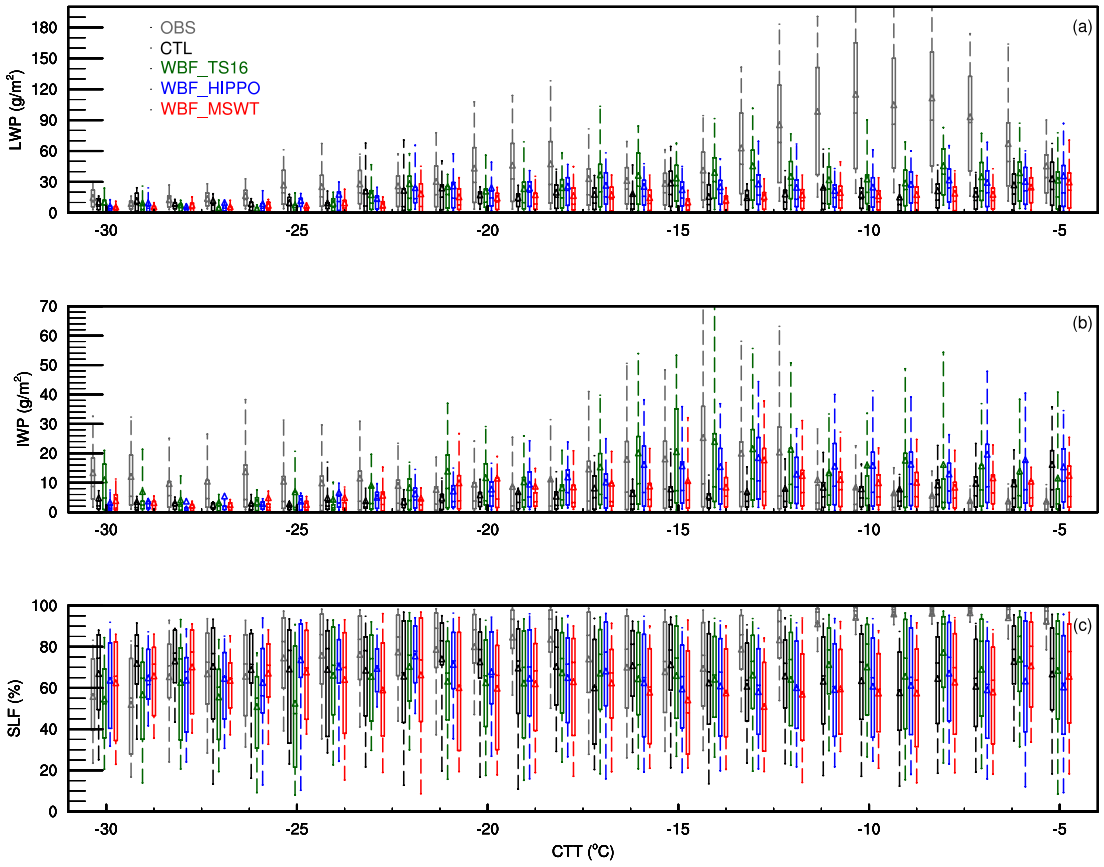

Figure 3.12. Statistics of observed single-layer stratiform mixed-phase cloud (grey) as a function of CTT and modeled low-level mixed-phase clouds from CTL (black) and sensitivity experiments (green: WBF_TS16, blue: WBF_HIPPO, and red: WBF_MSWT) at Utqiaġvik. (a)-(c) are for LWP, IWP, and SLF, respectively. The box-

and-whisker plots are the same as in Figure 3.10. (Reprinted from Zhang, Liu et al., (2019).)

To better understand the influence of changes in WBF process on SLF in low-level mixed-phase clouds, Figure 3.12 shows the statistics of mixed-phase cloud water as a function of CTT. Figure 3.12a shows an apparent LWP dependence on temperature. There is an LWP maximum at -10℃ and a minimum near -15℃. The minimal LWP at -15℃ can be associated with fast ice depositional growth that effectively consumes supercooled liquid water (Korolev, 2008). Such a rapid ice growth feature is demonstrated by Figure 3.12b where an IWP local peak is centered at -14℃. Unfortunately, model simulations indicate insignificant relations between LWP and CTT. Although IWP does not have an obvious relation to CTT in CTL, the IWP maximum near -14℃ is better simulated in WBF_TS16, WBF_HIPPO, and WBF_MSWT, implying the importance of accurate treatment of WBF process in controlling the ice phase microphysics in modeled mixed-phase clouds. Figure 3.12c shows a pronounced SLF minimum around -15℃ in observed mixed-phase clouds; and SLF is close to 100% at temperatures warmer than -10℃. However, all model experiments poorly simulate these SLF features as a function of temperature. The modeled low SLF bias at warm temperatures is mainly related to the underestimation of LWP in mixed-phase clouds.

3.4.3. Microphysical process budget analysis

In previous sections, the influence of representation of heterogeneous distribution between liquid and ice on simulated cloud properties are examined in both SCM and global simulations. To understand the role of modified WBF process on other microphysical processes, budget of process tendencies for cloud liquid, cloud ice, rain, and snow hydrometeors are investigated. Process tendencies are averaged between 9 and 13 October, outputted from SCM simulations. Single-layer boundary-layer mixed-phase clouds are examined here.

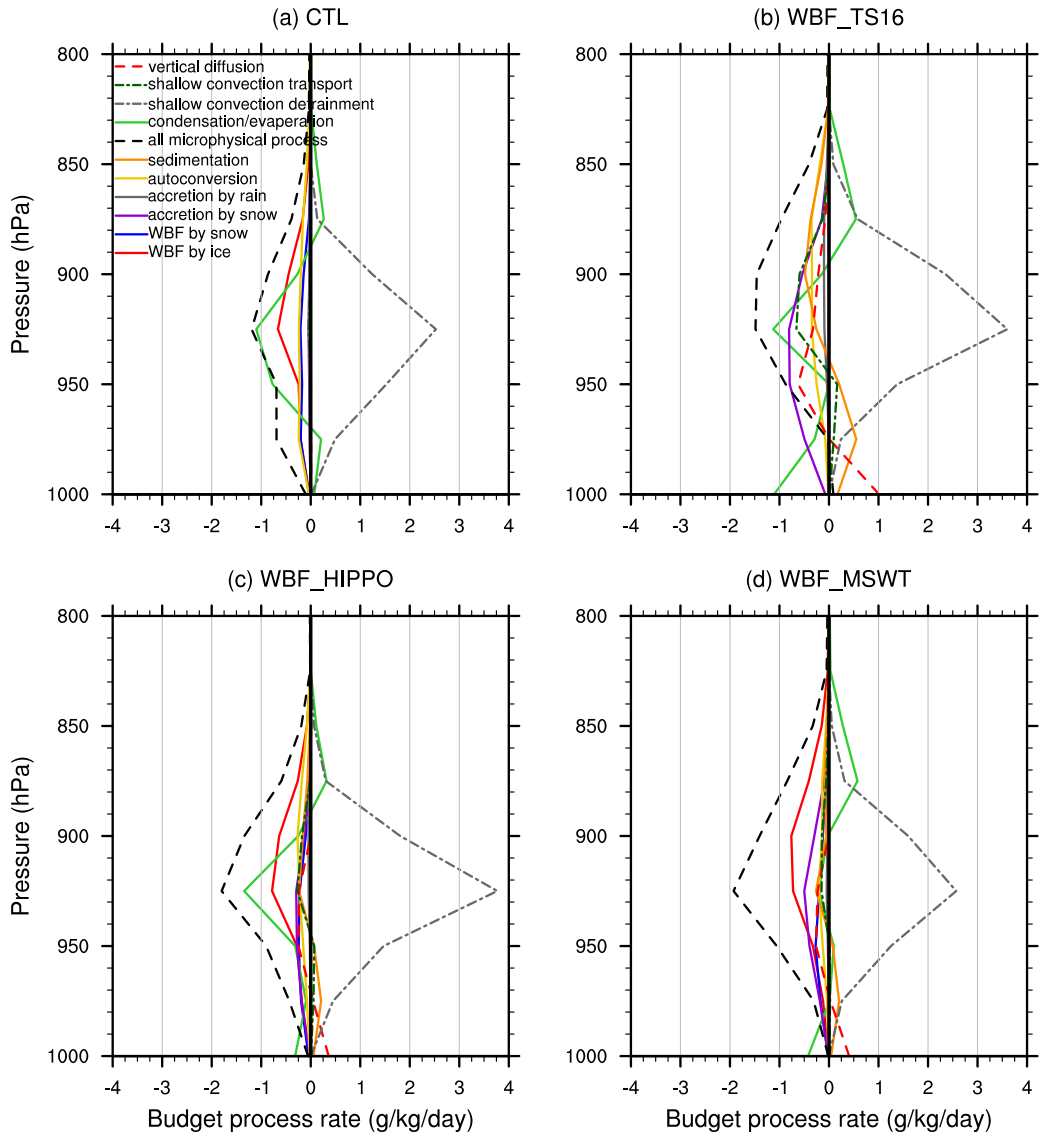

Figure 3.13. Process tendency budgets associated with cloud liquid water mass mixing ratio. Cloud microphysical processes, condensation/evaporation from cloud macrophysics, and other physical processes from shallow convection and PBL turbulence schemes are included. Tendencies from CTL and three sensitivity experiments are averaged between 9-13 October 2004. (Reprinted from Zhang, Liu et al., (2019).)

Figure 3.13 compares process tendencies of simulated cloud liquid water mass mixing ratio between CTL and sensitivity experiments. We include cloud microphysical processes, liquid condensation from cloud macrophysics, detrainment and transport from shallow convection, as well as transports via PBL turbulence in the tendency budgets. As shown in Figure 3.13, detrainment of cloud liquid from shallow convection dominates the liquid water source in all simulations. Liquid condensation also plays an important role near the cloud top (850-900 hPa). Evaporation in cloud macrophysics and several microphysical processes are responsible for the loss of liquid water mass mixing ratio. For example, in CTL (Figure 3.13a), WBF process with respect to ice and snow is the major sink to transfer cloud liquid into ice phase in mixed-phase clouds. Large changes are found in process tendencies in three sensitivity experiments. Compared to CTL, the WBF process is substantially reduced in WBF_TS16. However, accretion of liquid by snow, as well as vertical diffusion by PBL turbulence and shallow convection transport become more efficient to consume available liquid. Increased liquid water sinks through vertical diffusion and shallow convection transport are the result of interactions between cloud microphysics and other physical parameterizations. On the other hand, stronger detrainment of cloud liquid from shallow convection leads to larger amounts of LWC in WBF_TS16. For WBF_HIPPO and WBF_MSWT, although the WBF process indicates small differences compared to CTL, other processes show noticeable changes. For instance, compensating source from accretion by snow offsets the decreased sink of WBF process. Note that, based on the heterogeneous distribution between liquid and ice, the probability of accretion of liquid droplets by snow particles should also be reduced.

Therefore, the increase of accretion process implies that the heterogeneous spatial distribution of cloud hydrometeors is not reflected consistently throughout microphysical processes. A sensitivity test will be conducted in section 3.4.4 to illustrate the effect of a consistent treatment on simulated mixed-phase clouds.

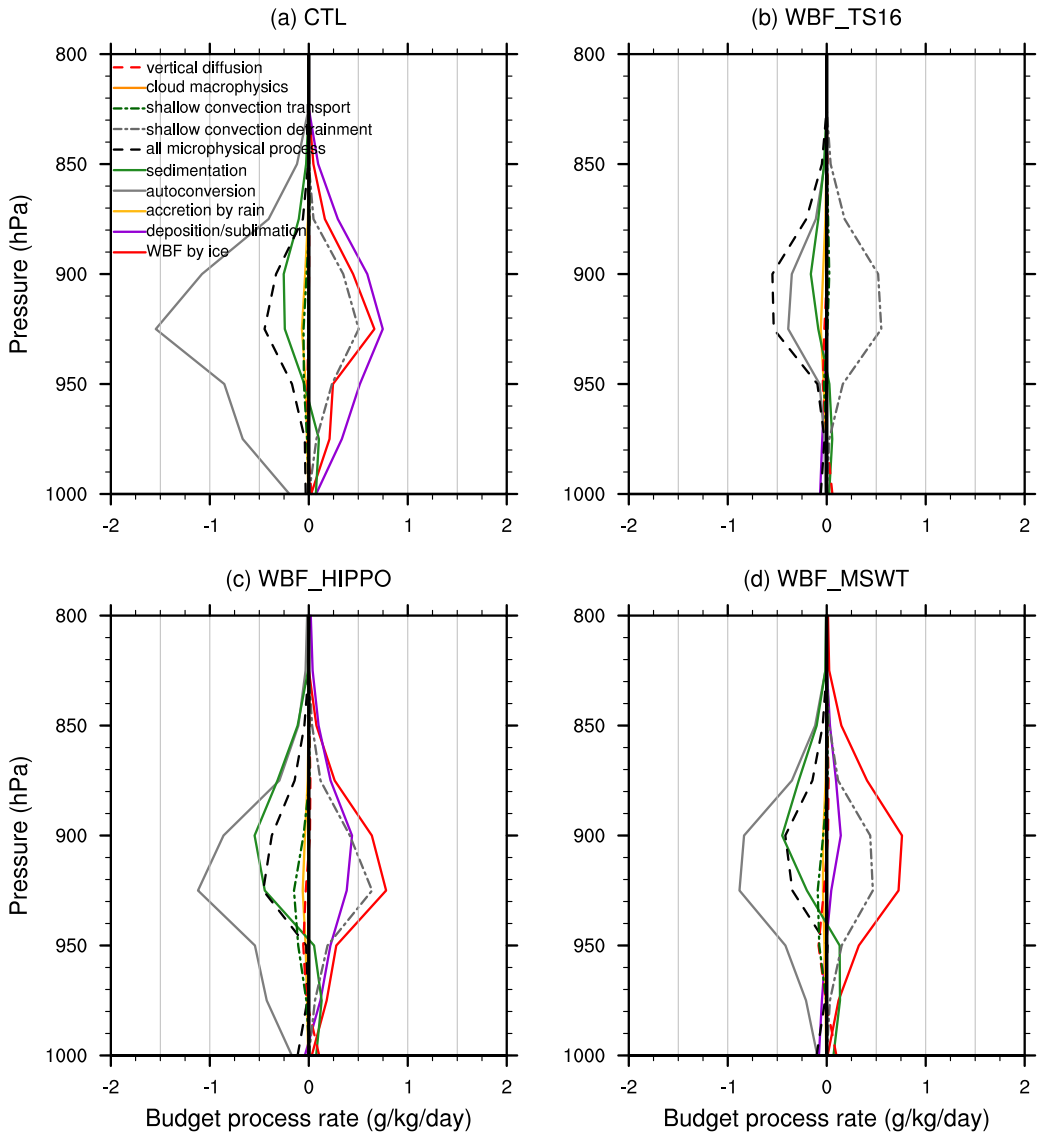

Figure 3.14. Same as Figure 3.13, but for cloud ice physical processes. (Reprinted from Zhang, Liu et al., (2019).)

Figure 3.14 shows the budget of process tendencies for cloud ice water mass mixing ratio. In general, there are three major sources contributing to cloud ice in CTL. WBF process at the expense of liquid water, ice depositional growth at the expense of

water vapor, and detrainment of cloud ice from shallow convection produce the majority of IWC in examined mixed-phase clouds. Note that the WBF process and ice depositional growth at the expense of water vapor are parameterized as two separate microphysical processes in the MG microphysics. The WBF process consumes available liquid water that coexists with cloud ice, whereas the ice deposition is calculated after all cloud liquid has been removed within one time step. Thus, the indication of ice deposition infers whether liquid droplets is completely or partially consumed in the model.

Comparing three sensitivity experiments to CTL, Figure 3.14 shows that the WBF process and ice deposition are completely inhibited in WBF_TS16; and the depositional growth of ice particles is also decreased in WBF_HIPPO and WBF_MSWT. These features imply that the occurrence of partial removal of cloud liquid becomes more frequent when WBF process is modified. Meanwhile, because of the fast autoconversion of cloud ice to snow, snow water plays an important role in solid phase cloud hydrometeors. Large amounts of cloud ice particles are converted to snow in CAM5 and induce efficient collection of liquid droplets and rain drops. As shown in Figure 3.15, with increased LWC in WBF_TS16, accretion of liquid and collection of rain by snow are largely enhanced. These explain the little sensitivity of IWC/IWP to perturbations of WBF process discussed in previous sections.

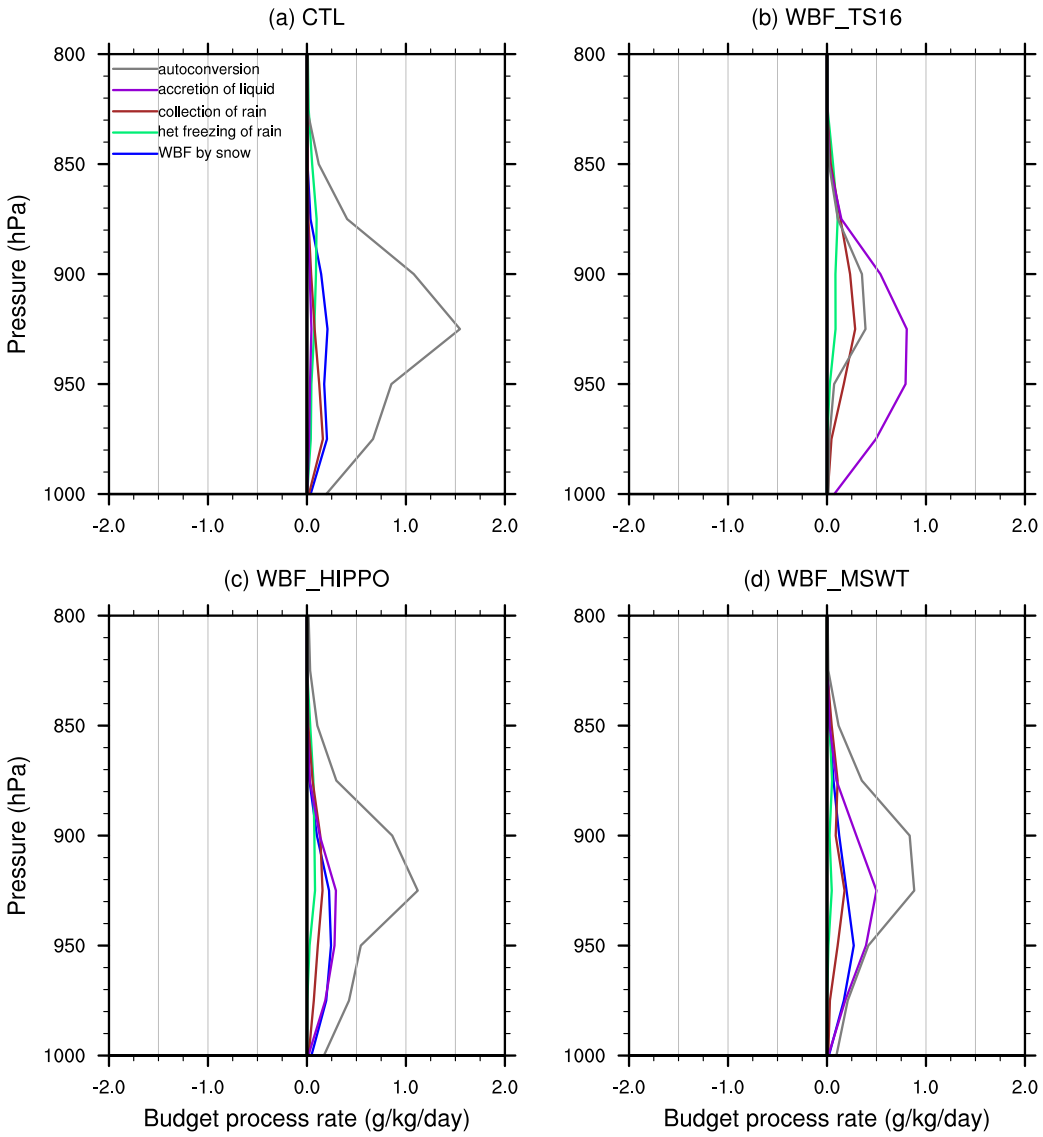

Figure 3.15. Same as Figure 3.13, but for snow water mass mixing ratio. (Reprinted from Zhang, Liu et al., (2019).)

3.4.4. Sensitivity experiments with accretion and model vertical resolution

As mentioned in earlier sections, a consistent representation of heterogeneous structure in all parameterizations is critical for mixed-phase clouds. In this section, the

consistent treatment as in WBF_TS16 is applied to accretion of liquid droplets and rain drops by snow particles. Because WBF_TS16 is equivalent to slowing down the WBF process by a factor of 10^6, a same perturbation factor is applied to accretion processes related to snow. This sensitivity experiment is defined as WBF_TS16_ACC in Table 3.1.

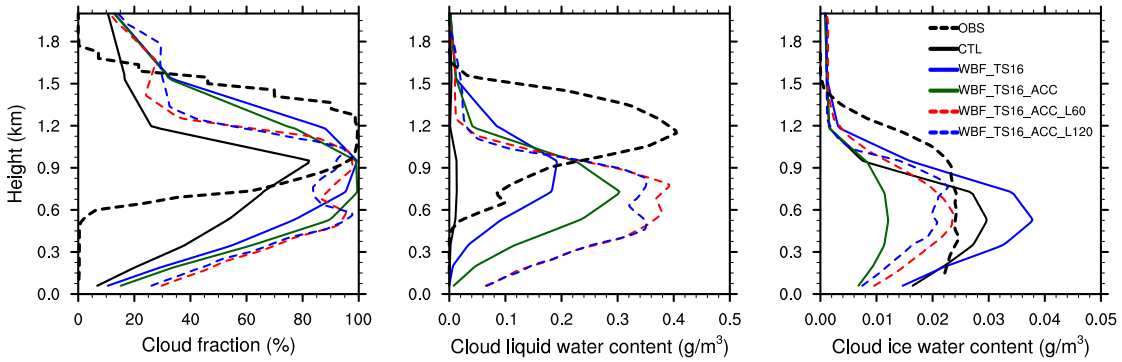

Figure 3.16. Vertical profiles of cloud fraction (left), cloud liquid water content (middle), and cloud ice water content (right) averaged between 1200 UTC 9 October and 1200 UTC 10 October during M-PACE. Cloud fraction observations are from ARSCL, and LWC and IWC profiles are retrieved by Shupe et al. (2008). Solid black lines represent the SCM CTL, solid blue lines for WBF_TS16, and solid green lines for WBF_TS16_ACC. Dashed lines are for sensitivity experiments with different vertical resolutions, as red for 60 vertical layers and blue for 120 vertical layers. (Reprinted from Zhang, Liu et al., (2019).)

Figure 3.16 shows the vertical profiles of cloud fraction, LWC, and IWC averaged between 9 and 10 October during the M-PACE field campaign. Despite the minimal change in cloud fraction and cloud boundaries (base and top height), one interesting feature is that LWC profiles simulated by WBF_TS16_ACC becomes

substantially larger than WBF_TS16 (increase by 150%). The overestimated IWC in WBF_TS16 is also alleviated.

Barrett et al. (2017b) demonstrated that vertical resolution is imperative for model to well maintain liquid water layers in simulated mixed-phase clouds. Therefore, we perform two additional experiments (WBF_TS16_ACC_L60 and WBF_TS16_ACC_L120 in Table 3.1) to test the impact of increasing vertical resolution. With vertical resolution increased to 60 and 120 layers, respectively, these two sensitivity experiments ultimately reproduce comparable LWC and IWC to ground-based remote sensing observations (Figure 3.16). Therefore, we conclude that consistent treatments in all cloud microphysical processes are important to represent the heterogeneous distribution between cloud hydrometeors. Fine vertical resolution also helps to better resolve structures of macrophysical and microphysical properties in Arctic mixed-phase clouds.

3.5. Discussion and conclusion

In this chapter, three different assumptions are incorporated to the WBF process to represent heterogeneous distribution between liquid droplets and ice crystals in mixed-phase clouds in CAM5. The examined assumptions are: (1) a partial homogeneous mixture within observed mixed-phase clouds during the HIPPO field campaign; (2) an idealized pocket structure of pure liquid and pure ice on the size of 100 m, uniformly distributed in model grids; and (3) a mass-weighted water vapor mass mixing ratio to replace the saturated environment with respect to liquid. The response of

Arctic mixed-phase cloud properties to the WBF process perturbation is investigated in both SCM and global CAM5 simulations. Model results are evaluated with ARM ground-based remote sensing retrievals at the Arctic Utqiaġvik site.

Model results illustrate that WBF process becomes less efficient after introducing our modifications. The mass growth of ice and snow at the expense of cloud liquid is then largely decreased. For the M-PACE case study, simulated amount of mixed-phase cloud LWC and the maintenance of cloud liquid layer are substantially improved compared to the default simulation. A better phase partitioning feature is achieved in simulated Arctic mixed-phase clouds, being more comparable to observations. The change of model simulated liquid phase is found to be linearly proportional to perturbation factors applied in the WBF process calculation. Comparing WBF_TS16 to WBF_HIPPO and WBF_MSWT, a larger LWC increase is associated with a stronger reduction in the WBF process rate. Despite the remaining low bias in liquid phase, simulated cloud phase partitioning is most comparable to observations in WBF_TS16. However, simulated IWC/IWP indicates less sensitivity to modified WBF treatments.

In terms of the influence on cloud seasonality, low-level mixed-phase clouds are more frequently simulated at the NSA Utqiaġvik site in boreal spring and fall, and the frequency of occurrence is underestimated during summertime in three sensitivity nudging simulations. Modeled CTT and SLF also exhibit improvements and the high bias of IWP in mixed-phase clouds is alleviated, especially for boreal summer. Among the three sensitivity experiments, WBF_TS16 shows the most prominent SLF increase. Furthermore, with perturbed WBF process, the temperature dependence of IWP on CTT

is better simulated in CAM5, implying the importance of accurate WBF process treatment in regulating ice phase microphysics.

Through a budget analysis of process tendencies, we find that detrained liquid water from shallow convection is enhanced using modified WBF process. This explains the LWC increase in sensitivity experiments and it is the result of interactions between cloud microphysics and other physical processes. One conclusion we draw from the budget analysis is that the occurrence of total removal of liquid water become less frequent with modified WBF process. This is reflected by the smaller tendency of ice depositional growth of ice particles at the expense of water vapor in WBF_HIPPO and WBF_MSWT. Another interesting pattern in our budget analysis is that other ice phase related processes, such as accretion of liquid droplets and rain drops by snow particles, are largely enhanced, even though the WBF process being substantially inhibited. The increased microphysical processes compensate the smaller growth of IWC due to reduced WBF process, and this is mainly responsible for the little sensitivity of IWC and IWP to WBF process change. Based on WBF_TS16, we further apply a consistent factor to accretion processes by snow. Sensitivity simulations show a much more comparable LWC and IWC vertical profiles to observations. We therefore note the importance of a consistent treatment in all microphysical process regarding the representation of cloud heterogeneity in GCM. Moreover, consistent to Barrett et al. (2017b), we also find that finer vertical model resolution can help to better maintain liquid layer in simulated mixed-phase clouds.

Learned from three different assumptions in our sensitivity experiments, the WBF process in current CAM5 is so efficient that cloud liquid water cannot be well preserved in mixed-phase clouds. Thus, we advocate that a physically based representation of heterogeneous distribution between liquid and ice, rather than a tunable parameter, will help to improve the simulated mixed-phase cloud phase partitioning. By representing the outcome of such a heterogenous pattern, improved cloud microphysics should better represent what actually happens in real clouds. Since large biases exist in large-scale moisture forcing, future work is encouraged to address a similar question but in a less-biased forcing framework. On the other hand, previous studies show that other mechanisms, such as changes in ice particle size distribution (Harrington et al., 1999; Jiang et al., 2000; Morrison & Pinto, 2006; Pinto, 1998; Solomon et al., 2009), changes in ice nucleation (Fridlind et al., 2012; Xie et al., 2013), and influence from turbulence (Furtado et al., 2016), can also be responsible for decreasing (increasing) sinks (sources) of supercooled liquid water in modeled mixed-phase clouds. Those processes require further understanding to purse an accurate parameterization in GCMs and to reduce the uncertainty in model simulation of high-latitude mixed-phase clouds.

CHAPTER IV

UNDERSTANDING CHANGES IN SIMULATED PHASE PARTITIONING OF SINGLE-LAYER ARCTIC MIXED-PHASE CLOUDS IN THE E3SMV1 DEVELOPMENT*

4.1. Background

As introduced in Chapter II, the U.S. DOE E3SMv1 model was developed based on the NCAR CESM1 with a number of significant modifications in model physics parameterizations. In previous evaluation work about EAMv1, it has been found that simulated mixed-phase cloud phase partitioning (i.e., SLF) changes substantially compared to CAM5. For example, over the Southern Ocean, Zhang, Xie et al. (2019) showed that EAMv1 simulated SLF is substantially larger than CAM5 at temperatures colder than -13℃. Compared to satellite retrievals, simulated liquid phase cloud fraction is largely overestimated, and the model underestimates ice phase cloud fraction between temperatures -20℃ and -30℃ in both hemispheres. Such model behaviors contradict results in CAM5 revealed by Kay et al. (2016). The large difference in simulated mixed-phase clouds leads to a smaller bias in shortwave cloud radiative effect in EAMv1 (Rasch et al., 2019). Zhang, Xie et al. (2019) attributed the increased liquid phase clouds from CAM5 to EAMv1 mainly to a slower WBF process, caused by an artificial slowing

*Reprinted with permission from "Toward Understanding the Simulated Phase Partitioning of Arctic Single-Layer Mixed-Phase Clouds in E3SM" by Meng Zhang, 2020. *Earth and Space Science*, 7, e2020EA001125, Copyright 2020 by AGU.

down factor of 0.1. However, SLF bias relative to the observation remains, even after the tuning parameter being removed. Thus, the remaining discrepancy implies that mixed-phase cloud phase partitioning is also influenced by changes in other cloud physics schemes.

Xie et al. (2018) summarized the effect of changes in cloud physics scheme on simulated cloud climatology during the EAMv1 development. In general, there are three major changes in schemes associated with mixed-phase cloud regime. First, EAMv1 replaces the temperature dependent Meyers et al. (1992) ice nucleation scheme with the CNT scheme for mixed-phase clouds (Hoose et al., 2010; Wang et al., 2014). Immersion/condensation, deposition, and contact freezing of supercooled liquid droplets are now linked to aerosol properties. Second, a simplified high-order turbulence closure scheme (CLUBB) is used to unify the treatment of processes in PBL turbulence, shallow convection, and cloud macrophysics (Golaz et al., 2002; Larson, 2017; Larson & Golaz, 2005). As detrained cloud condensate from shallow convection can participate in the growth of liquid droplets and ice particles in stratiform clouds, the introduction of CLUBB can influence modeled mixed-phase cloud properties. Third, EAMv1 is updated to the second version of two-moment stratiform cloud microphysics scheme (MG2) (Gettelman & Morrison, 2015). The accretion of liquid droplets by raindrops becomes dominant over the liquid-to-rain autoconversion, which is more comparable to cloud-resolving model simulations (Gettelman et al., 2015).

In this chapter, we aim to understand how these three changes of cloud physics parameterization would impact the EAMv1 simulated mixed-phase clouds. We will

conduct a process-level analysis, with a particular focus on single-layer mixed-phase clouds in high Arctic.

4.2. Model experiments

EAMv1 provides the flexibility to switch model parameterizations between newly incorporated schemes and their precursors in CAM5. Therefore, we can understand which physics parameterization change is most responsible for the model behavior change in simulated mixed-phase clouds. Table 4.1 lists the control and three sensitivity experiments for this study. To exclude the effect of artificial tuning on the WBF process mentioned earlier, CTL simulation keeps every setting the same as default EAMv1, except modifying the slowing down factor "berg_eff_factor" from 0.1 to 1.0. The first sensitivity experiment (MEYERS) is based on CTL, but we further switch the CNT ice nucleation scheme to the Meyers scheme that were used in CAM5. By comparing CTL to MEYERS in the analysis, the effect of heterogenous ice nucleation on changes in simulated mixed-phase cloud properties can be identified. The second experiment (UW) uses the University of Washington shallow convection, PBL turbulence, and cloud macrophysics schemes to replace the CLUBB parameterization. The difference between CTL and UW simulations reveals the effect of CLUBB on mixed-phase clouds. Lastly, UW_MG1 experiment is designed from the UW experiment, but we further switch the MG2 microphysics to MG1. The role of updated cloud microphysics can then be examined via understanding the difference between UW_MG1 and UW experiments.

Table 4.1. *Summary of Physical Parameterizations in EAMv1 Simulations (Reprinted from Zhang et al., (2020))*

Experiment	Configurations	Note
CTL	Parameter "berg_eff_factor" change to 1.0	Same as default EAMv1, but use the value 1.0 for the parameter that controls the WBF rate.
MEYERS	Same as CTL, but replace the CNT ice nucleation scheme (Wang et al., 2014) with Meyers et al. (1992)	Examine the effect of heterogeneous ice nucleation. Note that the Meyers scheme generally produces higher INP number concentrations than CNT.
UW	Same as CTL, but replace CLUBB with the CAM5 UW shallow convection, PBL turbulence, and cloud macrophysical schemes (Park and Bretherton, 2009; Bretherton and Park 2009; Park et al. 2014)	Examine the effect of CLUBB.
UW_MG1	Same as UW, except using the MG1 microphysics	Examine the effect of updated cloud microphysics.

For each experiment shown in Table 4.1, a series of 3-day hindcasts are initialized between 30 September 2004 and 31 October 2004 to cover the M-PACE field campaign. Large-scale states are described by the ECMWF ERA-Interim reanalysis (Dee et al., 2011). To avoid the spin-up issue, day-2 (24 – 48 hr) hindcast results are analyzed. We extract model outputs on the land grid that is closest to the ARM NSA Utqiaġvik site to validate hindcast simulations.

4.3. Results

4.3.1. Modeled cloud properties

EAMv1 short-term hindcast simulations are evaluated with multiple observations in the M-PACE field campaign. Figure 4.1 shows the time-pressure cross sections of occurrence of frequency between simulated and ARSCL retrieved clouds. Same observed cloud patterns are shown here as in Chapter III. We hence focus on the discrepancy of simulated cloud fraction against observations and the differences between different sensitivity experiments.

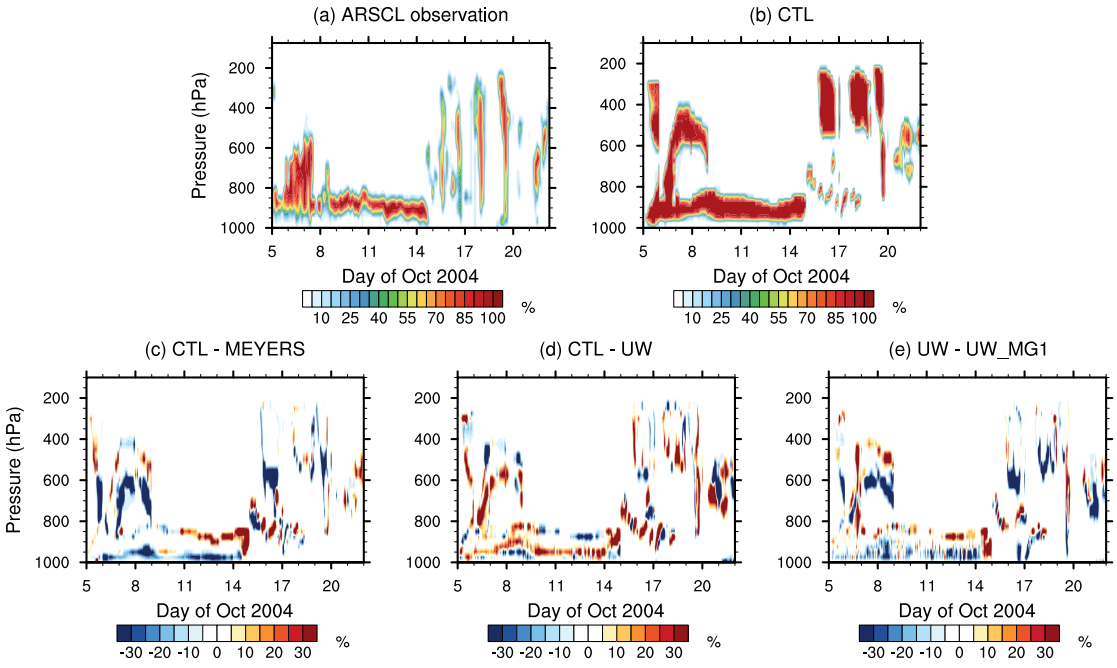

Figure 4.1. Time-pressure cross sections of cloud fraction at the NSA Utqiaġvik site during the M-PACE field campaign. (a) is observed frequency of occurrence of clouds from the ARSCL algorithm. (b) is simulated cloud fraction from CTL. (c)-(e) are the differences in simulated cloud fraction between CTL and MEYERS (c), CTL and UW

(d), and UW and UW_MG1 (e). Unit: %. Note that CTL utilizes CLUBB, MG2, and CNT parameterizations, while three sensitivity experiments have changes of Meyers et al. (1992) ice nucleation (MEYERS), UW shallow convection, PBL turbulence, and cloud macrophysics parameterizations (UW), and both UW schemes and MG1 cloud microphysics (UW_MG1), respectively. (Reprinted from Zhang et al., (2020).)

Compared to observed clouds, CTL hindcast well simulates the temporal evolution of multilayer (5-8 October) and single-layer clouds (9-14 October), as well as deep frontal clouds (16-20 October). The better model performance here than SCAM5 can be the result of more reasonable large-scale atmospheric circulations (e.g., wind, temperature, and moisture) prescribed in hindcast simulations. Simulated cloud fraction is close to 100% in CTL, which is slightly larger than observations. Moreover, low biases are found in simulated cloud base, defined as the lowest level with non-zero cloud fraction.

Compared to CTL, cloud boundaries in sensitivity experiments indicate noticeable sensitivity to the parameterization change. For example, changing ice nucleation scheme from Meyers to CNT during EAMv1 development leads to the higher cloud top and cloud base, suggesting a more comparable cloud structure to observations (Figure 4.1c). Meanwhile, it is shown in Figure 4.1d that the use of CLUBB parameterization decreases both cloud base and cloud top heights. Because cloud fraction is determined via relative humidity in UW cloud macrophysics scheme (Park et al., 2014), the more decoupled clouds from surface in UW experiments can be largely explained by the drier atmosphere near surface (figure not shown). By comparing UW to UW_MG1, MG2 cloud microphysics also improves simulated cloud layer height.

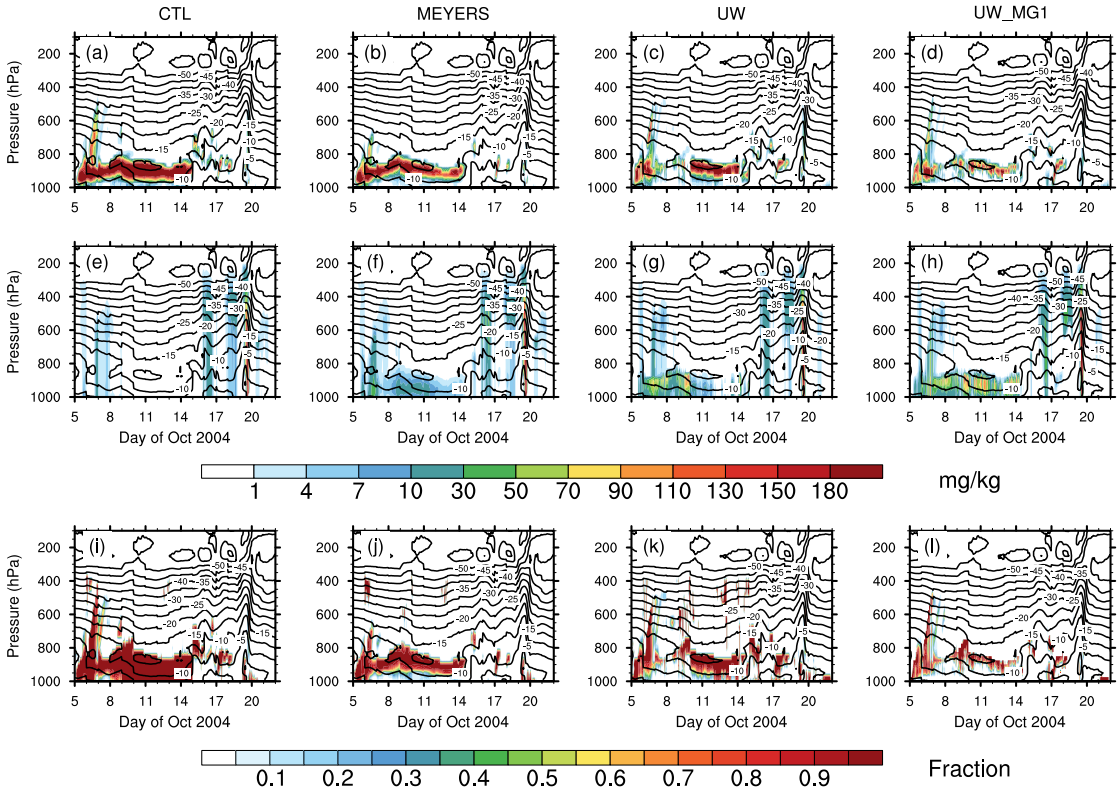

Figure 4.2. Time-pressure cross sections of simulated total cloud liquid water mass mixing ratio (including rain water mass; upper panel), total cloud ice water mass mixing ratio (including snow water mass; middle panel), and supercooled liquid fraction (lower panel) during the M-PACE field campaign from CTL, MEYERS, UW, and UW_MG1 (from left to right). (a)-(d) are for cloud liquid water, (e)-(h) are for cloud ice water mass, and (i)-(l) are for supercooled liquid fraction. Contours represent the ambient temperature in the unit of °C. (Reprinted from Zhang et al., (2020).)

Although the overall cloud structure is well reproduced for the M-PACE field campaign, substantial differences are found in simulated LWC and IWC with different combinations of model schemes. Figure 4.2 shows time-pressure cross sections of LWC, IWC, and SLF in CTL and three sensitivity experiments. Same as the analysis in Chapter III, rain and snow water mass mixing ratios are added to LWC and IWC, respectively. One unexpected feature we found in Figure 4.2 is the over-dominant supercooled liquid

water in CTL simulated single-layer boundary-layer mixed-phase clouds between 8 and 14 October. IWC is negligible in single-layer clouds at temperatures -14℃, while IWC remains profound for multilayer and deep clouds. Such model behavior in single-layer mixed-phase clouds is in substantial contrast to previous M-PACE results in CAM5 (as shown in section 3.4.1, and also in Liu et al., 2011; Xie et al., 2008, 2013). With artificial tuning parameter having been removed in WBF process, the underestimated IWC is most likely result from the low bias in ice particle formation in mixed-phase cloud microphysics. Due to the small amount of IWC, SLF is found to be close to 1 throughout all cloud layers, especially in single-layer mixed-phase clouds (Figure 4.2i).

As shown in Figure 4.2, simulated cloud phase partitioning indicates large disagreements for single-layer low-level cloud period in different sensitivity experiments, but clouds are quite similar in all four experiments between 5-8 and 15-22 October. Therefore, in the following sections, we will provide an in-depth evaluation and analysis for the model response to changes in model schemes, focusing on single-layer low-level mixed-phase clouds during 8-14 October.

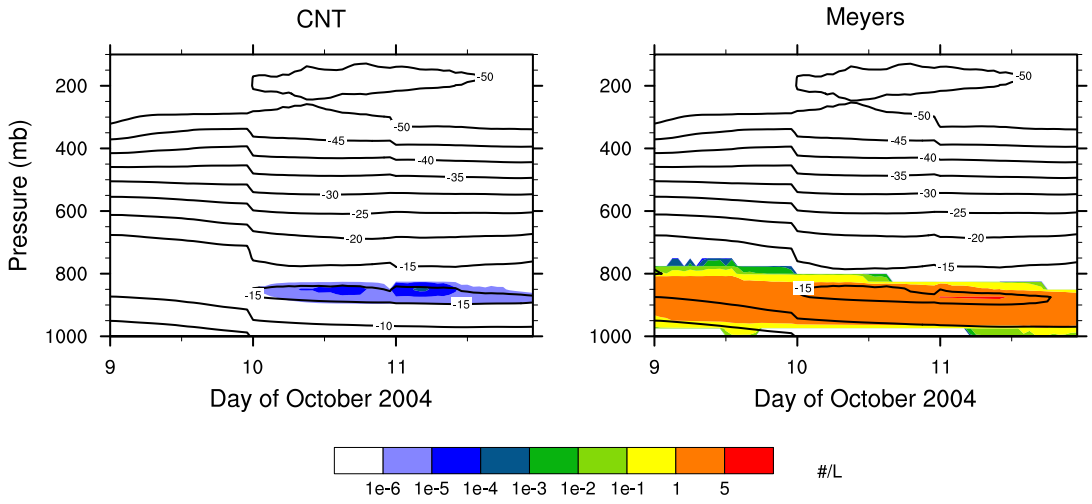

Figure 4.3. Simulated number concentration of ice nucleating particles between 9 and 11 October during the M-PACE. Left panel is from CNT ice nucleation, and Meyers scheme is shown in the right panel. Contours represent the ambient temperature in the unit of °C.

Compared to CTL, larger IWC is generated in MEYERS experiment. This reveals that the use of CNT ice nucleation scheme in EAMv1 leads to lower IWC in mixed-phase clouds. Figure 4.3 shows the simulated INP number concentration between 9-11 October, and we find the CNT ice nucleation forms 4-5 orders of magnitude lower INP concentration than Meyers scheme at temperatures warmer than -15℃. Consistent results were found in earlier studies (DeMott et al., 2010; Shi & Liu, 2019). In addition, CLUBB and MG2 parameterizations are also found to play important roles to reduce IWC, as comparing CTL to UW and UW to UW_MG1 experiments, respectively. Even though the sequence of updating number concentration of liquid droplets due to activation has been changed in MG2, the difference shown between UW and UW_MG1 is mainly due to the higher liquid to rain accretion rate. Conversion from liquid to ice

becomes less efficient as more liquid being collected by raindrops. In three sensitivity experiments, simulated SLF corresponds well to LWC. The dominance of liquid water becomes less profound in simulated single-layer mixed-phase clouds when Meyers ice nucleation, UW schemes, and MG1 cloud microphysics are utilized.

Consistent with the lack of total IWC and low INP number concentration, very small amounts of cloud ice particles ($< 0.01\ L^{-1}$) are generated in CTL during our examined single-layer period (Figure 4.4). It is clear that three updated cloud physics schemes in EAMv1 (i.e., CNT, CLUBB, MG2) substantially reduce simulated ice particle number concentrations. Among three schemes, the impact from CLUBB and MG2 tends to be stronger than CNT.

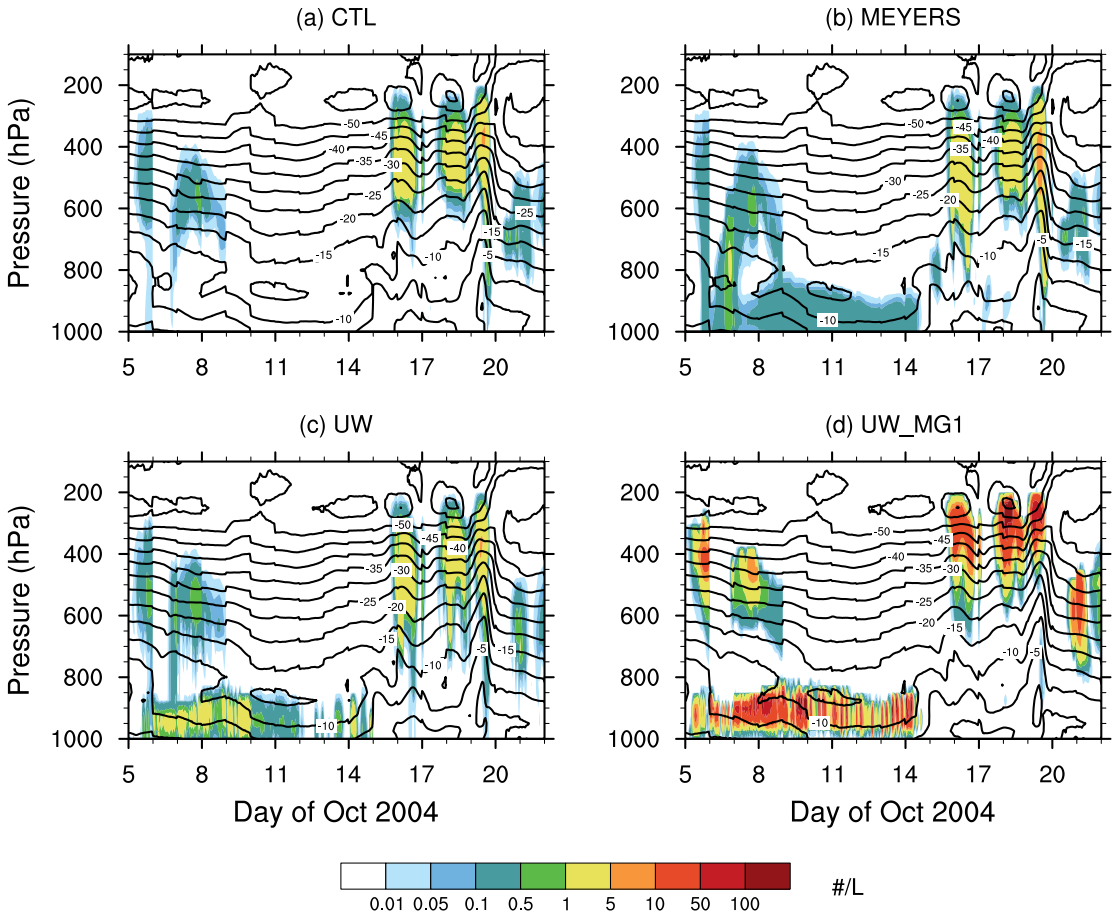

Figure 4.4. Time-pressure cross sections of simulated grid mean cloud ice number concentrations for the M-PACE. (a) CTL, (b) MEYERS, (c) UW, and (d) UW_MG1. Contours represent the ambient temperature in the unit of °C. (Reprinted from Zhang et al., (2020).)

To quantitatively estimate the underestimation of cloud ice in EAMv1, Figure 4.5 compares the LWP and IWP from day-2 hindcast results against the ACRED dataset. Four EAMv1 experiments are shown in different color lines, and markers represent different retrieval products in ACRED. Note that we only focus on the single-layer stratiform mixed-phase clouds here (9 to 15 October). One interesting result from Figure

4.5 is that CTL simulated IWP is underestimated by 3-4 orders of magnitude, despite the comparable LWP to ground-based observations. Comparing CTL to MEYERS and UW, we find that uses of the CNT ice nucleation scheme and CLUBB increase LWP but generate less IWP for examined single-layer mixed-phase clouds. More LWP and less IWP are also produced with the introduction of MG2 cloud microphysics when UW is compared with UW_MG1. Furthermore, compared to CTL, UW_MG1 substantially decreases LWP and increases IWP in simulated single-layer clouds. We note that when Meyers ice nucleation is further used in mixed-phase cloud regime in UW_MG1, the phase partitioning pattern becomes more comparable to previous CAM5 studies (not shown). The similarity between UW_MG1 and CAM5 demonstrates that changes in dynamic core, vertical and horizontal resolutions, and model tuning to achieve the TOA radiative balance should not be the main reason for the largely underestimated IWC/IWP found here, but the low bias is more related to changes in physics parameterizations.

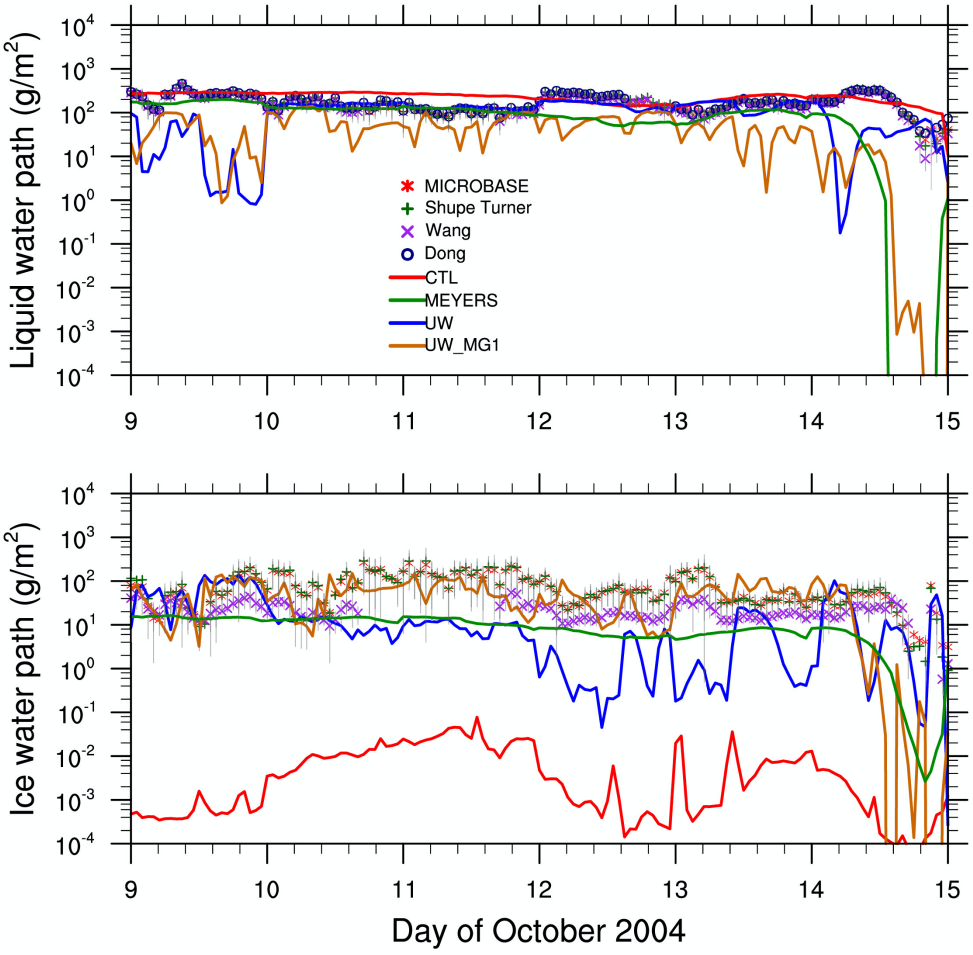

Figure 4.5. Time series of LWP (including rain; upper panel) and IWP (including snow; lower panel) from the EAMv1 and the ARM ACRED dataset between 9-15 October. CTL is presented by red line, MEYERS by green line, UW in blue line, and UW_MG1 in brown line. For the ACRED dataset, grey lines represent one standard deviations for each data point. (Reprinted from Zhang et al., (2020).)

Figure 4.6 compares the distribution of EAMv1 simulated SLF as a function of normalized cloud height against in-situ measurements onboard the UND Citation aircraft. Aircraft observations were processed by McFarquhar et al. (2007). In-situ data obtained on 9, 10, and 12 October during the M-PACE field campaign were used to

validate vertical structures of microphysical properties (e.g., LWC and IWC) in single-layer mixed-phase clouds. Note that cloud altitude is normalized between 0 and 1, where 0 and 1 referring to cloud base and cloud top, respectively. In this figure, simulated clouds from hindcasts are defined as total water mass mixing ratios larger than 0.001 g kg^{-1}.

Figure 4.6a shows that observed SLF increases with normalized cloud height, and it is larger than 80% at cloud top. Cloud ice tends to dominate in the lower cloud layers, with SLF smaller than 40%. This cloud structure pattern is persistent throughout three-day observations. It is obvious in Figure 4.6b that CTL substantially overestimates SLF in single-layer mixed-phase clouds. Simulated SLF in 9, 10, and 12 October is approximately 100% all the time. This is expected as IWC is nearly missing during examined time period. Compared to CTL, despite the underestimated SLF near cloud base, MEYERS better reproduces observed vertical distribution of SLF as a function of cloud height. The overestimated INP number concentration in Meyers ice nucleation scheme leads to higher ice number concentration, as well as the larger IWC than CTL, which explains the discrepancy between CTL and MEYERS. Compared to observations, the underestimated SLF near the surface in MEYERS can be the result of too much INP number concentration near cloud base. Meanwhile, the feature that SLF increasing with cloud height is captured by the use of UW schemes on 10 and 12 October, whereas such trend being poorly produced on 9 October. Note that 9 October is a transitional period in terms of large-scale environments. Surface temperature had decreased by ~5℃ until 9 October due to the cold air advection over the pack ice (Verlinde et al., 2007). The

difference, in terms of SLF patterns between 9 October and 10 and 12 October, can be result from the inadequate representation of this transition period in UW parameterizations. UW_MG1, in which MG2 is replaced by MG1, fails to reproduce the observed SLF feature, indicating that the use of MG2 microphysics improves the model behavior in single-layer mixed-phase cloud properties.

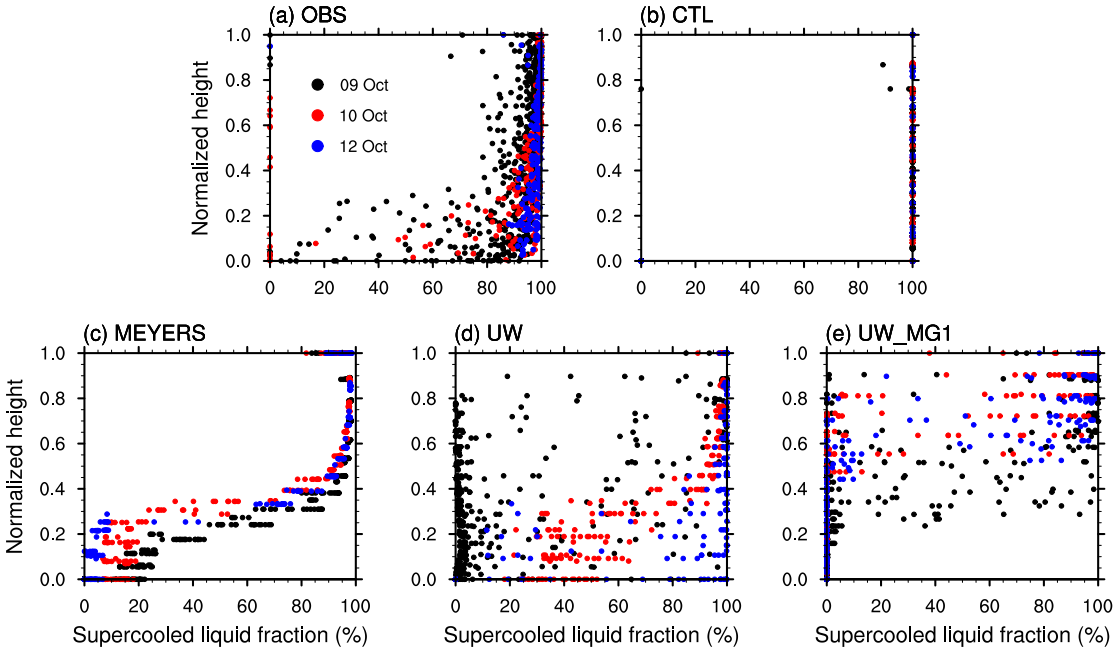

Figure 4.6. Distribution of supercooled liquid fraction as a function of normalized height in clouds. (a) In-situ measurements obtained from the University of North Dakota Citation aircraft (McFarquhar et al., 2007) on 9 October (black dots), 10 October (red dots), and 12 October (blue dots) during the M-PACE field campaign. (b)-(e) Results of model simulations from CTL, MEYERS, UW, and UW_MG1, respectively. Model results are sampled on 9, 10, 12 October which correspond to the same time period in measurements. (Reprinted from Zhang et al., (2020).)

4.3.2. Mass budget analysis

In this section, we will discuss detailed cloud microphysical process budgets for four hydrometeors – cloud liquid, cloud ice, rain, and snow – in single-layer mixed-phase clouds. Process tendency rates are integrated over the whole cloud layer and are averaged between 9-11 October using day-2 hindcast simulations. Our goal here is to understand which cloud process, due to scheme changes, plays the most important role in changes of simulated mixed-phase cloud properties. An in-depth discussion of how different parameterizations are interacted in the formation of cloud hydrometeors is provided in Zhang et al. (2018). In this study, only impacts of shallow convection, cloud macrophysics, ice nucleation, and cloud microphysics are investigated.

4.3.2.1. Impact of heterogenous ice nucleation

Figure 4.7 shows that liquid condensation constitutes the formation of cloud liquid condensates in both CTL and MEYERS. Note that liquid condensation is calculated from the assumed PDF function in CLUBB parameterization (Bogenschutz et al., 2012; Golaz et al., 2002). Although there are 4-5 orders of magnitude lower INP number concentration in CNT compared to Meyers ice nucleation scheme (Figure 4.3), minimal impacts are expected on the formation of cloud liquid water. Therefore, liquid condensation tendencies are comparable in both experiments.

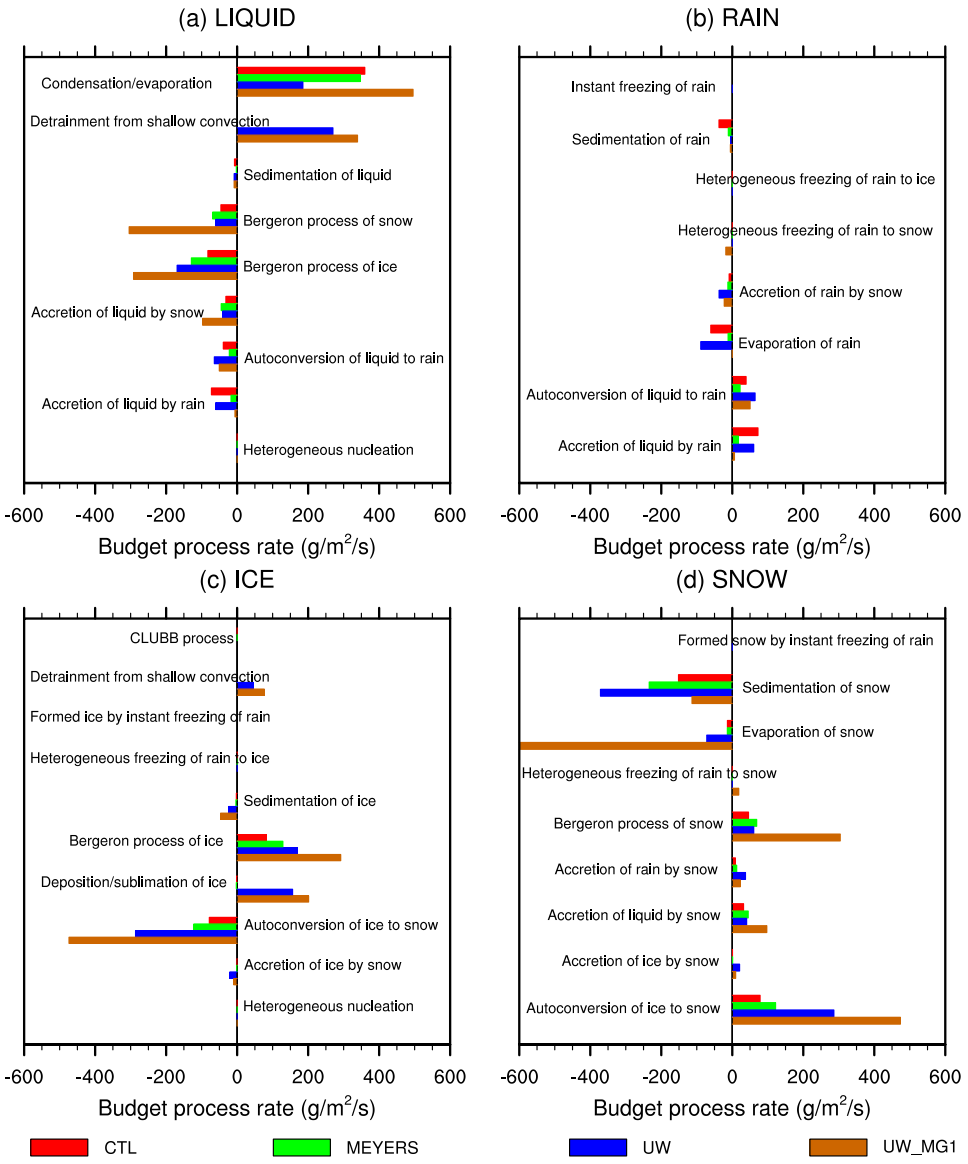

Figure 4.7. Budgets of vertically integrated cloud physical process tendencies of (a) cloud liquid, (b) rain, (c) cloud ice, and (d) snow hydrometeors from the short-term hindcast day-2 results. CTL is shown in red bars and MEYERS is in green bars. Blue bars represent UW, and brown bars for UW_MG1. The vertically integrated process rates are averaged over 3-day period between 9 and 11 October 2004 during the M-PACE field campaign. (Reprinted from Zhang et al., (2020).)

With a very small amount of INP generated in CTL, cloud ice mass growth processes are active at limited rates. For example, the loss of liquid water is weakly activated via WBF process with respect to ice and snow, as well as accretion by snow particles. Ice to snow autoconversion occurs efficiently, but snow particles tend to fall out of clouds and leave negligible total IWC in simulated mixed-phase clouds. This is the reason for underestimated ice in CTL during the M-PACE. Compared to CTL, larger ice phase associated process tendencies are shown in MEYERS. Besides the stronger WBF process, the enhanced ice nucleation also changes the pathway whether liquid droplets are collected by raindrops or snow particles. In MEYERS, the collection of liquid droplets by snow becomes more effective than that by rain, which is contrary to CTL. Here we highlight that the number concentration of ice particles, nucleated from primary ice production, is critical for Arctic single-layer low-level mixed-phase clouds. The heterogeneous ice nucleation is more important through its impact on cloud ice number concentration, rather than on mass mixing ratio. As shown in Figure 4.7a, the mass contribution from heterogenous ice nucleation is quite minimal, which is because of the small mass of newly formed ice crystals. Therefore, we believe that ice formation from CNT is too weak to trigger effective ice mass growth at temperatures warmer than -15℃. This partially explains why simulated IWC is largely underestimated in EAMv1 and why it is so different compared to CAM5.

4.3.2.2. Impact of CLUBB

Comparing UW to CTL, the role of CLUBB can be analyzed. In UW experiment, liquid condensation is calculated by cloud macrophysics (Park et al., 2014), and shallow convection is determined via Park and Bretherton (2009). This separated treatment makes cloud liquid water not only be condensed in saturated atmosphere with respect to liquid, but also be detrained from shallow convection. On the other hand, since CLUBB implicitly determines the total liquid production by integrating over the saturated portion of its PDF function, detrainment and condensation cannot be diagnosed separately in CTL.

Similar features are found for cloud ice budget as presented in liquid budget (Figure 4.7c). In UW, ice particles detrained from shallow convection together with ice nucleated from heterogeneous ice nucleation participate in the growth of ice mass mixing ratio in cloud microphysics. We emphasize the importance of initial ice (either from shallow convection detrainment or from heterogeneous ice nucleation) here, as one prerequisite for ice mass growth is the sufficient ice particles formed before the calculation of microphysical processes. As noted in section 2.1.2, ice phase process is currently not explicitly considered in CLUBB's PDF approach. Instead, ice mass mixing ratio is only treated via the turbulent transport in an eddy diffusion scheme; and such eddy diffusion transport is found relatively inactive in the examined mixed-phase clouds (included in CLUBB process in Figure 4.7c). Compared to UW, without the initial ice detrained from shallow convection, growth of total IWC becomes substantially weaker in CTL. For example, the WBF process with respect to ice and ice depositional growth at

the expense of water vapor largely contribute to the source of cloud ice mass mixing ratio in UW. However, ice deposition is never shown in CTL. As mentioned in section 3.4.3, ice deposition is a process after all liquid water being consumed at the expense of cloud ice. The indication of this ice deposition in UW implies that available liquid water has been completely removed at certain time step or at certain cloud layers. Furthermore, ice to snow autoconversion and the snow accretion of liquid droplets and raindrops are also enhanced in UW, which further attributes to the increased (decreased) IWC (LWC) in examined mixed-phase clouds

4.3.2.3. Impact of MG2

The effect of changing MG1 cloud microphysics to MG2 can be understood by examining UW and UW_MG1. It is shown in Figure 4.7 that MG2 microphysics largely decreases process tendencies such as the WBF process and snow accretion. We note that changes in process tendencies between UW and UW_MG1 are mainly attributed by the prognostic treatment of mass and number mixing ratios of rain and snow hydrometeors in MG2. Consistent with earlier studies, MG2 microphysics simulates a stronger accretion process than autoconversion to convert liquid droplets to raindrops. Although total IWC becomes smaller in UW than UW_MG1, no significant difference is found in major ice production mechanisms between these two experiments. For instance, same schemes are utilized for heterogeneous ice nucleation and shallow convection detrainment. Therefore, we believe the change in cloud microphysics should not be a major reason for the model behavior change during EAMv1 development. However, the

larger IWC in UW_MG1 is result from the stronger detrainment of ice particles from shallow convection. This later induces stronger growth of ice particles through microphysics. Nevertheless, noted by Gettelman et al. (2015), MG2 microphysics has a strong sensitivity to ice particle number. The change in initial ice number concentration thus has a stronger impact on cloud processes in MG2 than MG1.

4.3.3. Phase partitioning over the Southern Ocean

To evaluate the sensitivity of simulated mixed-phase cloud phase partitioning to heterogeneous ice nucleation and CLUBB over the Southern Ocean, we replot the Figure 8 in Zhang, Xie et al. (2019) and include a number of sensitivity experiments. Sensitivity simulations are performed for 2007 with nudging technique.

Figure 4.8 shows the simulated cloud SLF as a function of temperature. Orange solid and dashed lines are the same as in Zhang, Xie et al. (2019), which represent the EAMv1 simulations using default model configuration with and without the WBF process tuning factor. Compared to satellite observations (Hu et al., 2010), both experiments overestimate SLF at temperatures colder than -20℃ and they consistently produce a dented curving feature near -10℃. Using Meyers ice nucleation scheme, model simulated mixed-phase clouds underestimate SLF at any given temperatures between 0℃ and -40℃. Such a feature is similar to CAM5 simulation.

Revealed in our budget analysis of cloud ice water during the M-PACE field campaign, the lack of detrained ice from shallow convection in CLUBB substantially reduces the ice mass growth rate in cloud microphysics. In this section, we introduce a

modified treatment to CLUBB to determine the phase of condensed water from CLUBB based on temperature. This treatment was previously used in Park and Bretherton (2009) shallow convection scheme but has been deactivated in EAMv1. As shown in Figure 4.8, modified CLUBB parameterization (solid black line) improves the SLF simulation at temperatures below -20℃ and makes the model comparable to observations. However, biases can still be identified in warm temperature range. According to Kay et al. (2016) and Wang et al. (2018), changing the threshold temperature over which all detrained cloud condensate is liquid from 268 to 253 K can largely increase simulated SLF in CAM5. When the same change is introduced to CLUBB and deep convection scheme at the same time in EAMv1, it is interesting to notice that the curvature near -10℃ is much improved (dashed black line). Therefore, it is demonstrated that a modified treatment of detrainment process in CLUBB and deep convection facilitates a better mixed-phase cloud phase partitioning feature in EAMv1.

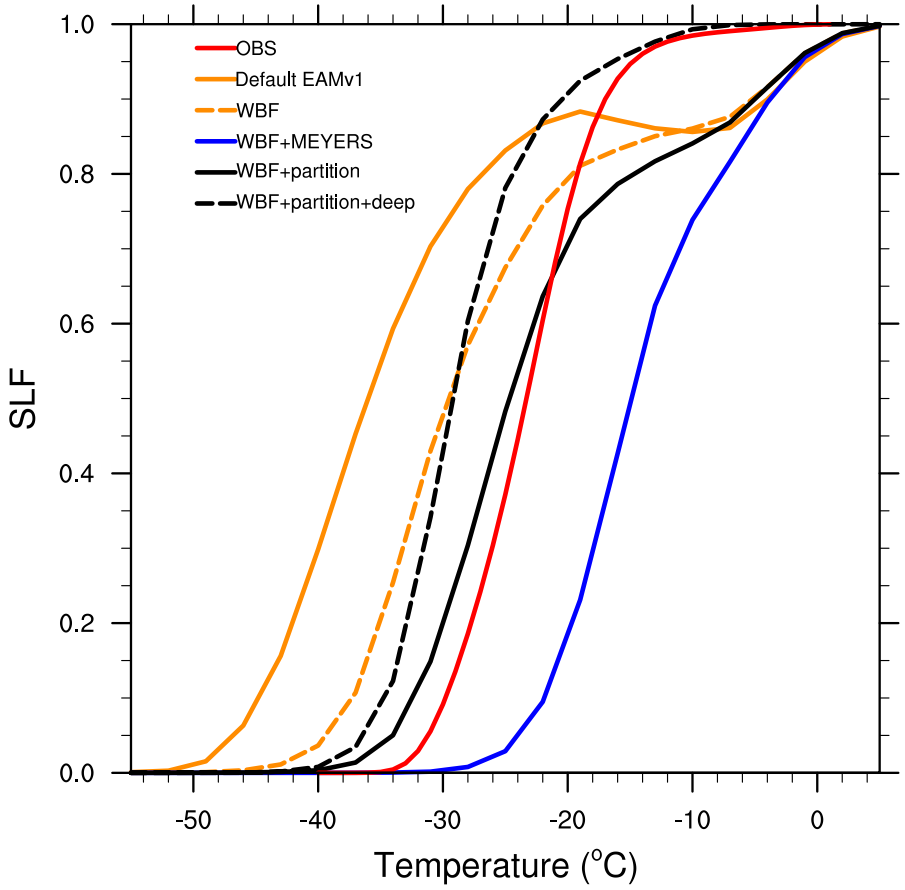

Figure 4.8. Simulated mixed-phase cloud SLF from EAMv1 sensitivity experiments as a function of temperature. SLF is averaged over the latitudes between 30°S and 80°S using one-year nudging model results. Red line represents observations from Hu et al. (2010). Orange solid line is the EAMv1 simulation with default model configuration and orange dashed line is EAMv1 model without the tuning factor on WBF process. Blue line shows the experiment using Meyers et al. (1992) ice nucleation scheme. Black solid line indicates the experiment incorporated with modified treatment of shallow convection detrainment in CLUBB, while black dashed line modifies the detrainment for both CLUBB and deep convection.

4.4. Summary and discussion

In this chapter, we perform short-term hindcast simulations to examine the model response to changes in physics parameterization. Three mixed-phase cloud associated

parameterizations, updated during the development of U.S. DOE EAMv1, are investigated to understand their impact on model behavior change in Arctic mixed-phase cloud properties relative to CAM5, which is the predecessor of EAMv1. We focus on single-layer low-level mixed-phase clouds during the M-PACE field campaign.

Hindcast results show that simulated total ice water mass mixing ratio is substantially lower than observations, also CAM5. Total liquid water, on the other hand, is slightly overestimated. Tracing back individual changes made in EAMv1 schemes, the CNT ice nucleation, CLUBB parameterization, and MG2 microphysics are found to lead to a reduced IWC during the examined cloud period. A detailed budget analysis of microphysical process tendency reveals that the production of initial ice particles plays an important role in ice mass growth. Heterogeneous ice nucleation and detrainment from shallow convection are largely responsible for the formation of ice particles that participate in microphysical processes, such as the WBF process and collision and coalescence between different hydrometeors. In the default EAMv1, when CNT and CLUBB are used to replace Meyers ice nucleation and UW schemes (i.e., shallow convection and cloud macrophysics) that were used in CAM5, a very small amount of initial ice is passed to cloud microphysics. Ice mass growth processes are then become less effective due to their strong sensitivity to ice particle number concentration. Because MG2 microphysics does not impact the formation of initial ice particles, we therefore conclude that change of MG2 should not be a primary cause for the underestimated IWC. The introduction of CNT and CLUBB is more important.

We note that, along with changing UW to CLUBB, the treatment of PBL turbulence has also been changed. However, in our short-term hindcast simulations, the difference of vertical updraft and potential temperature between CLUBB and UW schemes is not significant. Therefore, the change in PBL treatment should not contribute much to the phase partitioning change in mixed-phase clouds in this study.

We highlight that the issue examined here is mostly associated with single-layer boundary-layer mixed-phase clouds in EAMv1. Particularly, the problem of insufficient ice from CNT ice nucleation is most critical at warm temperature regime (warmer than -15℃). As aerosol properties have been considered in the CNT parameterization, deficiency in aerosol schemes can also degrade the performance of CNT in mixed-phase clouds due to aerosol-cloud interactions. For example, EAMv1 underestimates the high-latitude dust transport from mid-latitude source regions; and it misses the important INP source from Arctic local dust and biological aerosols. These underestimated INP number concentration over the Arctic can lead to biased phase partitioning of high-latitude mixed-phase clouds in models (Shi & Liu, 2019). Future model development is advocated to address the treatment of aerosol emission and scavenging to achieve an accurate spatial and vertical aerosol distribution in the atmosphere. In terms of the CLUBB parameterization, although a similar approach used in Park and Bretherton (2009) to partition condensed and detrained cloud water based on temperature has been tested and proved to improve the phase partitioning of simulated mixed-phase clouds over the Southern Ocean, ice phase assumptions should also be included in CLUBB's PDF parameterization in the future. Moreover, other microphysical processes, such as

secondary ice production, are not reasonably parameterized in the current model scheme. This can be the result of poorly understood ice multiplication processes in mixed-phase clouds in real atmosphere (Field et al., 2017). More efforts are required to understand these less constrained processes in mixed-phase cloud simulation in GCMs.

Although this study is purely based on one single location during the M-PACE field campaign, we expect that the underestimated (overestimated) cloud ice (liquid) is a common feature in EAMv1 simulated mixed-phase clouds beyond this ARM site (figures not shown). In the next chapter, results at other locations will be provided. As cloud feedback and climate sensitivity are strongly regulated by the phase partitioning of mixed-phase clouds (Tan & Storelvmo, 2019; Tan et al., 2016), biases in low-level mixed-phase clouds identified in this study may introduce uncertainties to E3SM estimated cloud phase feedback (Golaz et al., 2019; Zelinka et al., 2020), which is also of interest in future studies.

CHAPTER V

UNDERSTANDING THE HEMISPHERIC DIFFERENCES IN MIXED-PHASE CLOUD PROPERTIES FROM OBSERVATIONS AND E3SM SIMULATIONS

5.1. Background

Aerosols play an important role in modulating cloud properties and cloud radiative effect by changing number concentrations of cloud condensate nuclei (CCN) and sizes of liquid droplets (Andreae et al., 2005; Bellouin et al., 2020; McCoy et al., 2020). With the same amount of liquid water mass mixing ratio, increasing CCN number concentration decreases liquid droplet effective radius. Clouds then become more reflective and can generate a stronger cooling on the climate system (Twomey, 1977). Less efficient collection and accretion between liquid particles also reduces the cloud precipitation efficiency, and then extend cloud longevity (Albrecht,1989; Rosenfeld et al., 2008). On the other hand, some aerosol species can serve as INPs to change ice phase cloud properties (Choi et al., 2010; DeMott et al., 2015; Vergara-Temprado et al., 2018). For example, higher concentration of mineral dust, which are found to be effective INPs, can enhance the glaciation of mixed-phase clouds (Shi & Liu, 2019). More precipitation and shorter cloud lifetime are then expected due to the glaciation effect of INP on mixed-phase clouds (Lohmann, 2002). However, the net aerosol indirect effect on mixed-phase clouds remains uncertain.

Previous studies have shown that mixed-phase cloud properties have strong hemispheric differences in high-latitude regions. Zhang et al. (2018) used A-Train CloudSat and CALIPSO measurements to examine the characteristics of ice production in mixed-phase cloud regime in two hemispheres. They found that measured radar reflectivity is larger in the Northern Hemisphere (NH) than in the Southern Hemisphere (SH) under constrained cloud top temperatures and liquid water path for the same type of clouds. There is also a stronger seasonal variation in radar reflectivity in NH, implying the larger ice production in mixed-phase clouds compared to SH. Using ground-based remote sensing measurements, Zhang, Vogelmann et al. (2019) found consistent differences in stratiform mixed-phase cloud properties between Utqiaġvik site (Arctic) and McMurdo station (Antarctic). For example, higher and colder cloud top and thicker ice layer depth were found over the Antarctic, and larger supercooled liquid fraction was observed at McMurdo compared to Utqiaġvik site. Meanwhile, mixed-phase clouds at McMurdo have larger liquid droplet number concentration, smaller ice water content, and lower ice number concentration compared to the Arctic mixed-phase clouds. These hemispheric contrast in ice production activity can be partially attributed to the higher aerosol loadings in NH. Different thermodynamic conditions, large-scale circulations, and topography in two hemispheres are also believed to contribute to such differences in cloud macrophysical and microphysical properties (Silber et al., 2018, 2019), but further studies are required.

Compared to a relatively pristine environment over the Southern Ocean in SH, Arctic is more polluted, especially during the Arctic haze season when high aerosol

concentrations are transported from lower latitude regions (Luo et al., 2015). The strong contrast in background aerosol concentrations between the Arctic and Antarctic provides an ideal experimental field to understand the aerosol impact on cloud microphysical properties. In this study, we will focus on single-layer stratiform mixed-phase clouds observed and simulated in high-latitude regions. Firstly, we plan to evaluate the EAMv1 performance on simulated hemispheric differences in mixed-phase cloud macrophysical and microphysical properties against satellite and ground-based retrievals. Secondly, how aerosols and atmospheric thermodynamics would influence mixed-phase cloud properties under constrained environments between two hemispheres will be analyzed.

5.2. Model simulations

Simulated mixed-phase clouds from EAMv1 are evaluated with both satellite and ground-based remote sensing retrievals of single-layer stratiform mixed-phase clouds. The default EAMv1 configuration is used in our model simulation, except that we remove the tuning parameter of 0.1 on WBF process. Horizontal wind (U and V) and temperature (T) fields are nudged towards the ERA-Interim reanalysis data, and we perform model simulations on the 1-degree horizontal resolution. Simulations are run from November 2015 to December 2016 with the first two months for spin-up. Simulation period is chosen to cover the AWARE field campaign. Three-hourly high frequency outputs are used to sample single-layer stratiform mixed-phase clouds from the model.

5.3. Results

5.3.1. Cloud macrophysical properties

In this section, we compare EAMv1 simulated mixed-phase cloud properties to single-layer stratiform mixed-phase clouds measured by ground-based remote sensing instruments. Mixed-phase clouds from the model simulation are sampled in a similar method as discussed in Chapter III, but we change a few thresholds in cloud height definition. In EAMv1 parameterization, simulated clouds at layers below 700 hPa are classified as low-level clouds, while mid-level clouds are defined when they are between 700 hPa land 400 hPa altitude. To account for the possible mid-level single-layer stratiform mixed-phase clouds measured in observations, a cutoff threshold of 600 hPa is used at Utqiaġvik site, and clouds lower than 400 hPa altitude are sampled in our simulations at the Antarctic McMurdo station. The reason for different cutoff thresholds in two hemispheres is because Antarctic mixed-phase clouds during the AWARE field campaign were found overall to have higher top heights compared to clouds observed in the Arctic (Silber et al., 2018, 2019; Zhang, Vogelmann et al., 2019). More discussion about the sensitivity of sampled clouds to the choice of these thresholds will be provided in following paragraphs. We note that the cloud top height cutoff is not applied in observations, the discrepancy in cloud definition between model and observation could influence our results. This effect will be examined in the next step.

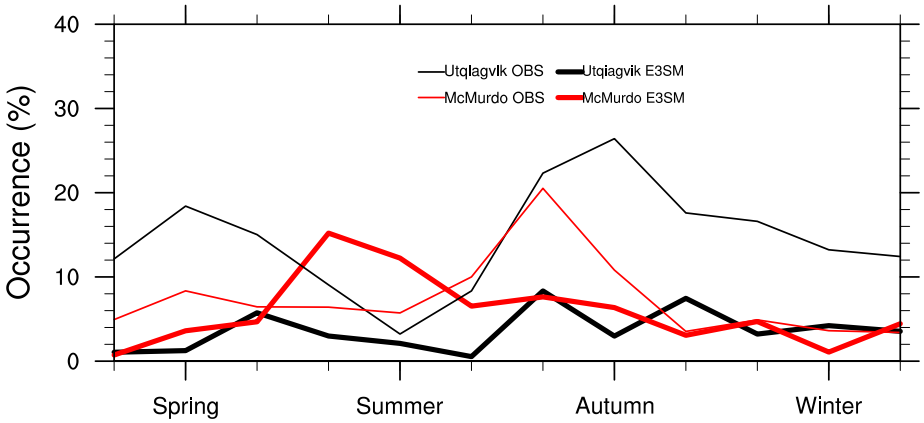

Figure 5.1. Monthly single-layer stratiform mixed-phase cloud frequency of occurrence at Utqiaġvik and McMurdo in ground-based remote sensing measurements (thin lines) and EAMv1 simulations (thick lines). Cloud frequency of occurrence is grouped into boreal and austral seasons, respectively.

Figure 5.1 shows the comparison of monthly cloud frequency of occurrence between model and observations at Utqiaġvik site and McMurdo station. Observed frequency of occurrence is derived as the ratio between number of lidar profiles that containing single-layer stratiform mixed-phase clouds and number of total lidar profiles. It is shown that single-layer stratiform mixed-phase clouds are more frequently observed in the Arctic than its Antarctic counterpart throughout the years. The feature of higher cloud occurrence in autumn than other seasons is shown in both hemispheres. The lowest frequency of occurrence was observed in boreal summer and austral winter in the Arctic and Antarctic, respectively. For EAMv1 simulations, cloud frequency of occurrence is calculated as the number of outputs including sampled single-layer stratiform mixed-phase clouds divided by the number of total outputs, Model results are averaged over nine surrounding grids to the grid point that is closest to individual

observational sites. Compared to observations, it is shown in Figure 5.1 that EAMv1 simulation largely underestimates cloud frequency of occurrence at Utqiaġvik site, but it captures the cloud occurrence seasonal variability. We note that the underestimated mixed-phase cloud occurrence is probably caused by an overestimated frequency of occurrence of pure liquid phase clouds between temperature range from -40℃ to 0℃. During the AWARE field campaign, EAMv1 simulated mixed-phase clouds have comparable frequency of occurrence to the ground-based remote sensing measurements in austral winter. However, the model misrepresents the peak occurrence of mixed-phase clouds in austral summertime. We note that overestimated cloud occurrence during summer is mostly related to mixed-phase clouds at higher altitudes. In a sensitivity test using 600 hPa cutoff threshold to sample single-layer stratiform mixed-phase clouds at McMurdo, such overestimation is much alleviated. However, compared to other seasons, a higher cloud occurrence remains in summer in model simulations, no matter which threshold being used. Such a larger cloud occurrence can be attributed to the warmer and moister summer atmosphere in the Antarctic, while cold and dry air (e.g., surface temperature colder than -17℃) dominates the rest of the year. Meanwhile, lower tropospheric stability (LTS), defined as the difference of potential temperature between surface and 700 hPa, is found to play a potential role in influencing the high occurrence of simulated Antarctic mixed-phase clouds. With lower LTS simulated during austral summertime (figure not shown), the less stable atmosphere favors more cloud formation than other seasons.

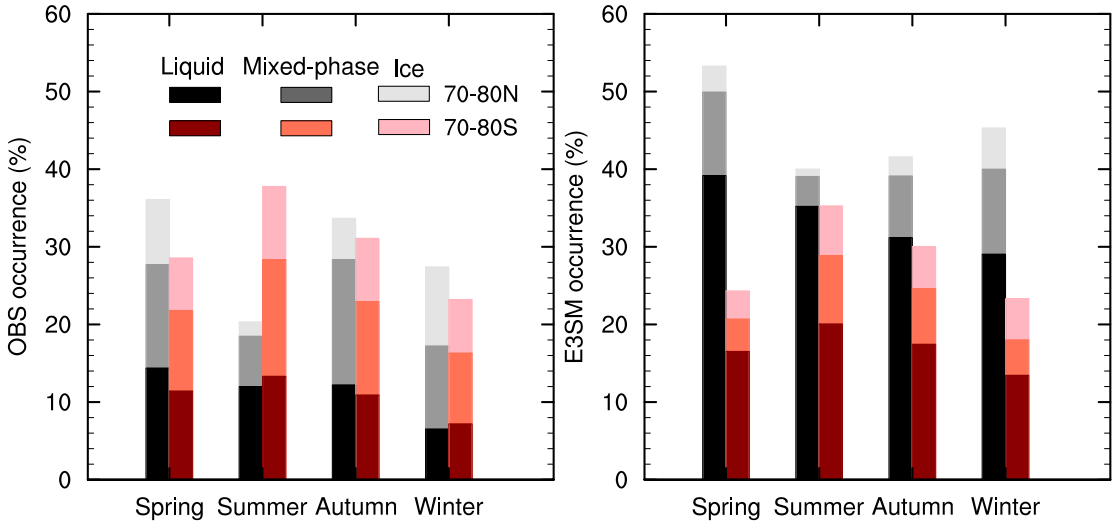

Figure 5.2. Seasonal mean frequency of occurrence of low-level single-layer stratiform clouds averaged between 70-80° latitude bands over the Arctic and Antarctic regions. EAMv1 simulated clouds are compared to the 2B-CLDCLASS-LIDAR products retrieved using CloudSat and CALIPSO measurements. Frequency of occurrence of low-level single-layer stratiform clouds in pure liquid phase, pure ice phase, and mixed-phase are defined and averaged for both latitude bands, and then grouped to boreal and austral seasons.

Figure 5.2 shows the averaged frequency of occurrence of pure liquid phase, pure ice phase, and mixed-phase single-layer low-level stratiform clouds relative to all clouds from the 2B-CLDCLASS-LIDAR product and model simulations. Cloud frequency of occurrence is averaged between latitude bands from 70° to 80° in both hemispheres. Simulated pure liquid (ice) phase clouds are defined similarly as mixed-phase clouds, except we allow total IWC (LWC) smaller than 0.001 g kg^{-1}. Note that clouds from EAMv1 are sampled using the same cutoff threshold of 600 hPa in both hemispheres in this analysis, so that similar types of clouds (e.g., stratocumulus and stratus) are used in comparison. Although defined clouds differ slightly between Figures 5.1 and 5.2 at

McMurdo, insignificant difference is found in the phase partitioning pattern in cloud frequency of occurrence. Therefore, the satellite retrievals provide complimentary dataset for our understanding on the model performance of frequency of occurrence of three cloud phases at two ARM sites.

As illustrated in Figure 5.2, relative to total cloudy sky conditions, simulated clouds are more dominated by pure liquid phase than by mixed-phase between 70-80°N latitude band. Such a partitioning feature between liquid phase and mixed-phase is substantially different compared to CloudSat and CALIPSO satellite retrievals, in which retrieved low-level stratiform mixed-phase clouds are more frequent. The shift of simulated cloud phase from mixed-phase to pure liquid phase is consistent to our conclusions in Chapter IV. This is because the observed mixed-phase clouds during the M-PACE field campaign have been simulated as a structure that is overly dominated by liquid water with little ice produced in EAMv1. Such a biased cloud structure, however, is now categorized into pure liquid phase in the current study. In addition, compared to satellite retrievals, even though the total occurrence of low-level clouds (sum of occurrence of three cloud phases) in the Arctic is overestimated by EAMv1, the frequency of occurrence of pure ice phase is underestimated. This result further illustrates that cloud ice water is underestimated in the mixed-phase temperature regime. At latitude band between 70-80°S, although the total occurrence of low-level clouds becomes more comparable to satellite measurements, most of the features shown in the Arctic still hold for the Antarctic clouds. Consistent to ground-based remote sensing measurements, the same seasonality of mixed-phase cloud frequency of occurrence is

found in the 2B-CLDCLASS-LIDAR product. For example, over the Arctic region, mixed-phase clouds have minimal occurrence during the boreal summertime, and they are more frequently observed in boreal autumn and spring. Over the Antarctic, on the other hand, observations show a maximum cloud occurrence during austral warm season and clouds become relatively less frequent during austral winter. In spite of the biased cloud frequency of occurrence, EAMv1 is capable to simulate comparable seasonal variations to the observation.

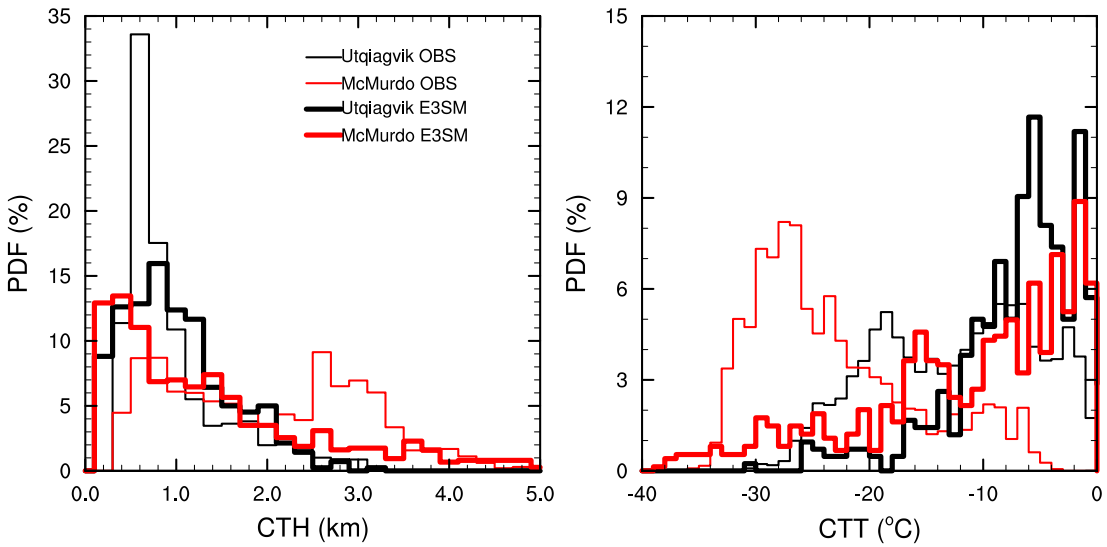

Figure 5.3. Probability of distribution of cloud top height (left) and top temperature (right) in single-layer stratiform mixed-phase clouds at Utqiaġvik and McMurdo. Ground-based measurements are represented in thin lines while EAMv1 simulations are shown with thick lines.

Figure 5.3 shows the probability of distribution of single-layer stratiform mixed-phase cloud top height and top temperature from ground-based retrievals and EAMv1 simulations at Utqiaġvik and McMurdo. Cloud top height (CTH) and CTT in model results are the altitude and grid mean temperature at the highest level where single-layer stratiform mixed-phase cloud is defined. It is clear that clouds observed at Utqiaġvik tend to have lower top heights than at McMurdo. CTH of single-layer stratiform mixed-phase clouds observed from Utqiaġvik has a peak probability around 0.6 km, while the CTH peaks are around 0.8 km and 2.6 km at McMurdo. There is a wider distribution of CTH at McMurdo station compared to Utqiaġvik site. For simulated stratiform mixed-phase clouds, CTH in the Arctic shows a similar local maximum around 0.8 km, but its probability is substantially underestimated. Simulated clouds also tend to have higher probability of CTH between 1.0 and 2.0 km than observations at Utqiaġvik. Even though EAMv1 overall captures the wider CTH distribution at McMurdo than at Utqiaġvik, the probability of CTH near 3.0 km remains too low and there are too frequent CTH lower than 0.5 km at McMurdo. We note that the higher CTH during the AWARE field campaign can be partially related to the higher cutoff threshold applied in cloud sampling. The similarities in hemispheric contrast of CTH between model and observation suggest that using different thresholds to filter target clouds at these two locations is probably necessary. As discussed in previous studies, observed higher CTH in single-layer stratiform mixed-phase clouds is probably the result of strong katabatic flow from topographic effect over the Antarctic region (Bromwich et al., 2012). Due to the use of coarse horizontal resolution, such topographic effect on cloud formation may

not be well simulated in our model. Therefore, in future studies, an investigation using high resolution model is necessary to figure out the impact of complex topography on high latitude mixed-phase cloud properties. Furthermore, the large probability of CTH below 0.6 km at Utqiaġvik implies that single-layer stratiform mixed-phase clouds formed in the Arctic is mostly within PBL. As discussed in Morrision et al. (2012), Arctic stratiform mixed-phase clouds are commonly generated and maintained through complex interactions between cloud top radiative cooling, turbulence, large-scale dynamics, surface fluxes, and cloud microphysics. The formation mechanisms for mixed-phase clouds in the Arctic and Antarctic can be different. More analysis is required.

Corresponding to the higher CTH at McMurdo, observed CTT also indicates larger probabilities at colder temperatures compared to Utqiaġvik. For example, in remote sensing retrievals, single-layer stratiform mixed-phase clouds have two local peaks of probability near -8℃ and -20℃ at Utqiaġvik, while the peak at McMurdo is at -28℃. The cold CTT in the Antarctic could also be related to the pristine environment with less INPs to glaciate mixed-phase clouds and the cold atmosphere there. Inconsistent to observations, simulated CTT in EAMv1 has pronounced probabilities at temperatures warmer than -10℃ at both locations. These warm biases can be related to the low bias in CTH in simulated stratiform mixed-phase clouds. Regardless of the biased CTT distribution, the hemispheric difference that CTT in the Antarctic has higher probabilities at cold temperature range (e.g., colder than -25℃) than Arctic is well captured.

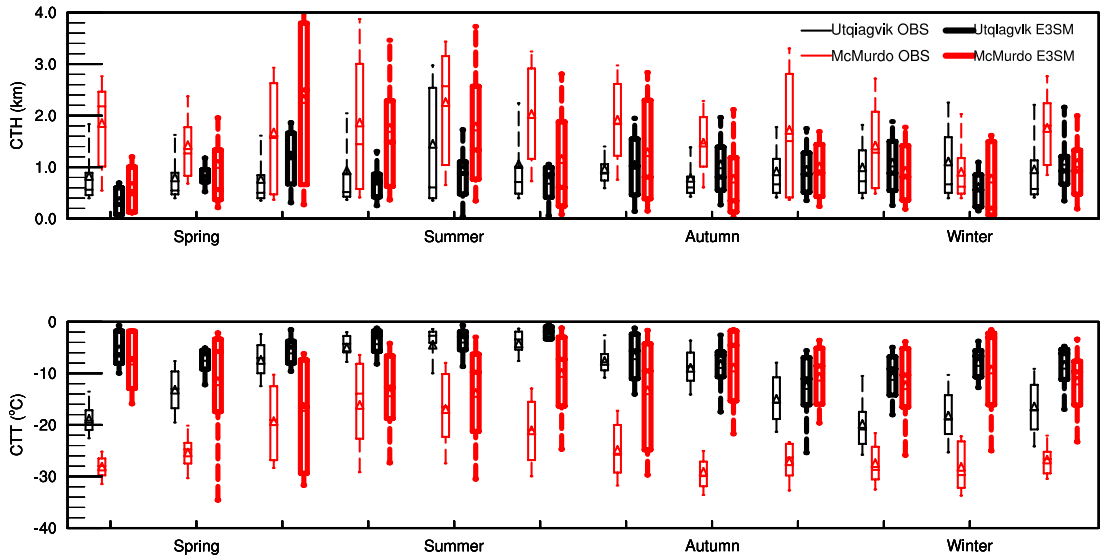

Figure 5.4. Monthly statistics of CTH (upper panel) and CTT (bottom panel) of single-layer stratiform mixed-phase clouds at Utqiaġvik and McMurdo in observations and model simulations. The box-and-whisker plots provide 10th, 25th, 50th, 75th, and 90th percentiles of the monthly statistics, and the means are shown by triangles.

Monthly statistics of observed and simulated CTH and CTT in single-layer stratiform mixed-phase clouds are presented in Figure 5.4. In both ground-based remote sensing measurements and EAMv1 simulations, higher CTH is shown during austral summer at McMurdo. Ground-based retrievals also indicate a CTH maximum in boreal summer at Utqiaġvik, but such CTH peaks are not simulated in EAMv1. It is shown in Figure 5.4 that a strong seasonal variation is simulated in CTH at McMurdo, which is consistent to observations. However, compared to observed mixed-phase clouds, a smaller contrast between warm and cold seasons is simulated at Utqiagivk.

Figure 5.4 shows that CTT of single-layer stratiform mixed-phase clouds corresponds well to CTH. For instance, colder (warmer) CTT is found largely associated

with higher (lower) CTH in individual months. With a reasonable model performance in CTH in terms of its hemispheric difference, the substantial CTT contrast between two hemispheres is also well captured by EAMv1. In a given season, colder temperature is simulated at McMurdo than Utqiaġvik. However, compared to observations, despite the comparable CTH in simulated mixed-phase clouds in winter at both locations, warm bias can still be found in CTT, especially at Utqiaġvik. The reason for these warm biases requires further examination in our future studies.

By examining the monthly mean LTS at two ARM sites, a stronger seasonal variation of LTS is found at McMurdo than at Utqiaġvik (figure not shown). Lower LTS is both observed and simulated during austral summer, accompanied with a larger LTS in austral winter. Such seasonality is less substantial in the Arctic. Figure 5.5 shows that CTH tends to be positively correlated to LTS at both McMurdo and Utqiaġvik. By conducting a linear regression between CTH and LTS, it is interesting that the regression coefficient (i.e., slope) between CTH and LTS at McMurdo is larger than at Utqiaġvik. Such a feature is illustrated in both observations and model results, which suggests that the higher CTH at McMurdo is probably generated by the stronger thermodynamic instability in low-level atmosphere.

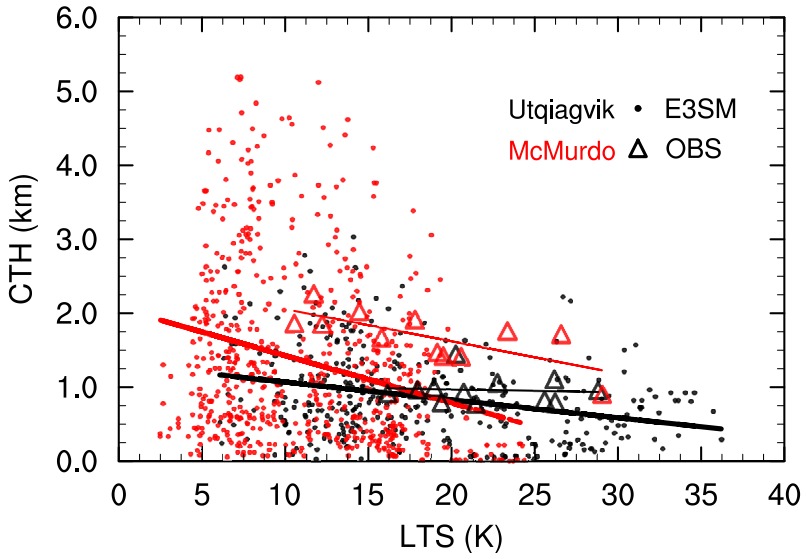

Figure 5.5. Relations of CTH of single-layer stratiform mixed-phase clouds as a function of LTS at Utqiaġvik and McMurdo. 3-hourly model results are indicated by dots, and monthly observational data is shown in triangles. Solid lines represent linear regressions between CTH and LTS. Red lines are for McMurdo and black lines are for Utqiaġvik. Thick solid lines represent model results while observations are shown in thin solid lines.

5.3.2. Cloud microphysical properties

In previous sections, we evaluate cloud macrophysical properties, such as cloud frequency of occurrence, CTH, and CTT, simulated by EAMv1 against ground-based remote-sensing measurements. Differences in single-layer stratiform mixed-phase cloud properties between the Arctic and Antarctic regions are examined. In this section, we further evaluate how well EAMv1 model simulates stratiform mixed-phase cloud microphysical properties at Utqiaġvik and McMurdo.

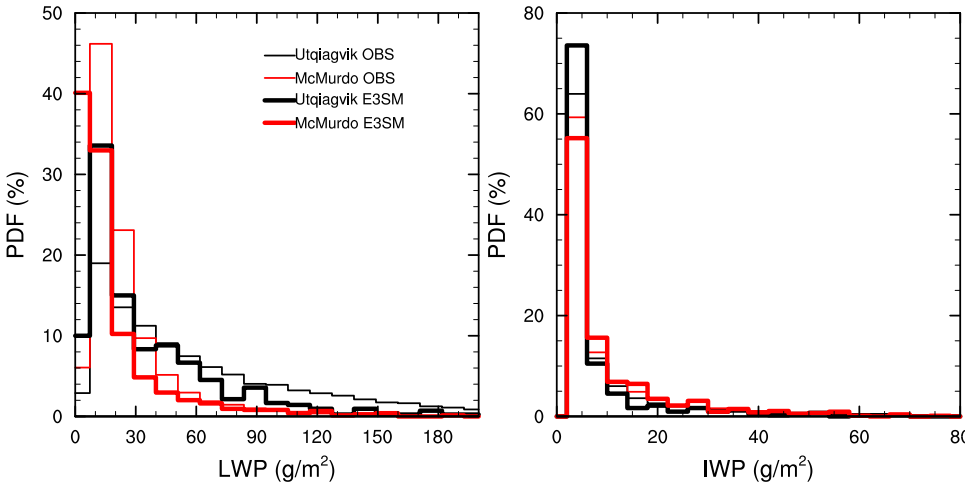

Figure 5.6. Same as Figure 5.3, but for LWP (left) and IWP (right) in single-layer stratiform mixed-phase clouds.

Figure 5.6 indicates the probability of distribution of LWP and IWP in single-layer stratiform mixed-phase clouds at Utqiaġvik and McMurdo. It is shown that although observed stratiform mixed-phase clouds have a peak probability of LWP around 20 g m^{-2} at both Utqiaġvik and McMurdo, clouds at McMurdo have substantially larger probability of LWP smaller than 20 g m^{-2}. On the other hand, LWP in stratiform mixed-phase clouds at Utqiaġvik are more commonly greater than 50 g m^{-2}. The overall larger LWP in stratiform mixed-phase clouds in the Arctic than Antarctic results from the greater liquid-dominant layer thickness observed at Utqiaġvik (Zhang, Vogelmann et al., 2019). For EAMv1 simulated mixed-phase clouds, the LWP distribution difference observed between Utqiaġvik and McMurdo is generally reproduced. However, model tends to underestimate the probability of LWP greater than 90 g m^{-2} and overestimate the probability of small LWP value of 20 g m^{-2} at Utqiaġvik. Despite the overestimated

probability of LWP smaller than 10 g m^{-2}, LWP probability distribution at McMurdo is comparable to the observation.

In terms of IWP probability distribution, model simulated stratiform mixed-phase clouds share many similarities to the observation at both locations. For example, in spite of the CTT difference between Utqiaġvik and McMurdo, the PDF of observed IWP in single-layer stratiform mixed-phase clouds is essentially comparable at Utqiaġvik and McMurdo. Although biases are shown in modeled CTH and CTT, EAMv1 simulates a similar IWP distribution compared to observed stratiform mixed-phase clouds. In contrast to the underestimated IWP revealed in Chapter IV, we note that the comparable IWP distribution here is concluded by analyzing sampled mixed-phase clouds with a strict definition. Clouds that are dominated by supercooled liquid water, like what produced by EAMv1 during the M-PACE field campaign, have been excluded in this analysis. Those clouds are now categorized into pure liquid phase clouds whose frequency of occurrence are largely overestimated compared to observations. If we include the liquid dominated clouds as mixed-phase clouds, consistent results to Chapter IV will then be presented.

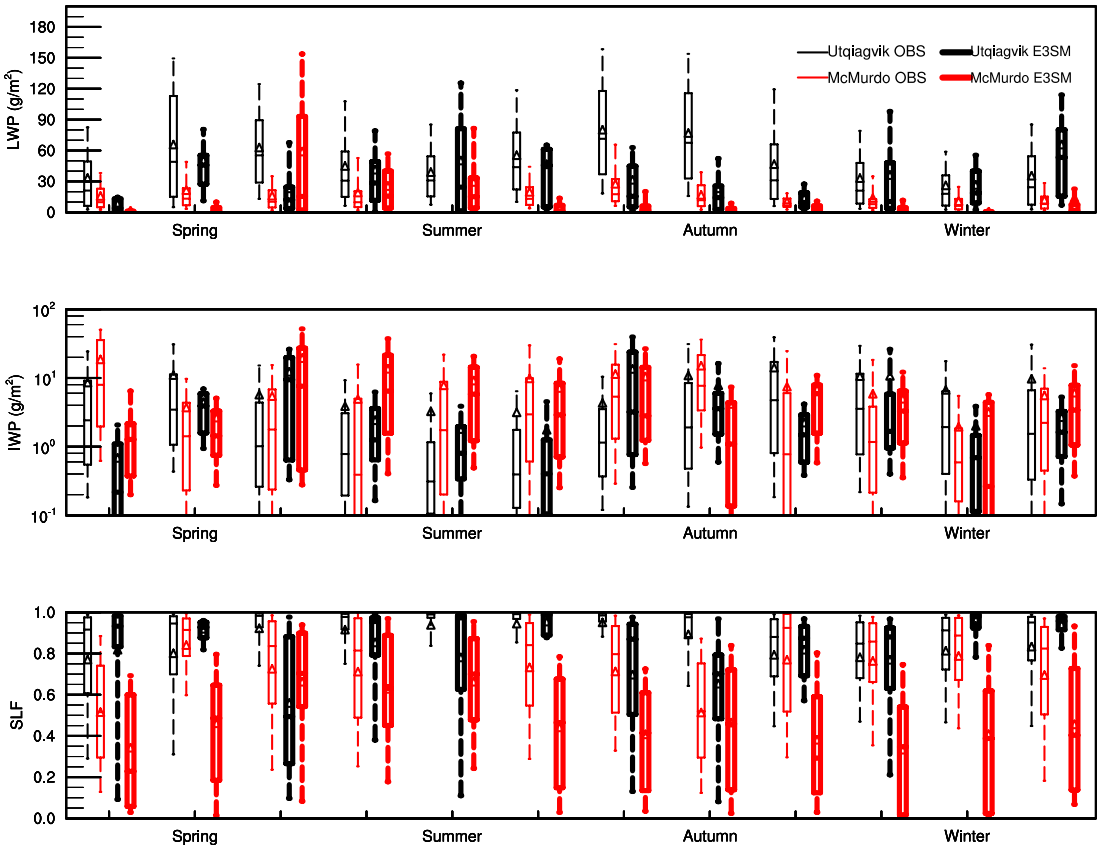

Figure 5.7. Same as Figure 5.4, but for LWP (upper panel), IWP (middle panel), and SLF (lower panel) for single-layer stratiform mixed-phase clouds.

Figure 5.7 compares the monthly statistics of LWP, IWP, and SLF at Utqiaġvik and McMurdo between model and observations. Consistent to Figure 5.6, observed mixed-phase clouds have overall larger LWP at Utqiaġvik compared to McMurdo throughout the years. With relatively smaller IWP at Utqiaġvik, SLF in observations tends to be greater than clouds measured at McMurdo. In terms of the seasonality of cloud microphysical properties, LWP and IWP in observed stratiform mixed-phase clouds exhibit larger values during autumn and spring at both locations. SLF shows

relatively smaller values during spring and autumn seasons due to the larger IWP in observed mixed-phase clouds.

One important feature for EAMv1 simulation is that the observed hemispheric contrast in cloud microphysical property statistics is generally captured during most of the months. For example, simulated Arctic mixed-phase clouds contain greater LWP and SLF than the Antarctic; and the hemispheric contrast in modeled IWP is consistent to observations during summertime. We note that, at Utqiaġvik site, large LWP values mostly occur during boreal spring and autumn in remote sensing retrievals. Therefore, the too low LWP probability at values greater than 90 g m^{-2} (shown in Figure 5.6) can be attributed to the LWP underestimation in these seasons in EAMv1. Underestimated liquid droplet number concentration and effective radius in simulated stratiform mixed-phase clouds possibly explain the reason for such underestimation, but further validation is required. At McMurdo, despite of the overestimated LWP in austral late spring and early summer, simulated LWP is comparable to ground-based retrievals during most seasons. The large LWP in austral spring and summer can be attributable to the overestimated mixed-phase cloud occurrence in EAMv1.

Even with the hemispheric difference captured in cloud phase partitioning, biases are still found in simulated SLF for individual month. Substantially low SLF is simulated during most of the seasons (i.e., except November and April) at McMurdo and in May, July, September, and October at Utqiaġvik. We should emphasize that results shown here have excluded the influence of mixed-phase clouds that is similar to what

simulated by EAMv1 during the M-PACE field campaign. Therefore, larger values of IWP are shown in our sampling.

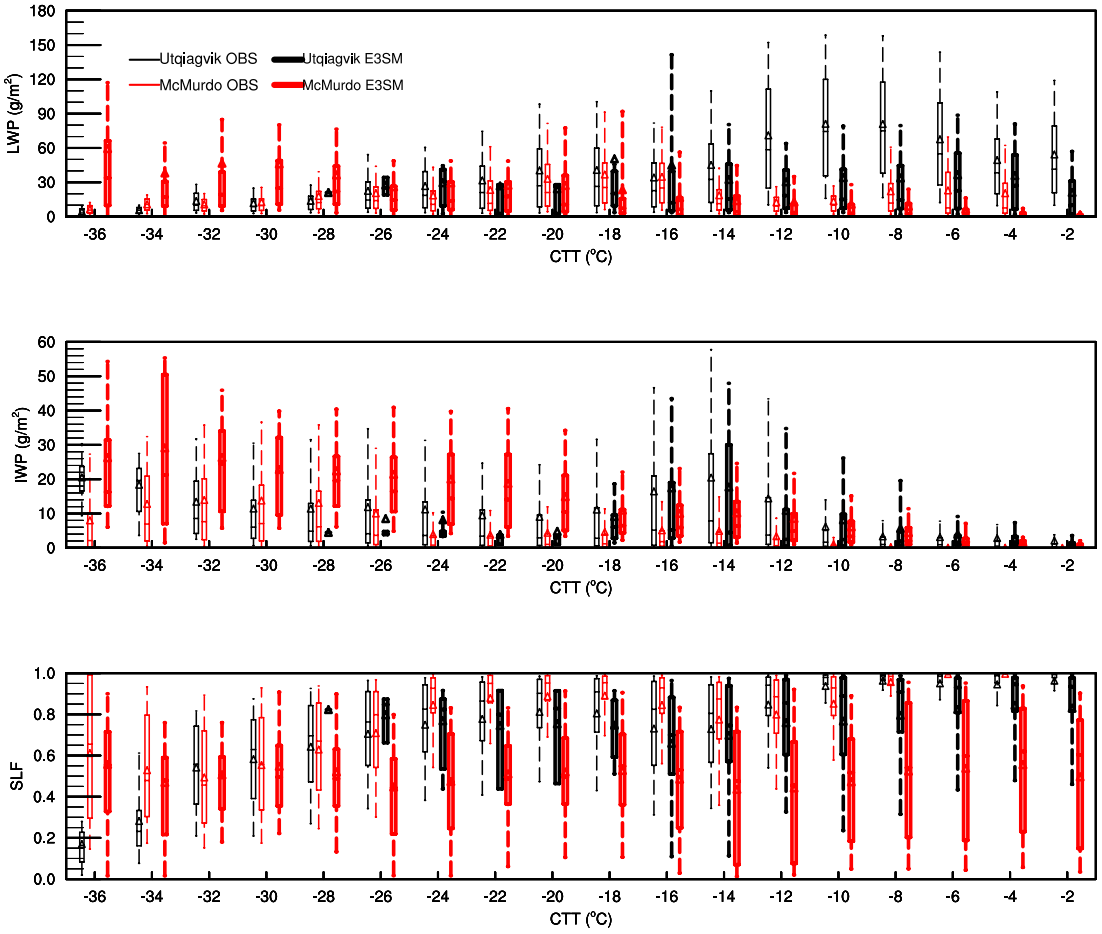

Figure 5.8. Statistics of single-layer stratiform mixed-phase cloud microphysical properties (LWP in upper panel, IWP in middle panel, and SLF in lower panel) as a function of CTT at Utqiaġvik and McMurdo in EAMv1 simulations and observations. The box-and-whisker plots are the same as in Figure 5.4.

Figure 5.8 shows the statistic relationship of LWP, IWP, and SLF as a function of CTT at Utqiaġvik and McMurdo. Significant temperature dependence of LWP, IWP, and SLF is observed in single-layer stratiform mixed-phase clouds. At Utqiaġvik, there are two local maximums in LWP at -10℃ and -20℃, respectively; and a local minimal LWP is centered around -16℃. Correspondingly, a local IWP peak is found near -14℃, which is consistent to the results from theoretical studies that ice depositional growth is most efficient within this temperature range to consume liquid water via WBF process (Fukuta & Takahashi, 1999; Korolev, 2008). SLF observed in Arctic mixed-phase clouds shows an increasing tendency towards warm temperatures. SLF becomes close to 1.0 at temperatures warmer than -10℃ and it decreases to smaller than 0.4 when temperature becomes as cold as -34℃. On the other hand, the relation between mixed-phase cloud microphysical properties and CTT at McMurdo differs largely from Utqiaġvik site. It is shown in Figure 5.8 that the LWP local peak is observed near -18℃ at McMurdo; and IWP has a local maximum centered at -34℃. The distribution of LWP and IWP maxima moving towards colder temperature at McMurdo also supports that mixed-phase clouds tend to be located at higher altitudes and colder temperatures compared to Utqiaġvik. Furthermore, consistent to Utqiaġvik, SLF minima are shown at -14℃ at McMurdo, which correlate to the LWP minima and IWP maxima at this temperature range. For a given temperature from -24℃ to -14℃, larger SLF is shown at McMurdo than Utqiaġvik. Such a pattern was reported to be consistent to Tan et al. (2014) who also found less supercooled cloud fraction in NH than SH using spaceborne lidar measurements (Zhang, Vogelmann et al., 2019).

For simulated temperature dependence of LWP, IWP, and SLF, it is interesting to find that LWP, IWP, and SLF at Utqiaġvik have tendencies to distribute towards temperatures warmer than -24℃, and the distribution of these three properties shifts to colder temperatures at McMurdo. For example, large values of simulated LWP occur mainly at temperatures between -18℃ and -4℃ in the Arctic mixed-phase clouds. The simulated IWP maximum is also centered at -14℃, which is consistent to measurements at Utqiaġvik. With a slightly increasing LWP tendency and a decreasing IWP tendency towards warm temperature range, SLF at Utqiaġvik increases with increasing temperature. In contrast, at McMurdo, large values of LWP and IWP are more dominated at temperatures colder than -20℃ in EAMv1, and LWP and IWP become smaller at warm temperature range. As a result, simulated SLF at McMurdo is relatively small, and it is lower than Utqiaġvik at given temperatures from -26℃ to -2℃. Such hemispheric differences in LWP, IWP, and SLF temperature dependency imply that mechanisms regulating mixed-phase cloud microphysical properties could be different in these two high-latitude regions. Note that using a higher cutoff threshold to sample stratiform mixed-phase clouds at McMurdo may also influence our analysis here. More investigations will be necessary to understand why modeled mixed-phase clouds show such different temperature dependence features in two hemispheres.

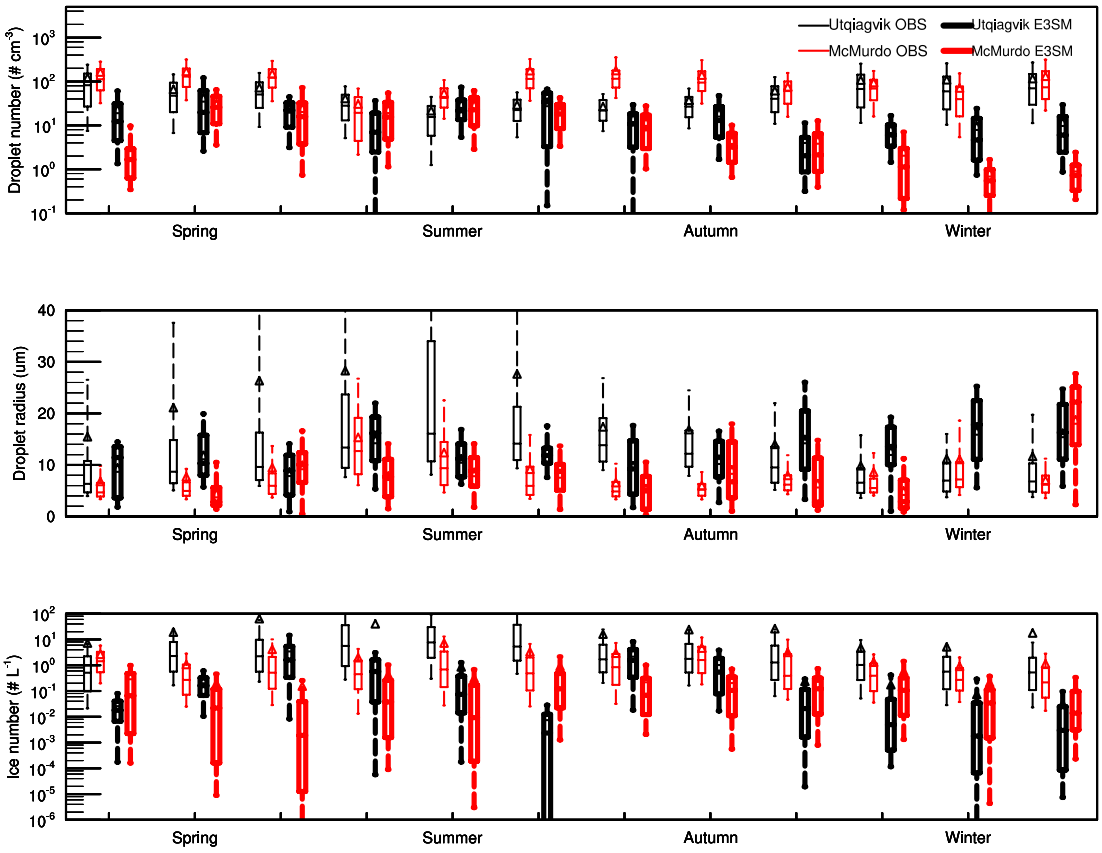

Figure 5.9. Same as Figure 5.4, but for number concentrations of cloud liquid droplet (upper panel) and droplet effective radius (middle panel), as well as number concentrations of ice crystals (lower panel) for single-layer stratiform mixed-phase clouds.

Figure 5.9 shows the monthly statistics of number concentrations of cloud liquid droplets and ice crystals and effective radius of liquid droplets in EAMv1 simulated and observed single-layer stratiform mixed-phase clouds. In ground-based remote sensing measurements, droplet number concentration and effective radius are derived for liquid-dominated layers. In general, larger liquid droplet number concentrations are measured at McMurdo than at Utqiaġvik except for wintertime. It is also shown that smaller liquid

droplet effective radius is obtained during the AWARE field campaign compared to the Arctic mixed-phase clouds. Meanwhile, lower number concentration of cloud liquid droplets and larger droplet size are observed during summer in both hemispheres. The anticorrelation between droplet number concentration and effective radius is expected. For EAMv1 simulations, the seasonal variation in liquid droplet number concentration is not accurately simulated. For example, simulated liquid droplets have the lowest number concentrations in boreal autumn at Utqiaġvik and in austral winter at McMurdo, respectively. Insignificant difference is also simulated in droplet number between the two sites during warm seasons, but the hemispheric difference becomes overestimated during cold seasons. From summer to autumn, the size of simulated cloud droplets is larger in the Arctic, where higher aerosol loading and slightly higher liquid droplet concentration are produced in the atmosphere at the same time. This suggests that the relation between liquid droplet concentration and effective radius is opposite between model and observation during this period. Compared to observations, with underestimated liquid droplet number concentration during winter at both locations, droplet effective radius is overestimated in simulated stratiform mixed-phase clouds. Nevertheless, during most of the seasons, the droplet size difference between Utiqagvik and McMurdo is overall simulated in EAMv1.

Cloud ice particles also show noticeable differences between Utqiaġvik and McMurdo in observations. Larger ice particle concentrations are measured in the Arctic as the result of stronger dust emissions in the NH than SH. From late spring to early autumn, such observed feature is captured in EAMv1. However, an opposite pattern in

hemispheric difference is simulated from late autumn to winter, during which larger cloud ice number concentration is at McMurdo than Utqiaġvik in simulated mixed-phase clouds. This discrepancy is probably because there is a biased local dust emission simulated near McMurdo station in EAMv1, which leads to substantially overestimated dust mass concentrations over the Antarctica (figure not shown). The effect of this local dust emission will be examined in a separate sensitivity experiment.

5.3.3. Aerosol effect on cloud properties

Earlier studies revealed that the Antarctic atmosphere is a relatively pristine environment, and the Arctic has more pollutants due to anthropogenic activities and continental emissions (e.g., dust) (McCoy et al., 2020). In addition to the impact from different thermodynamic conditions in two hemispheres, aerosols are also believed to play an important role modulating mixed-phase cloud properties. In this section, we will focus on the aerosol effect on cloud properties by understanding the linkage between aerosol and cloud differences at Utqiaġvik and McMurdo.

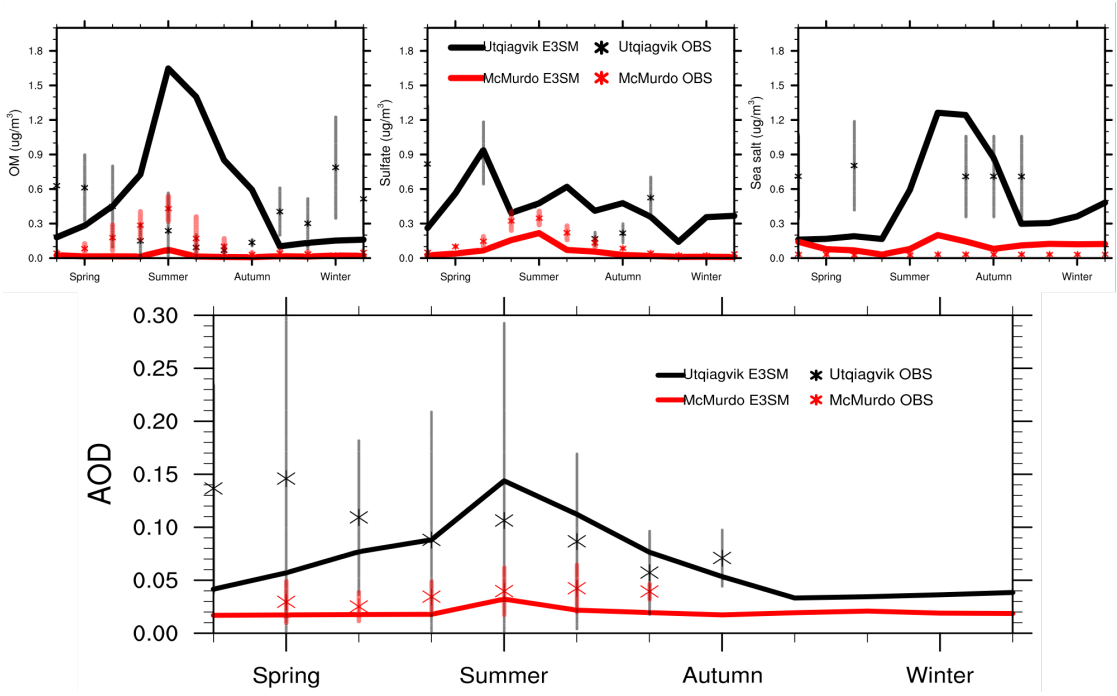

Figure 5.10. Monthly mean aerosol mass concentrations and total aerosol optical depth at 500 nm observed during the AWARE field campaign and at Utqiaġvik site. EAMv1 simulations are monthly averaged values at McMurdo and Utqiaġvik. Straight lines represent one standard deviation in observations for each month.

Figure 5.10 shows the comparison between observed aerosol mass concentration at Utqiaġvik and McMurdo and EAMv1 simulations. Simulated total AOD is also compared to CSPHOT measurements from ARM dataset. Note that the mass concentration of OM is obtained using FTIR spectroscopy spectra. Sea salt particle mass concentration is calculated based on Bates et al. (2012), and non-sea salt sulfate mass concentration is derived using XRF measurement based on (Liu et al., 2018). Figure 5.10 indicates that total AOD measured during the AWARE field campaign is lower than the climatology aerosol total AOD over the Arctic. Especially during the Arctic haze spring,

measured AOD at Utqiaġvik is nearly one order of magnitude larger than at McMurdo. Over the Antarctic region, larger AOD is found during austral summer and relatively low AOD is observed in rest of the season. By examining aerosol mass concentration in different composites, OM, sulfate, and sea salt aerosols are found to contribute to the high Arctic AOD during boreal springtime. Earlier studies have reported that the high aerosol mass concentration in boreal spring in the Arctic is mainly attributable to aerosol transport from mid-latitude source regions (Brock et al., 2011; Shindell et al., 2008; Wu et al., 2018). Meanwhile, during the AWARE field campaign, organics that resulted from sea bird deposits and human activities at McMurdo station, and non-sea salt sulfate formed from oxidation of DMS are largely responsible for the high Antarctic AOD in austral summer (Lubin et al., 2020). We note that due to the data availability, here we only show the aerosol composition of OM, sulfate, and sea salt. More dataset will be collected in the next step to evaluate other aerosol species (e.g., dust).

In terms of model simulations, larger AOD is simulated at Utqiaġvik than McMurdo all year round. However, while the peak summer AOD is the same as observation at McMurdo, EAMv1 inaccurately generates a peak AOD during boreal summer. The biased low AOD during spring haze period suggests that model probably underestimates the aerosol transport from mid-latitudes (Wu et al., 2020). It is found that sea salt and OM aerosols dominate the high AOD in both hemispheres in EAMv1 simulations, which means the seasonal variation in simulated OM is opposite to surface aerosol observations at Utqiaġvik. During the Arctic haze season, we find that sulfate is one of the dominant aerosol species in model simulations.

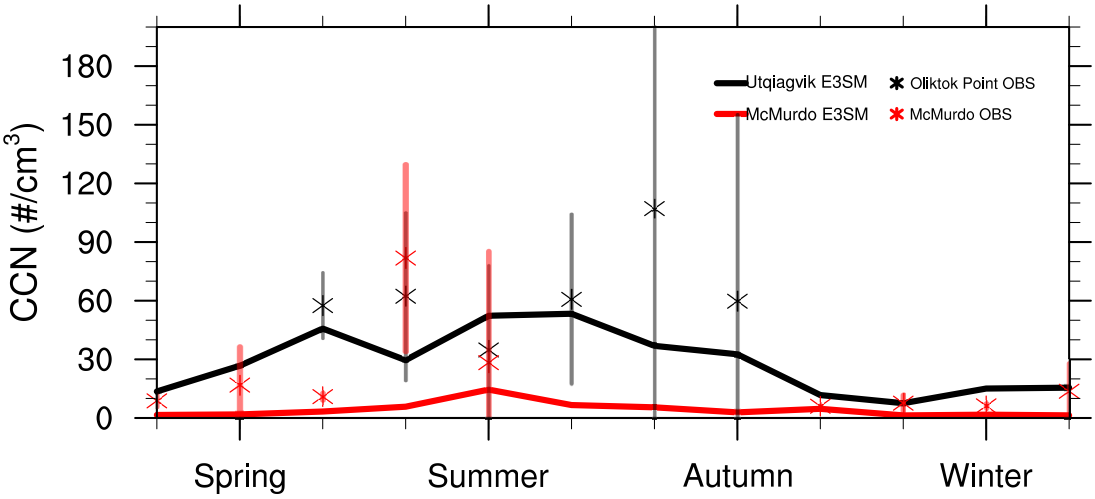

Figure 5.11. Monthly mean CCN number concentration at 0.1% supersaturation between observation and EAMv1 simulation. Measured CCN concentration is during the AWARE field campaign at McMurdo and from 2017 to 2019 at Oliktok Point over the Arctic. Straight lines represent one standard deviation in observed CCN for each month.

Differences in aerosol concentrations between the Arctic and Antarctic are reflected in observed CCN number concentrations (Figure 5.11). Compared to McMurdo, with higher aerosol concentrations, larger CCN number concentrations are both observed and simulated in the Arctic. However, we also notice that, during summer, insignificant difference is observed in CCN concentration between two hemispheres. Note that observed Arctic CCN number concentration is obtained at Oliktok Point. Different local emissions are expected between Oliktok Point and Utqiaġvik. At McMurdo, the high CCN concentration can be explained by the large aerosol hygroscopicity parameter, which makes aerosol more readily to be activated as CCN

(Herenz et al., 2018, 2019; Liu et al., 2018). Meanwhile, the complex terrain around McMurdo station can also favor stronger droplet activation. Therefore, more CCNs are formed during certain time period.

Different from observations, Figure 5.11 also shows that substantially lower CCN number concentration is simulated at McMurdo than Utqiaġvik. This is consistent to the lower cloud liquid droplet number concentration simulated at McMurdo except for summer. However, more effort is required, and more observational dataset is necessary for further investigation of the relation between aerosol, CCN, and liquid droplet concentrations in future studies.

5.4. Summary and discussion

In this study, we utilize DOE ARM ground-based remote sensing measurements to evaluate EAMv1 simulated high-latitude mixed-phase clouds. Single-layer stratiform mixed-phase clouds are derived at Utqiaġvik site and during the AWARE field campaign at McMurdo station. 2B-CLDCLASS-LIDAR product retrieved from CloudSat and CALIPSO measurements is also used to provide complimentary cloud dataset for our model validation. Cloud macrophysical and microphysical properties and their hemispheric difference between two locations are examined.

Through sampling simulated clouds that are most comparable to observed single-layer stratiform mixed-phase clouds at both sites, we find that EAMv1 underestimates frequency of occurrence of the target mixed-phase clouds. The underestimation at Utqiaġvik is found more significant than McMurdo. Overestimated frequency of

occurrence of pure liquid phase clouds explains the underestimation of mixed-phase cloud occurrence. In other words, EAMv1 tends to produce more clouds in pure liquid phase rather than mixed-phase at given supercooled environment. Regardless of biased frequency of occurrence in stratiform mixed-phase clouds, macrophysical properties, such as CTH and CTT, are generally produced in simulated stratiform mixed-phase clouds. For example, the wider probability distribution of CTH and CTT at McMurdo is captured by the model. The tendency that mixed-phase clouds at McMurdo have higher CTH and colder CTT than at Utqiaġvik is also simulated, which is consistent to observations. However, the probabilities of CTH higher than 2.0 km and CTT colder than -20℃ are substantially smaller in modeled mixed-phase clouds. This accompanies with the issue that stratiform mixed-phase clouds in EAMv1 are too low and too warm at both Utqiaġvik and McMurdo compared to ground-based measurements. Furthermore, we find the higher CTH at McMurdo is well correlated to the smaller LTS in both observation and model results. Our regression analysis shows that a larger regression coefficient is shown at McMurdo than at Utqiaġvik. This suggests that atmospheric stability can be important to understand the hemispheric difference in mixed-phase cloud properties.

For stratiform mixed-phase cloud microphysical properties, despite the overestimated probability of small LWP values at McMurdo and Utqiaġvik, the probability distributions of LWP and IWP are comparable between EAMv1 and remote sensing measurements. Monthly statistics of simulated mixed-phase cloud LWP and IWP also exhibit similar seasonal variations compared to observation. The analysis of

temperature dependence of LWP, IWP, and SLF indicates substantial discrepancies between Utqiaġvik and McMurdo, implying the dominated mechanism modulating mixed-phase cloud properties could be different at two high-latitude sites. Further examination will be necessary to understand processes that result in such hemispheric difference in mixed-phase clouds. Moreover, annual variability is expected in the statistics of mixed-phase cloud properties in the Arctic in different years (Shupe et al., 2006). The use of one-year model results may not be representative for simulated Arctic mixed-phase clouds. Therefore, analysis using multi-year simulations will be conducted in the next step.

Analysis of aerosol properties and their impact on CCN and cloud microphysical properties is also performed in the current study. However, only preliminary results have been discussed. In our future studies, more investigations are required to understand the impact of different aerosol loading between two hemispheres on stratiform mixed-phase cloud properties. Moreover, with complex topographic effect on cloud formation over the Antarctic region, high resolution simulation is important in future work to better resolve complicated terrains near the McMurdo. The topographic effect on local dynamics and its influence on cloud formation can then be better examined. Finally, we note that our artificial definition of single-layer stratiform mixed-phase clouds from GCM simulation may not sample the same mixed-phase clouds as observed. The heterogeneity of cloud top temperature and top heights are both neglected in simulated mixed-phase clouds. Therefore, the use of ground-based radar and lidar simulator or satellite simulator in the future will help to improve the consistency in our model-

observation comparison, and they will merit a better understanding about the model performance in simulated clouds.

CHAPTER VI

CONCLUSION AND FUTURE DIRECTION

6.1. Conclusions

Mixed-phase clouds are frequently observed over high-latitude regions. Due to the distinct radiative properties between liquid droplets and ice crystals, phase partitioning between liquid and ice is known as one of the key parameters in mixed-phase clouds that can largely influence the surface energy balance and impact the high-latitude climate change. In the past decades, although substantial progresses have been achieved in the understanding and representation of cloud processes in mixed-phase clouds, unconstrained parameterizations of cloud microphysics in GCMs still contribute to large uncertainties in simulated mixed-phase cloud phase partitioning.

In this dissertation, we utilize comprehensive observational datasets to understand how well current GCMs represent high-latitude mixed-phase clouds. In CAM5, we represent the heterogeneous distribution between liquid droplets and ice crystals through modifying the WBF process in cloud microphysics parameterization. The impact of modified WBF process on mixed-phase cloud simulation is evaluated against data measured during the DOE ARM M-PACE field campaign. In our experiments, three assumptions are made to improve the representation of liquid droplet and ice crystal heterogenous distribution. First, we assume a partial homogeneous mixture that observed in the HIPPO in-situ measurements. Second, an idealized pocket structure is assumed to uniformly distribute within each model grid cell. Third, a mass-

weighted treatment is applied to replace the use of saturated water vapor mass mixing ratio in the WBF process calculation. We show that the WBF process becomes less efficient after introducing these three modifications, leading to a better phase partitioning feature in simulated Arctic mixed-phase clouds. During the M-PACE field campaign, cloud LWC and the maintenance of liquid water layer become more comparable to ground-based remote sensing measurements in SCAM5. The improvement of cloud liquid water mass mixing ratio is found to be proportional to the magnitude of perturbation factors used in WBF process. We also find that IWP/IWC is less sensitive to our WBF process modifications. This is because snow mass coming from accretion of liquid droplets and raindrops tends to compensate the reduced WBF process, leaving insignificant changes in simulated ice phase water content. Despite the better phase partitioning pattern in SCAM5, consistent improvements are shown in global simulations when compared to long-term ground-based measurements. Through a separate sensitivity experiment, we illustrate the importance of a consistent treatment in representing cloud heterogeneity in different microphysical processes. Meanwhile, increasing vertical resolution in GCMs is also found helpful to improve the simulation of mixed-phase cloud vertical profiles.

By moving to an updated state-of-the-art ESM developed by U.S. DOE, we investigate the reason why simulated mixed-phase cloud phase partitioning in EAMv1 substantially changed from its precursor CAM5. Short-term hindcast simulations are performed for the M-PACE field campaign to isolate the impact of physics scheme change during EAMv1 development on mixed-phase cloud properties. It is interesting to

find that simulated total ice water mass mixing ratio is currently lower than observations. Total liquid water, however, is slightly overestimated. Such a model behavior change will exert substantial differences in surface energy budget compared to previous model schemes. Budget analysis of hindcast results presents that the production of initial ice particles is important for accurately simulating mixed-phase cloud properties in EAMv1. The ice production from either heterogeneous ice nucleation or detrainment from shallow convection can provide such initial ice particles, and they subsequently go through mass growth processes such as ice deposition and collision and coalescence to gain mass and generate mixed-phase clouds. However, with the incorporation of CNT ice nucleation scheme and CLUBB parameterization in EAMv1, very small amounts of initial ice are formed at temperatures warmer than -15℃. This is because the CNT scheme tends to underestimate ice particle number concentration within this relatively warm temperature range, compared to the Meyers scheme which was previously used in CAM5. On the other hand, with the lack of ice phase process in CLUBB, minimal cloud ice water is then detrained from CLUBB to stratiform cloud microphysics scheme, which also explains the decrease of initial ice production. In a sensitivity experiment, incorporating detrained ice from CLUBB determined cloud condensate shows promising improvements in simulated mixed-phase clouds.

Finally, we utilize ARM long-term ground-based remote sensing measurements at Utqiaġvik site and the AWARE field campaign data at McMurdo to evaluate EAMv1 simulated high-latitude stratiform mixed-phase clouds in terms of their hemispheric difference. We find that when defining stratiform mixed-phase clouds as liquid and ice

water coexisted in the model, EAMv1 underestimates the frequency of occurrence of observed single-layer stratiform mixed-phase clouds at Utqiaġvik and McMurdo. By analyzing the complimentary spaceborne remote sensing measurements, we find that EAMv1 tends to overestimate the frequency of occurrence of pure liquid phase clouds within mixed-phase regime over both Arctic and Antarctic regions. Cloud macrophysical and microphysical properties and their hemispheric difference between two locations are also examined. In general, the hemispheric difference in probability distribution of CTH and CTT is simulated between Utqiaġvik and McMurdo in EAMv1. The model well captures the tendency that mixed-phase clouds have higher CTH and colder CTT at McMurdo than at Utqiaġvik. However, too warm and too low biases still exist in individual simulated clouds. It is shown that there is a positive correlation between LTS and CTH in both observation and model at both locations. The stronger correlation at McMurdo than at Utqiaġvik suggests that atmospheric stability can be important to interpret the hemispheric difference in high-latitude mixed-phase clouds. In terms of cloud microphysical properties, model simulated mixed-phase clouds show overall comparable probability distribution of LWP and IWP and their monthly statistics compared to ground-based measurements. However, too large probability is simulated for small LWP values at both sites. Compared to McMurdo, the feature that single-layer stratiform mixed-phase clouds have larger SLF at Utqiaġvik is well simulated. Our preliminary results also suggest that the dominated mechanism regulating mixed-phase cloud properties could be different at McMurdo and Utqiaġvik. Differences in atmospheric thermodynamics (e.g., temperature, moisture) and aerosols are believed to

play important roles between the two locations. Further investigation is required to fully understand those hemispheric difference in stratiform mixed-phase cloud properties shown in our comparison.

6.2. Future directions

In this dissertation, we performed a number of sensitivity simulations to understand the response of simulated mixed-phase cloud properties to selected microphysical processes. In Chapter III, our examination about the impact of modified WBF process on mixed-phase clouds is performed using the single column version of CAM5. Biases have been found in the atmospheric states prescribed by large-scale forcing. Therefore, addressing the similar science question under a less biased forcing framework is encouraged. On the other hand, many other factors can also introduce uncertainties to the simulation of high-latitude mixed-phase clouds in GCMs. Future work is advocated to understand effects of factors such as changing ice particle size distribution, ice nucleation scheme, and turbulence representation on simulated clouds. Meanwhile, cloud microphysics parameterization can be sensitive to changes in model resolution. Especially for the heterogeneous distribution between liquid droplets and ice crystals in mixed-phase clouds, with an increased horizontal resolution, these structures would be numerically resolved using a 0.25° grid spacing. The response of cloud microphysical processes to changes in horizontal resolution is of interest in future studies.

With the substantial model behavior change from CAM5 to EAMv1, deficiencies in model parameterization associated with aerosol processes require further understanding. This is because current GCMs become more complex to treat aerosol and cloud interactions, where large uncertainties remain in our knowledge. For example, EAMv1 is found to underestimate high-latitude dust transport from mid-latitude source regions. The representation of local dust emission over the Arctic is also insufficient, while the potential INP contribution from biogenic species is neglected. Thus, future model development is encouraged to obtain better treatments of aerosol emission and aerosol scavenging processes, which would help to achieve an accurate spatial and vertical aerosol distribution in GCMs. Moreover, with underestimated contribution from secondary ice production to simulated ice particles in mixed-phase clouds, more efforts are required to understand secondary ice production related processes. Including better constrained ice multiplication mechanisms in cloud microphysics will have a large impact on simulated mixed-phase cloud properties, as well as their global climate effects.

For stratiform mixed-phase clouds over the Antarctic, their difference in macrophysical and microphysical properties from the Arctic clouds is briefly analyzed in this dissertation. In our next step, aerosol effect resulted from the large difference in aerosol loading and aerosol properties between two hemispheres will be investigated with more efforts. The topographic effect on cloud formation at McMurdo station is also interesting to have more comprehensive analysis. High resolution simulation will be helpful. Furthermore, using radar and lidar simulator developed for both ground-based

and spaceborne instruments will help to improve the consistency in our model-observation comparison. By removing discrepancies between GCM and instrument measurements, simulator combined model validation can benefit our interpretation of simulated cloud properties when comparing to remote sensing data.

Note that our model simulations are mainly examined during the M-PACE field campaign at a single location in the Arctic. It is also important to understand the global impact of modifications in WBF process, as well as changes in heterogenous ice nucleation schemes on mixed-phase clouds. Alterations in mixed-phase cloud radiative effect are expected due to changes in the phase partitioning of simulated clouds. In future studies, it is necessary to repeat sensitivity experiments designed in this dissertation studies for long-term simulations, so that how cloud climatology and global energy budget would response to different treatments in WBF process and ice nucleation can be examined. Moreover, cloud feedback and climate sensitivity have been found to be strongly influenced by the phase partitioning of mixed-phase clouds due to their ubiquitous coverage and distinct radiative effect (Tan & Storelvmo, 2019; Tan et al., 2016). For example, the high incidence of mixed-phase clouds over the Southern Ocean can largely modulate the surface albedo in that region. The strength of negative cloud phase feedback is also mostly associated with mixed-phase cloud properties represented in GCMs (Bodas-Salcedo et al., 2019; Gettelman et al., 2019; Zelinka et al., 2020). Which cloud process and through which mechanism can mixed-phase clouds change cloud feedback and climate sensitivity is of interest in future studies. It is also interesting

to test how changes in mixed-phase cloud phase partitioning due to our modifications in WBF process and CLUBB would impact future climate projection.

Last but not the least, because different earth system components are closely coupled with each other, changes in clouds and atmosphere could exert substantial impacts on sea surface temperature and ocean circulations, along with changes in ice sheets and glaciers in the cryosphere. Experiments using coupled simulation will facilitate our understanding about the interactions between different earth system components when introducing modifications in cloud microphysics.

REFERENCES

Albrecht, B. A. (1989). Aerosols, cloud microphysics, and fractional cloudiness. *Science*, 245, 1227-1230. https://doi.org/10.1126/science.245.4923.1227

Andreae, M., Jones, C. & Cox, P. (2005). Strong present-day aerosol cooling implies a hot future. *Nature*, 435, 1187-1190. https://doi.org/10.1038/nature03671

Bates, T. S., Quinn, P. K., Frossard, A. A., Russell, L. M., Hakala, J., Petäjä, T., et al. (2012). Measurements of ocean derived aerosol off the coast of California. *Journal of Geophysical Research: Atmospheres*, 117, D00V15, https://doi.org/10.1029 /2012JD017588

Barrett, A. I., Hogan, R. J., & Forbes R. M. (2017a). Why are mixed-phase altocumulus clouds poorly predicted by large-scale models? Part 1. Physical processes. *Journal of Geophysical Research: Atmospheres*, 122, 9903-9926. https://doi.org/10.1002/2016JD026321

Barrett, A. I., Hogan, R. J., & Forbes, R. M. (2017b). Why are mixed-phase altocumulus clouds poorly predicted by large-scale models? Part 2. Vertical resolution sensitivity and parameterization. *Journal of Geophysical Research: Atmospheres*, 122, 9927-9944. https://doi.org/10.1002/2016JD026322

Bellouin, N., Quaas, J., Gryspeerdt, E., Kinne, S., Stier, P., Watson-Parris, D., et al. (2020). Bounding global aerosol radiative forcing of climate change. *Reviews of Geophysics*, 58, e2019RG000660. https://doi.org/10.1029/2019RG000660

Bennartz, R., Shupe, M. D., Turner, D. D., Walden, V. P., Steffen, K., Cox, C. J., et al. (2013). July 2012 Greenland melt extent enhanced by low-level liquid clouds. *Nature*, 496, 83-86. https://doi.org/10.1038/nature12002

Bergeron, T. (1935). 'On the physics of clouds and precipitation'. pp. 156-178 in *Proces Verbaux de l'Association de Météorologie, International Union of Geodesy and Geophysics*, Paris, France

Bodas-Salcedo, A., Mulcahy, J. P., Andrews, T., Williams, K. D., Ringer, M. A., Field, P. R., & Elsaesser, G. S. (2019). Strong dependence of atmospheric feedbacks on mixed-phase microphysics and aerosol-cloud interactions in HadGEM3. *Journal of Advances in Modeling Earth Systems*, 11, 1735–1758. https://doi.org/10.1029/2019MS001688

Bogenschutz, P. A., Gettelman, A., Morrison, H., Larson, V. E., Craig, C., & Schanen, D. P. (2013). Higher-order turbulence closure and its impact on climate simulations in

the Community Atmosphere Model. *Journal of Climate*, 26(23), 9655–9676. https://doi.org/10.1175/JCLI-D-13-00075.1

Bogenschutz, P. A., Gettelman, A., Morrison, H., Larson, V. E., Schanen, D. P., Meyer, N. R., et al. (2012). Unified parameterization of the planetary boundary layer and shallow convection with a higher-order turbulence closure in the Community Atmosphere Model: single-column experiments. *Geoscientific Model Development*, 5, 1407-1423. https://doi.org/10.5194/gmd-5-1407-2012, 2012

Bretherton, C. S. & Park, S. (2009). A New Moist Turbulence Parameterization in the Community Atmosphere Model. *Journal of Climate*, 22, 3422-3448. https://doi.org/10.1175/2008JCLI2556.1

Brock, C. A., Cozic, J., Bahreini, R., Froyd, K. D., Middlebrook, A. M., McComiskey, A., et al. (2011). Characteristics, sources, and transport of aerosols measured in spring 2008 during the aerosol, radiation, and cloud processes affecting Arctic Climate (ARCPAC) Project. *Atmospheric Chemistry and Physics*, 11, 2423-2453. https://doi.org/10.5194/acp-11-2423-2011

Bromwich, D. H., Nicolas, J. P., Hines, K. M., Kay, J. E., Key, E. L., Lazzara, M. A., et al. (2012). Tropospheric clouds in Antarctica. *Reviews of Geophysics*, 50, RG1004. https://doi.org/10.1029/2011RG000363

Brown, P. R. & Francis, P. N. (1995). Improved Measurements of the Ice Water Content in Cirrus Using a Total-Water Probe. *Journal of Atmospheric and Oceanic Technology*, 12, 410-414. https://doi.org/10.1175/1520-0426(1995)012<0410:IMOTIW>2.0.CO;2

Chen, J. P., Hazra, A., & Levin, Z. (2008). Parameterizing ice nucleation rates using contact angle and activation energy derived from laboratory data. *Atmospheric Chemistry and Physics*, 8, 7431-7449. https://doi.org/10.5194/acp-8-7431-2008

Choi, Y. S., Lindzen, R. S., Ho, C. H., & Kim, J. (2010). Space observations of cold-cloud phase change. *Proceedings of the National Academy of Sciences*, 107, 11,211-11,216. https://doi.org/10.1073/pnas.1006241107

Clothiaux, E. E., Ackerman, T. P., Mace, G. G., Moran, K. P., Marchand, R. T., Miller, M. A., & Martner, B. E. (2000). Objective determination of cloud heights and radar reflectivities using a combination of active remote sensors at the ARM CART sites. *Journal of Applied Meteorology and Climatology*, 39, 645-665. https://doi.org/10.1175/1520-0450(2000)039%3C0645:ODOCHA%3E2.0.CO;2

Cohen, J., Zhang, X., Francis, J., Jung, T., Rwok, R., Overland, J. et al. (2020). Divergent consensuses on Arctic amplification influence on midlatitude severe winter

weather. *Nature Climate Change*, 10, 20-29. https://doi.org/10.1038/s41558-019-0662-y

D'Alessandro, J. J., Diao, M., Wu, C., Liu, X., Jensen, J. B., & Stephens, B. B. (2019). Cloud phase and relative humidity distributions over the Southern Ocean in austral summer based on in situ observations and CAM5 simulations. *Journal of Climate*, 32, 2781-2805. https://doi.org/10.1175/JCLI-D-18-0232.1

de Boer, G., Eloranta, E. W., & Shupe, M. D. (2009). Arctic Mixed-Phase Stratiform Cloud Properties from Multiple Years of Surface-Based Measurements at Two High-Latitude Locations. *Journal of the Atmospheric Science*, 66, 2874-2887. https://doi.org/10.1175/2009JAS3029.1

Dee, D. P., Uppala, S. M., Simmons, A. J., Berrisford, P., Poli, P., Kobayashi, S., et al. (2011). The ERA-Interim reanalysis: configuration and performance of the data assimilation system. *Quarterly Journal of the Royal Meteorological Society*, 137, 553-597. https://doi.org/10.1002/qj.828

DeMott, P. J., Prenni, A. J., Liu, X., Kreidenweis, S. M., Petters, M. D., Twohy, C. H., et al. (2010). Predicting global atmospheric ice nuclei distributions and their impacts on climate. *Proceedings of the National Academy of Sciences*, 107(25), 11217-11222. https://doi.org/10.1073/pnas.0910818107

DeMott, P. J., Prenni, A. J., McMeeking, G. R., Sullivan, R. C., Petters, M. D., Tobo, Y., et al. (2015). Integrating laboratory and field data to quantify the immersion freezing ice nucleation activity of mineral dust particles. *Atmospheric Chemistry and Physics*, 15(1), 393-409. https://doi.org/10.5194/acp-15-393-2015

Deser, C., Walsh, J. E., & Timlin, M. S. (2000). Arctic sea ice variability in the context of recent atmospheric circulation trends. Journal of Climate, 13, 617-633. https://doi.org/10.1175/1520-0442(2000)013<0617:ASIVIT>2.0.CO;2

Dong, X., & Mace, G. G. (2003). Profiles of low-level stratus cloud microphysics deduced from ground-based measurements. *Journal of Atmospheric and Oceanic Technology*, 20, 42-53. https://doi.org/10.1175/1520-0426(2003)020<0042:POLLSC>2.0.CO;2

Fan, J., Ghan, S., Ovchinnikov, M., Liu, X., Rasch, P. J., & Korolev, A. (2011). Representation of Arctic mixed-phase clouds and the Wegener-Bergeron-Findeisen process in climate models: Perspectives from a cloud-resolving study. *Journal of Geophysical Research: Atmospheres*, 116, D00T07. https://doi.org/10.1029/2010JD015375

Field, P. R., Lawson, R. P., Brown, P. R., Lloyd, G., Westbrook, C., Moisseev, D., et al. (2017). Secondary Ice Production: Current State of the Science and Recommendations for the Future. *Meteorological Monographs*, 58, 7.1-7.20. https://doi.org/10.1175/AMSMONOGRAPHS-D-16-0014.1

Findeisen, W. (1938). Kolloid-meteorologische Vorgäange bei Neiderschlags-bildung. *Meteorologiche Zeitschrift*, 55, 121-133

Frisch, A. S., Fairall, C. W. & Snider, J. B. (1995). Measurement of stratus cloud and drizzle parameters in ASTEX with Ka-band Doppler radar and a microwave radiometer. *Journal of the Atmospheric Science*. 52, 2788-2799. https://doi.org/10.1175/1520-0469(1995)052<2788:MOSCAD>2.0.CO;2

Fridlind, A. M., Ackerman, A. S., McFarquhar, G., Zhang, G., Poellot, M. R., DeMott, P. J., Prenni, A. J., & Heymsfield, A. J. (2007). Ice properties of single-layer stratocumulus during the Mixed-Phase Arctic Cloud Experiment: 2. Model results. *Journal of Geophysical Research: Atmospheres*, 112, D24202. https://doi.org/10.1029/2007JD008646

Fridlind, A., van Diedenhoven, M., B., Ackerman, A. S., Avramov, A., Mrowiec, A., Morrison, H., et al. (2012). A FIRE-ACE/SHEBA case study of mixed-phase Arctic boundary-layer clouds: Entrainment rate limitations on primary ice nucleation

processes. *Journal of the Atmospheric Sciences*, 69, 365-389. https://doi.org/10.1175/JAS-D-11-052.1

Frossard, A. A., Hawkins, L. N., Russell, L. M., Quinn, P. K., Upchurch, L., & Andrews, E. (2020). Submicron organic and elemental aerosol composition at Utgiagvik (Barrow), Alaska, from March 2008 to February 2010. In Atmospheric Aerosol Submicron Particle Composition including Organic Functional Group Concentrations at Arctic Locations. UC San Diego Library Digital Collections. https://doi.org/10.6075/J01N7ZN2

Fu, Q., & Hollars, S. (2004). Testing Mixed-Phase Cloud Water Vapor Parameterizations with SHEBA/FIRE-ACE Observations. *Journal of the Atmospheric Sciences*, 61, 2083-2091. https://doi.org/10.1175/1520-0469(2004)061<2083:TMCWVP>2.0.CO;2

Fukuta, N., & Takahashi, T. (1999). The growth of atmospheric ice crystals: A summary of findings in vertical supercooled cloud tunnel studies. *Journal of the Atmospheric Sciences*, 56(12), 1963-1979. https://doi.org/10.1175/1520-0469(1999)056<1963:TGOAIC>2.0.CO;2

Furtado, K., Field, P. R., Boutle, I. A., Morcrette, C. J., & Wilkinson, J. M. (2016). A Physically Based Subgrid Parameterization for the Production and Maintenance of

Mixed-Phase Clouds in a General Circulation Model. *Journal of the Atmospheric Sciences*, 73, 279-291. https://doi.org/10.1175/JAS-D-15-0021.1

Gettelman, A., Hannay, C., Bacmeister, J. T., Neale, R. B., Pendergrass, A. G., Danabasoglu, G., et al. (2019). High climate sensitivity in the Community Earth System Model Version 2 (CESM2). *Geophysical Research Letters*, 46, 8329–8337. https://doi.org/10.1029/2019GL083978

Gettelman, A., Liu, X., Ghan, S. J., Morrison, H., Park, S., Conley, A. J., et al. (2010). Global simulations of ice nucleation and ice supersaturation with an improved cloud scheme in the Community Atmosphere Model. *Journal of Geophysical Research: Atmospheres*, 115, D18216. https://doi.org/10.1029/2009JD013797

Gettelman, A., & Morrison, H. (2015). Advanced two-moment bulk microphysics for global models. Part I: Off-line tests and comparison with other schemes. *Journal of Climate*, 28(3), 1268-1287. https://doi.org/10.1175/JCLI-D-14-00102.1

Gettelman, A., Morrison, H., Santos, S., Bogenschutz, P. & Caldwell, P. M. (2015). Advanced Two-Moment Bulk Microphysics for Global Models. Part II: Global Model Solutions and Aerosol–Cloud Interactions. *Journal of Climate*, 28, 1288-1307. https://doi.org/10.1175/JCLI-D-14-00103.1

Golaz, J.-C., Caldwell, P. M., Van Roekel, L. P., Petersen, M. R., Tang, Q., Wolfe, J. D., et al. (2019). The DOE E3SM coupled model version 1: Overview and evaluation at standard resolution. *Journal of Advances in Modeling Earth Systems*, 11. https://doi.org/10.1029/2018MS001603

Golaz, J.-C., Larson, V. E., & Cotton, W. R. (2002). A PDF-based model for boundary layer clouds. Part I: Method and model description. *Journal of the Atmospheric Sciences*, 59(24), 3540–3551. https://doi.org/10.1175/1520-0469(2002)059<3540:APBMFB>2.0.CO;2

Harrington, J. Y., Reisin, T., Cotton, W. R., & Kreidenweis, S. M. (1999). Cloud resolving simulations of Arctic stratus. Part II: Transition-season clouds. *Atmospheric Research*, 51, 45-75. https://doi.org/10.1016/S0169-8095(98)00098-2

Hartmann, M., Adachi, K., Eppers, O., Haas, C., Herber, A., Holzinger, R., et al. (2020). Wintertime airborne measurements of ice nucleating particles in the high Arctic: A hint to a marine, biogenic source for ice nucleating particles. *Geophysical Research Letters*, 47, e2020GL087770. https://doi.org/10.1029/2020GL087770

He, M., Hu, Y., Chen, N., Wang, D., Huang, J., & Stamnes, K. (2019). High cloud coverage over melted areas dominates the impact of clouds on the albedo feedback in the Arctic. *Scientific Reports*, 9, 9529. https://doi.org/10.1038/s41598-019-44155-w

Herenz, P., Wex, H., Henning, S., Kristensen, T. B., Rubach, F., Roth, A., et al. (2018). Measurements of aerosol and CCN properties in the Mackenzie River delta (Canadian Arctic) during spring–summer transition in May 2014. *Atmospheric Chemistry and Physics*, 18(7), 4477-4496. https://doi.org/10.5194/acp-18-4477-2018

Herenz, P., Wex, H., Mangold, A., Laffineur, Q., Gorodestkaya, I. V., Fleming, Z. L., et al. (2019). CCN measurements at the Princess Elisabeth Antarctica Research Station during three austral summers. *Atmospheric Chemistry and Physics*, 19, 275-294. https://doi.org/10.5194/acp-19-275-2019

Hofer, S., Tedstone, A. J., Fettweis, X. & Bamber, J. L. (2019). Cloud microphysics and circulation anomalies control differences in future Greenland melt. *Nature Climate Change*, 9, 523-528. https://doi.org/10.1038/s41558-019-0507-8

Hoose, C., Kristjánsson, J. E., Chen, J. P., & Hazra, A. (2010). A classical-theory-based parameterization of heterogeneous ice nucleation by mineral dust, soot, and biological particles in a global climate model. *Journal of the Atmospheric Sciences*, 67, 2483-2503. https://doi.org/10.1175/2010JAS3425.1

Hsu, J., & Prather, M. J. (2009). Stratospheric variability and tropospheric ozone. *Journal of Geophysical Research: Atmospheres*, 114, D06102. https://doi.org/10.1029/2008JD010942

Hu, Y. X., Rodier, S., Xu, K. M., Sun, W. B., Huang, J. P., Lin, B., et al. (2010). Occurrence, liquid water content, and fraction of supercooled water clouds from combined CALIOP/IIR/MODIS measurements. *Journal of Geophysical Research: Atmospheres*, 115, D00H34. https://doi.org/10.1029/2009JD012384

Iacono, M. J., Delamere, J. S., Mlawer, E. J., Shephard, M. W., Clough, S. A., & Collins, W. D. (2008). Radiative forcing by long-lived greenhouse gases: Calculations with the AER radiative transfer models. *Journal of Geophysical Research: Atmospheres*, 113, D13103. https://doi.org/10.1029/2008JD009944

Ivanova, D. C., Mitchell, D. L., Arnott, W. P., & Poellot, M. (2001). A GCM parameterization for bimodal size spectra and ice mass removal rates in mid-latitude cirrus clouds. *Atmospheric Research*, 59-60, 89-113. https://doi.org/10.1016/S0169-8095(01)00111-9

Jiang, H., Cotton, W. R., Pinto, J. O., Curry, J. A., & Weissbluth, M. J. (2000). Cloud Resolving Simulations of Mixed-Phase Arctic Stratus Observed during BASE: Sensitivity to Concentration of Ice Crystals and Large-Scale Heat and Moisture

Advection. *Journal of the Atmospheric Sciences*, 57, 2105-2117. https://doi.org/10.1175/1520-0469(2000)057<2105:CRSOMP>2.0.CO;2

Kay, J. E., Bourdages, L., Miller, N. B., Morrison, A., Yettella, V., Chepfer, H. & Eaton, B. (2016). Evaluating and improving cloud phase in the Community Atmosphere Model version 5 using spaceborne lidar observations, *Journal of Geophysical Research: Atmospheres*, 121, 4162-4176. https://doi.org/10.1002/2015JD024699

Khanal, S., & Wang, Z. (2018). Uncertainties in MODIS-based cloud liquid water path retrievals at high latitudes due to mixed-phase clouds and cloud top height inhomogeneity. *Journal of Geophysical Research: Atmospheres*, 123. https://doi.org/10.1029/2018JD028558

Klein, S. A., McCoy, R. B., Morrison, H., Ackerman, A. S., Avramov, A., Boer, G. d., et al. (2009). Intercomparison of model simulations of mixed-phase clouds observed during the ARM Mixed-Phase Arctic Cloud Experiment. I: single-layer cloud. *Quarterly Journal of the Royal Meteorological Society*, 135: 979-1002. https://doi.org/10.1002/qj.416

Korolev, A. (2007). Limitations of the Wegener-Bergeron-Findeisen mechanism in the evolution of mixed-phase clouds. *Journal of the Atmospheric Sciences*, 64, 3372-3375. https://doi.org/10.1175/JAS4035.1

Korolev, A., & Field, P. R. (2008). The Effect of Dynamics on Mixed-Phase Clouds: Theoretical Considerations. *Journal of the Atmospheric Sciences*, 65, 66-86. https://doi.org/10.1175/2007JAS2355.1

Korolev, A., & Isaac, G. A. (2006). Relative humidity in liquid, mixed-phase, and ice clouds. *Journal of the Atmospheric Sciences*, 63, 2865-2880. https://doi.org/10.1175/JAS3784.1

Korolev, A. V. (2008). Rates of phase transformations in mixed-phase clouds. *Quarterly Journal of the Royal Meteorological Society*, 134, 595-608. https://doi.org/10.1002/qj.230

Korolev, A. V., Isaac, G. A., Cober, S. G., Strapp, J. W., & Hallett, J. (2003). Microphysical characterization of mixed-phase clouds. *Quarterly Journal of the Royal Meteorological Society*, 129, 39-65. https://doi.org/10.1256/gj.01.204

Korolev, A. V., & Mazin, I. P. (2003). Supersaturation of Water Vapor in Clouds. *Journal of the Atmospheric Sciences*, 60, 2957-2974. https://doi.org/10.1175/1520-0469(2003)060<2957:SOWVIC>2.0.CO;2

Korolev, A., McFarquhar, G., Field, P. R., Franklin, C., Lawson, P., Wang, Z., et al. (2017). Mixed-Phase Clouds: Progress and Challenges. *Meteorological Monographs*. 58, 5.1-5.50. https://doi.org/10.1175/AMSMONOGRAPHS-D-17-0001.1

Lance, S., Shupe, M. D., Feingold, G., Brock, C. A., Cozic, J., Holloway, J. S., et al. (2011). Cloud condensation nuclei as a modulator of ice processes in Arctic mixed-phase clouds, *Atmospheric Chemistry and Physics*, 11, 8003-015. https://doi.org/10.5194/acp-11-8003-2011.

Larson, V. E. (2017). CLUBB-SILHS: A parameterization of subgrid variability in the atmosphere. *ArXiv:1711.03675 [Physics]*. Retrieved from http://arxiv.org/abs/1711.03675

Larson, V. E., & Golaz, J.-C. (2005). Using probability density functions to derive consistent closure relationships among higher-order moments. *Monthly Weather Review*, 133(4), 1023-1042. https://doi.org/10.1175/MWR2902.1

Larson, V. E., Golaz, J. & Cotton, W. R. (2002). Small-Scale and Mesoscale Variability in Cloudy Boundary Layers: Joint Probability Density Functions. *Journal of the Atmospheric Sciences*, 59, 3519-3539. https://doi.org/10.1175/1520-0469(2002)059<3519:SSAMVI>2.0.CO;2

Lawson, P. R., & Gettelman, A. (2014). Impact of Antarctic clouds on climate. *Proceedings of the National Academy of Sciences*, 111(51), 18156-18161. https://doi.org/10.1073/pnas.1418197111

Liao, L., & Sassen, K. (1994), Investigation of relationships between Ka-band radar reflectivity and ice and liquid water contents. *Atmospheric Research*, 34, 231-248. https://doi.org/10.1016/0169-8095(94)90094-9

Liu, C.-L., & Illingworth, A. J. (2000). Towards more accurate retrievals of ice water content from radar measurement of clouds, *Journal of Applied Meteorology and Climatology*, 39, 1130-1146. https://doi.org/10.1175/1520-0450(2000)039<1130:TMAROI>2.0.CO;2

Liu, J., Dedrick, J., Russell, L. M., Senum, G. I., Uin, J., Kuang, C., et al. (2018). High Summertime Aerosol Organic Functional Group Concentrations from Marine and Seabird Sources at Ross Island, Antarctica, during AWARE. *Atmospheric Chemistry and Physics*, 18(12), 8571-8587. https://doi.org/10.5194/acp-18-8571-2018

Liu, X., Easter, R. C., Ghan, S. J., Zaveri, R., Rasch, P., Shi, X., et al. (2012). Toward a minimal representation of aerosols in climate models: Description and evaluation in

the Community Atmosphere Model CAM5. *Geoscientific Model Development*, 5, 709-739. https://doi.org/10.5194/gmd-5-709-2012

Liu, X., Ma, P.-L., Wang, H., Tilmes, S., Singh, B., Easter, R. C., et al. (2016). Description and evaluation of a new four-mode version of the Modal Aerosol Module (MAM4) within version 5.3 of the Community Atmosphere Model. *Geoscientific Model Development*, 9(2), 505-522. https://doi.org/10.5194/gmd-9-505-2016

Liu, X., Xie, S., Boyle, J., Klein, S. A., Shi, X., Wang, Z., et al. (2011). Testing cloud microphysics parameterizations in NCAR CAM5 with ISDAC and M-PACE observations. *Journal of Geophysical Research: Atmospheres*, 116, D00T11. https://doi.org/10.1029/2011JD015889

Liu, X., Xie, S., & Ghan, S. J. (2007). Evaluation of a new mixed-phase cloud microphysics parameterization with CAM3 single-column model and M-PACE observations. *Geophysical Research Letters*, 34, L23712. https://doi.org/10.1029/2007GL031446

Lohmann, U. (2002). A glaciation indirect aerosol effect caused by soot aerosols. *Geophysical Research Letters*, 29(4), https://doi.org/10.1029/2001GL014357.

Lohmann, U., Henneberger, J., Henneberg, O., Fugal, J. P., Bühl, J., & Kanji, Z. A. (2016). Persistence of orographic mixed-phase clouds. *Geophysical Research Letters*, 43, 10512-10519. https://doi.org/10.1002/2016GL071036

Lohmann, U. & Neubauer, D. (2018). The importance of mixed-phase and ice clouds for climate sensitivity in the global aerosol–climate model ECHAM6-HAM2. *Atmospheric Chemistry and Physics*, 18, 8807-8828. https://doi.org/10.5194/acp-18-8807-2018

Lubin, D., Zhang, D., Silber, I., Scott, R. C., Kalogeras, P., Battaglia, A., et al. (2020). The Atmospheric Radiation Measurement program West Antarctic radiation experiment. *Bulletin of the American Meteorological Society*, 101, E1069-E1091. https://doi.org/10.1175/BAMS-D-18-0278.1

Luo, T., Wang, Z., Zhang, D., Liu, X., Wang, Y., & Yuan, R. (2015). Global dust distribution from improved thin dust layer detection using A-train satellite lidar observations, *Geophysical Research Letters*, 42, 620-628. https://doi.org/10.1002/2014GL062111

Ma, H.-Y., Chuang, C. C., Klein, S. A., Lo, M.-H., Zhang, Y., Xie, S., et al. (2015). An improved hindcast approach for evaluation and diagnosis of physical processes in

global climate models. *Journal of Advances in Modeling Earth Systems*, 7, 1810-1827. https://doi.org/10.1002/2015MS000490

Ma, H.-Y., Xie, S., Klein, S. A., Williams, K. D., Boyle, J. S., Bony, S., et al. (2014). On the correspondence between mean forecast errors and climate errors in CMIP5 models. *Journal of Climate*, 27(4), 1781-1798. https://doi.org/10.1175/JCLI-D-13-00474.1

McCoy, D. T., Hartmann, D. L., Zelinka, M. D., Ceppi, P., & Grosvenor, D. P. (2015). Mixed-phase cloud physics and Southern Ocean cloud feedback in climate models. *Journal of Geophysical Research: Atmospheres*, 120, 9539-9554. https://doi.org/10.1002/2015JD023603

McCoy, D. T., Tan, I., Hartmann, D. L., Zelinka, M. D., & Storelvmo, T. (2016). On the relationships among cloud cover, mixed-phase partitioning, and planetary albedo in GCMs. *Journal of Advances in Modeling Earth Systems*, 8, 650-668. https://doi.org/10.1002/2015MS000589

McCoy, I. L., McCoy, D. T., Wood, R., Regayre, L., Watson-Parris, D., Grosvenor, D. P., et al. (2020). The hemispheric contrast in cloud microphysical properties constrains aerosol forcing. *Proceedings of the National Academy of Sciences*. https://10.1073/pnas.1922502117

McFarquhar, G. M., Zhang, G., Poellot, M. R., Kok, G. L., McCoy, R., Tooman, T., et al. (2007). Ice properties of single-layer stratocumulus during the Mixed-Phase Arctic Cloud Experiment: 1. Observations. *Journal of Geophysical Research: Atmospheres*, 112, D24201. https://doi.org/10.1029/2007JD008633

McLinden, C. A., Olsen, S. C., Hannegan, B. J., Wild, O., and Prather, M. J. (2000). Stratosphere ozone in 3-D models: A simple chemistry and the cross-tropopause flux, *Journal of Geophysical Research: Atmospheres*, 105(D11), 14,653–14,665. https://doi.org/10.1029/2000JD900124

Meyers, M. P., DeMott, P. J., & Cotton, W. R. (1992). New primary ice-nucleation parameterizations in an explicit cloud model. *Journal of Applied Meteorology and Climatology*, 31, 708-721. https;//doi.org/10.1175/1520-0450(1992)031<0708:NPINPI>2.0.CO;2

Morrison, H., de Boer, G., Feingold, G., Harrington, J., Shupe, M. D., & Sulia, K. (2012). Resilience of persistent Arctic mixed-phase clouds. *Nature Geoscience*, 5, 11-17. https://doi.org/10.1038/ngeo1332

Morrison, H., & Gettelman, A. (2008). A new two-moment bulk stratiform cloud microphysics scheme in the Community Atmosphere Model, version 3 (CAM3). Part

I: Description and numerical tests. *Journal of Climate*, 21, 3642-3659. https://doi.org/10.1175/2008JCLI2105.1

Morrison, H., McCoy, R. B., Klein, S. A., Xie, S., Luo, Y., Avramov, A., et al. (2009). Intercomparison of model simulations of mixed-phase clouds observed during the ARM Mixed-Phase Arctic Cloud Experiment. II: Multilayer cloud. *Quarterly Journal of the Royal Meteorological Society*, 135, 1003-1019. https://doi.org/10.1002/qj.415

Morrison, H., & Pinto, J. O. (2006). Intercomparison of Bulk Cloud Microphysics Schemes in Mesoscale Simulations of Springtime Arctic Mixed-Phase Stratiform Clouds. *Monthly Weather Review*, 134, 1880-1900. https://doi.org/10.1175/MWR3154.1

Morrison, H., van Lier-Walqui, M., Fridlind, A. M., Grabowski, W. W., Harrington, J. Y., Hoose, C., et al. (2020). Confronting the challenge of modeling cloud and precipitation microphysics. *Journal of Advances in Modeling Earth Systems*, 12, e2019MS001689. https://doi.org/10.1029/2019MS001689

Neale, R. B., Chen, C. C., Gettelman, A., Lauritzen, P. H., Park, S., Williamson, D. L., et al. (2010). Description of the NCAR community atmosphere model (CAM 5.0) (NCAR/TN-4861STR). Boulder, CO: National Center for Atmospheric Research. http://www.cesm.ucar.edu/models/cesm1.2/cam/docs/description/cam5_desc.pdf

Nicolas, J. P., Vogelmann, A. M., Scott, R. C., Wilson, A. B., Cadeddu, M. P., Bromwich, D. H., et al. (2017). January 2016 extensive summer melt in West Antarctica favoured by strong El Niño. *Nature Communications*, 8, 15799. https://doi.org/10.1038/ncomms15799

Niemand, M., Möhler, O., Vogel, B., Vogel, H., Hoose, C., Connolly, P., et al. (2012). A Particle-Surface-Area-Based Parameterization of Immersion Freezing on Desert Dust Particles. *Journal of the Atmospheric Sciences*, 69, 3077-3092. https://doi.org/10.1175/JAS-D-11-0249.1

O'Shea, S. J., Choularton, T. W., Flynn, M., Bower, K. N., Gallagher, M., Crosier, J., et al. (2017). In situ measurements of cloud microphysics and aerosol over coastal Antarctica during the MAC campaign. *Atmospheric Chemistry and Physics*, 17, 13049-13070. https://doi.org/10.5194/acp-17-13049-2017

Park, S., & Bretherton, C. S. (2009). The University of Washington shallow convection and moist turbulence schemes and their impact on climate simulations with the Community Atmosphere Model. *Journal of Climate*, 22, 3449-3469. https://doi.org/10.1175/2008JCLI2557.1

Park, S., Bretherton, C. S., & Rasch, P. J. (2014). Integrating Cloud Processes in the Community Atmosphere Model, Version 5. *Journal of Climate*, 27, 6821-6856. https://doi.org/10.1175/JCLI-D-14-00087.1

Phillips, V. T., Patade, J., S., Gutierrez, J., & Bansemer, A. (2018). Secondary Ice Production by Fragmentation of Freezing Drops: Formulation and Theory. *Journal of the Atmospheric Sciences*, 75, 3031-3070. https://doi.org/10.1175/JAS-D-17-0190.1

Phillips, T. J., Potter, G. L., Williamson, D. L., Cederwall, R. T., Boyle, J. S., Fiorino, M., et al. (2004). Evaluating Parameterizations in General Circulation Models: Climate Simulation Meets Weather Prediction. *Bulletin of the American Meteorological Society*, 85, 1903-1916. https://doi.org/10.1175/BAMS-85-12-1903

Pinto, J. O. (1998). Autumnal Mixed-Phase Cloudy Boundary Layers in the Arctic. *Journal of the Atmospheric Sciences*, 55, 2016-2038. https://doi.org/10.1175/1520-0469(1998)055<2016:AMPCBL>2.0.CO;2

Pistone, K., Eisenman, I., & Ramanathan, V. (2019). Radiative heating of an ice-free arctic ocean. *Geophysical Research Letters*, 46, 7474-7480. https://doi.org/10.1029/2019GL082914

Prenni, A. J., Harrington, J. Y., Tjernström, M., DeMott, P. J., Avramov, A., Long, C. N., et al. (2007). Can ice-nucleating aerosols affect arctic seasonal climate? *Bulletin of the American Meteorological Society*, 88(4), 541-550. https://doi.org/10.1175/BAMS-88-4-541

Rahimi, S., Liu, X., Wu, C., Lau, W. K., Brown, H., Wu, M., & Qian, Y. (2019). Quantifying snow darkening and atmospheric radiative effects of black carbon and dust on the South Asian monsoon and hydrological cycle: experiments using variable-resolution CESM. *Atmospheric Chemistry and Physics*, 19, 12025-12049. https://doi.org/10.5194/acp-19-12025-2019

Rahimi, S., Liu, X., Zhao, C., Lu, Z., & Lebo, Z. J. (2020). Examining the atmospheric radiative and snow-darkening effects of black carbon and dust across the Rocky Mountains of the United States using WRF-Chem, *Atmospheric Chemistry and Physics*. 20, 10911-10935. https://doi.org/10.5194/acp-20-10911-2020

Rasch, P. J., Xie, S., Ma, P.-L., Lin, W., Wang, H., Tang, Q., et al. (2019). An Overview of the Atmospheric Component of the Energy Exascale Earth System Model. *Journal of Advances in Modeling Earth Systems*, 11, 2377– 2411. https://doi.org/10.1029/2019MS001629

Rosenfeld, D., Lohmann, U., Raga, G. B., O'Dowd, C. D., Kulmala, M., Fuzzi, S., et al. (2008). Flood or drought: how do aerosols affect precipitation? *Science*, 321, 1309-1313. https://doi.org/10.1126/science.1160606

Sassen, K., Wang, Z., & Liu, D. (2008). Global distribution of cirrus clouds from CloudSat/Cloud-Aerosol Lidar and Infrared Pathfinder Satellite Observations (CALIPSO) measurements. *Journal of Geophysical Research: Atmospheres*, 113, D00A12. https://doi.org/10.1029/2008JD009972

Screen, J., & Simmonds, I. (2010). The central role of diminishing sea ice in recent Arctic temperature amplification. *Nature*, 464, 1334-1337. https://doi.org/10.1038/nature09051

Shi, Y., & Liu, X. (2019). Dust radiative effects on climate by glaciating mixed-phase clouds. *Geophysical Research Letters*, 46. https://doi.org/10.1029/2019GL082504

Shindell, D. T., Chin, M., Dentener, F., Doherty, R. M., Faluvegi, G., Fiore, A. M., et al. (2008). A multi-model assessment of pollution transport to the Arctic. *Atmospheric Chemistry and Physics*, 8, 5353-5372. https://doi.org/10.5194/acp-8-5353-2008

Shupe, M. D. (2011). Clouds at Arctic atmospheric observatories. Part II: Thermodynamic phase characteristics. *Journal of Applied Meteorology and Climatology*, 50, 645-661. https://doi.org/10.1175/2010JAMC2468.1

Shupe, M. D., Kollias, P., Persson, P. O. G., & McFarquhar, G. M. (2008). Vertical motions in Arctic mixed-phase stratiform clouds. *Journal of the Atmospheric Sciences*, 65, 1304-1322. https://doi.org/10.1175/2007JAS2479.1

Shupe, M. D., Matrosov, S. Y., & Uttal, T. (2006). Arctic Mixed-Phase Cloud Properties Derived from Surface-Based Sensors at SHEBA. *Journal of the Atmospheric Sciences*, 63, 697-711. https://doi.org/10.1175/JAS3659.1

Shupe, M. D., Uttal, T., & Matrosov, S. Y. (2005), Arctic cloud microphysics retrievals from surface-based remote sensors at SHEBA. *Journal of Applied Meteorology and Climatology*, 44, 1544-1562. https://doi.org/10.1175/JAM2297.1

Shupe, M. D., Walden, V. P., Eloranta, E., Uttal, T., Campbell, J. R., Starkweather, S. M., & Shiobara, M. (2011). Clouds at Arctic atmospheric observatories. Part I: Occurrence and macrophysical properties. *Journal of Applied Meteorology and Climatology*, 50(3), 626–644. https://doi.org/10.1175/2010JAMC2467.1

Silber, I., Verlinde, J., Cadeddu, M., Flynn, C. J., Vogelmann, A. M., & Eloranta, E. W. (2019). Antarctic cloud macrophysical, thermodynamic phase, and atmospheric inversion coupling properties at McMurdo Station—Part II: Radiative impact during different synoptic regimes. *Journal of Geophysical Research: Atmospheres*, 124, 1697-1719. https://doi.org/10.1029/2018JD029471

Silber, I., Verlinde, J., Eloranta, E. W., & Cadeddu, M. (2018). Antarctic cloud macrophysical, thermodynamic phase, and atmospheric inversion coupling properties at McMurdo Station: I. Principal data processing and climatology. *Journal of Geophysical Research: Atmospheres*, 123, 6099-6121. https://doi.org/10.1029/2018JD028279

Simpson, E. L., Connolly, P. J., & McFiggans, G. (2018). Competition for water vapour results in suppression of ice formation in mixed-phase clouds. *Atmospheric Chemistry and Physics*, 18, 7237-7250. https://doi.org/10.5194/acp-18-7237-2018.

Solomon, A., Morrison, H., Persson, O., Shupe, M. D., & Bao, J. (2009). Investigation of Microphysical Parameterizations of Snow and Ice in Arctic Clouds during M-PACE through Model-Observation Comparisons. *Monthly Weather Review*, 137, 3110-3128. https://doi.org/10.1175/2009MWR2688.1

Storelvmo, T., Kristjánsson, J. E., Lohmann, U., Iversen, T., Kirkevåg, A., & Seland, Ø. (2008). Modeling of the Wegener-Bergeron-Findeisen process—implications for aerosol indirect effects. *Environmental Research Letters*, 3, 045001. https://doi.org/10.1088/1748-9326/3/4/045001

Sun, J., Zhang, K., Wan, H., Ma, P.-L., Tang, Q., & Zhang, S. (2019). Impact of nudging strategy on the climate representativeness and hindcast skill of constrained EAMv1 simulations. *Journal of Advances in Modeling Earth Systems*, 11, 3911-3933. https://doi.org/10.1029/2019MS001831

Tan, I., & Storelvmo, T. (2016). Sensitivity study on the influence of cloud microphysical parameters on mixed-phase cloud thermodynamic phase partitioning in CAM5. *Journal of the Atmospheric Sciences*, 73, 709-728. https://doi.org/10.1175/JAS-D-15-0152.1

Tan, I., & Storelvmo, T. (2019). Evidence of strong contributions from mixed-phase clouds to Arctic climate change. *Geophysical Research Letters*, 46, 2894-2902. https://doi.org/10.1029/2018GL081871

Tan, I., Storelvmo, T., & Choi, Y.-S. (2014). Spaceborne lidar observations of the ice-nucleating potential of dust, polluted dust and smoke aerosols in mixed-phase clouds.

Journal of Geophysical Research: Atmospheres, 119, 6653-6665. https://doi.org/10.1002/2013JD021333

Tan, I., Storelvmo, T., & Zelinka, M. D. (2016). Observational constraints on mixed-phase clouds imply higher climate sensitivity. *Science*, 352, 224-227. https://doi.org/10.1126/science.aad5300

Tobo, Y., Adachi, K., DeMott, P. J., Hill, T. J., Hamilton, D. S., Mahowald N. M., et al. (2019). Glacially sourced dust as a potentially significant source of ice nucleating particles. *Nature Geoscience*. 12, 253-258. https://doi.org/10.1038/s41561-019-0314-x

Turner, D. (2005). Arctic mixed-phase cloud properties from AERI-lidar observations: Algorithm and results from SHEBA. *Journal of Applied Meteorology and Climatology*, 44, 427-444. https://doi.org/10.1175/JAM2208.1

Twomey, S. (1977). The Influence of Pollution on the Shortwave Albedo of Clouds. Journal of the Atmospheric Sciences, 34, 1149-1152. https://doi.org/10.1175/1520-0469(1977)034<1149:TIOPOT>2.0.CO;2

Vergara-Temprado, J., Miltenberger, A. K., Furtado, K., Grosvenor, D. P., Shipway B. J., Hill, A. A., et al. (2018). Strong control of Southern Ocean cloud reflectivity by

ice-nucleating particles. *Proceedings of the National Academy of Sciences*, 115(11), 2687-2692. https://doi.org/10.1073/pnas.1721627115

Verlinde, J., Harrington, J. Y., McFarquhar, G. M., Yannuzzi, V. T., Avramov, A., Greenberg, S., et al. (2007). The Mixed-Phase Arctic Cloud Experiment. *Bulletin of the American Meteorological Society*, 88, 205-222. https://doi.org/10.1175/BAMS-88-2-205

Wang, H., Easter, R. C., Rasch, P. J., Wang, M., Liu, X., Ghan, S. J., et al. (2013). Sensitivity of remote aerosol distributions to representation of cloud-aerosol interactions in a global climate model. *Geoscientific Model Development*, 6(3), 765–782. https://doi.org/10.5194/gmd-6-765-2013

Wang, Y., Liu, X., Hoose, C., & Wang, B. (2014). Different contact angle distributions for heterogeneous ice nucleation in the Community Atmospheric Model version 5. *Atmospheric Chemistry and Physics*, 14, 10411-10430. https://doi.org/10.5194/acp-14-10411-2014

Wang, Y., Zhang, D., Liu, X., & Wang, Z. (2018). Distinct contributions of ice nucleation, large-scale environment, and shallow cumulus detrainment to cloud phase partitioning with NCAR CAM5. *Journal of Geophysical Research: Atmospheres*, 123, 1132-1154. https://doi.org/10.1002/2017JD027213

Wang, Z. (2007). A refined two-channel microwave radiometer liquid water path retrieval for cold regions by using multiple-sensor measurements. *IEEE Geoscience and Remote Sensing Letters*, 4, 591-595. https://doi.org/10.1109/LGRS.2007.900752

Wang, Z., & Sassen, K. (2002). Cirrus cloud microphysical property retrieval using lidar and radar measurements: I. Algorithm description and comparison with in situ data. *Journal of Applied Meteorology and Climatology*, 41, 218-229. https://doi.org/10.1175/1520-0450(2002)041<0218:CCMPRU>2.0.CO;2

Wang, Z., Sassen, K., Whiteman, D. N., & Demoz, B. B. (2004). Studying altocumulus with ice virga using ground-based active and passive remote sensors. *Journal of Applied Meteorology and Climatology*, 43, 449-460. https://doi.org/10.1175/1520-0450(2004)043<0449:SAWIVU>2.0.CO;2

Wang, Z., Vane, D., Stephens, G., & Reinke, D. (2013). CloudSat Project: Level 2 combined radar and lidar cloud scenario classification product process description and interface control document. California Institute of Technology JPL, 61 pp.

Wegener, A. (1911). *Thermodynamik der Atmosphäre*, Johann Ambrosius Barth, Leipzig, Germany.

Williams, K. D. & Brooks, M. E. (2008). Initial Tendencies of Cloud Regimes in the Met Office Unified Model. *Journal of Climate*, 21, 833–840. https://doi.org/10.1175/2007JCLI1900.1

Wilson, T., Ladino, L., Alpert, P., Breckels, M. N., Brooks, I. M., Browse, J., et al. (2015). A marine biogenic source of atmospheric ice-nucleating particles. *Nature*, 525, 234-238. https://doi.org/10.1038/nature14986

Wofsy, S. C., Daube, B. C., Jimenez, R., Kort, E., Pittman, J. V., Park, S., et al. (2011). HIAPER Pole-to-Pole Observations (HIPPO): fine-grained, global-scale measurements of climatically important atmospheric gases and aerosols. *Philosophical Transactions of the Royal Society A*, 369, 2073-2086. https://doi.org/10.1098/rsta.2010.0313

Wu, M., Liu, X., Yu, H., Wang, H., Shi, Y., Yang, K., et al. (2020). Understanding Processes that Control Dust Spatial Distributions with Global Climate Models and Satellite Observations, *Atmospheric Chemistry and Physics*, 20, 13835-13855. https://doi.org/10.5194/acp-20-13835-2020

Wu, M., Liu, X., Zhang, L., Wu, C., Lu, Z., Ma, P.-L., et al. (2018). Impacts of aerosol dry deposition on black carbon spatial distributions and radiative effects in the

Community Atmosphere Model CAM5. *Journal of Advances in Modeling Earth Systems*, 10, 1150-1171. https://doi.org/10.1029/2017MS001219

Xie, S., Boyle, J., Klein, S. A., Liu, X., & Ghan, S. (2008). Simulations of Arctic mixed-phase clouds in forecasts with CAM3 and AM2 for M-PACE. *Journal of Geophysical Research: Atmospheres*, 113, D04211. https://doi.org/10.1029/2007JD009225

Xie, S., Klein, S. A., Yio, J. J., Beljaars, A. C. M., Long, C. N., & Zhang, M. (2006). An assessment of ECMWF analyses and model forecasts over the North Slope of Alaska using observations from the ARM Mixed-Phase Arctic Cloud Experiment. *Journal of Geophysical Research: Atmospheres*, 111, D05107. https://doi.org/10.1029/2005JD006509

Xie, S., Lin, W., Rasch, P. J., Ma, P.-L., Neale, R., Larson, V. E., et al. (2018). Understanding cloud and convective characteristics in version 1 of the E3SM atmosphere model. *Journal of Advances in Modeling Earth Systems*, 10, 2618-2644. https://doi.org/10.1029/2018MS001350

Xie, S., Liu, X., Zhao, C., & Zhang, Y. (2013). Sensitivity of CAM5-Simulated Arctic Clouds and Radiation to Ice Nucleation Parameterization. *Journal of Climate*, 26, 5981-5999. https://doi.org/10.1175/JCLI-D-12-00517.1

Xie, S., Ma, H.-Y., Boyle, J. S., Klein, S. A., & Zhang, Y. (2012). On the correspondence between short- and long-time-scale systematic errors in CAM4/CAM5 for the year of tropical convection. *Journal of Climate*, 25(22), 7937-7955. https://doi.org/10.1175/JCLI-D-12-00134.1

Xie, S., McCoy, R. B., Klein, S. A., Cederwall, R. T., Wiscombe, W. J., Jensen, M. P., et al. (2010). CLOUDS AND MORE: ARM Climate Modeling Best Estimate Data: A New Data Product for Climate Studies. *Bulletin of the American Meteorological Society*, 91(1), 13-20. https://doi.org/10.1175/2009BAMS2891.1

Xie, S., Zhang, M., Branson, M., Cederwall, R. T., Del Genio, A. D., Eitzen, Z. A., et al. (2005). Simulations of midlatitude frontal clouds by single-column and cloud-resolving models during the Atmospheric Radiation Measurement March 2000 cloud intensive operational period. *Journal of Geophysical Research: Atmosphere*, 110, D15S03. https://doi.org/10.1029/2004JD005119

Yasunari, T. J., Koster, R. D., Lau, W. K. M., & Kim, K.-M. (2015). Impact of snow darkening via dust, black carbon, and organic carbon on boreal spring climate in the Earth system. *Journal of Geophysical Research: Atmosphere*. 120, 5485-5503. https://doi.org/10.1002/2014JD022977

Yuan, J., Fu, Q., & McFarlane, N. (2006). Tests and improvements of GCM cloud parameterizations using the CCCMA SCM with the SHEBA data set. *Atmospheric Research*, 82, 222-238. https://doi.org/10.1016/j.atmosres.2005.10.009

Zelinka, M. D., Myers, T. A., McCoy, D. T., Po-Chedley, S., Caldwell, P. M., Ceppi, P., et al. (2020). Causes of higher climate sensitivity in CMIP6 models. *Geophysical Research Letters*, 47, e2019GL085782. https://doi.org/10.1029/2019GL085782

Zhang, D., Vogelmann, A., Kollias, P., Luke, E., Yang, F., Lubin, D., & Wang, Z. (2019). Comparison of Antarctic and Arctic single-layer stratiform mixed-phase cloud properties using ground-based remote sensing measurements. *Journal of Geophysical Research: Atmospheres*, 124. https://doi.org/10.1029/2019JD030673

Zhang, D., Wang, Z., Heymsfield, A., Fan, J., & Luo, T. (2014). Ice Concentration Retrieval in Stratiform Mixed-Phase Clouds Using Cloud Radar Reflectivity Measurements and 1D Ice Growth Model Simulations. *Journal of the Atmospheric Sciences*, 71, 3613-3635. https://doi.org/10.1175/JAS-D-13-0354.1

Zhang, D., Wang, Z., Kollias, P., Vogelmann, A. M., Yang, K., & Luo, T. (2018). Ice particle production in mid-level stratiform mixed-phase clouds observed with collocated A-Train measurements. *Atmospheric Chemistry and Physics,* 18, 4317-4327. https://doi.org/10.5194/acp-18-4317-2018.

Zhang, K., Rasch, P. J., Taylor, M. A., Wan, H., Leung, R., Ma, P.-L., et al. (2018). Impact of numerical choices on water conservation in the E3SM Atmosphere Model version 1 (EAMv1). *Geoscientific Model Development*, 11, 1971-1988. https://doi.org/10.5194/gmd-11-1971-2018

Zhang, K., Wan, H., Liu, X., Ghan, S. J., Kooperman, G. J., Ma, P.-L., et al. (2014). Technical Note: On the use of nudging for aerosol-climate model intercomparison studies. *Atmospheric Chemistry and Physics*, 14, 8631-8645. https://doi.org/10.5194/acp-14-8631-2014

Zhang, G. J., & McFarlane, N. A. (1995). Sensitivity of climate simulations to the parameterization of cumulus convection in the Canadian Climate Centre general circulation model. *Atmosphere-Ocean*, 33(3), 407-446. https://doi.org/10.1080/07055900.1995.9649539

Zhang, M., Liu, X., Diao, M., D'Alessandro, J. J., Wang, Y., Wu, C., et al (2019). Impacts of representing heterogeneous distribution of cloud liquid and Ice on phase partitioning of Arctic mixed-phase clouds. *Journal of Geophysical Research: Atmospheres*, 124, 13071-13090. https://doi.org/10.1029/2019JD030502

Zhang, M., Xie, S., Liu, X., Lin, W., Zhang, K., Ma, H.-Y., et al. (2020). Toward understanding the simulated phase partitioning of arctic single-layer mixed-phase clouds in E3SM. *Earth and Space Science*, 7, e2020EA001125. https://doi.org/10.1029/2020EA001125

Zhang, Y., Xie, S., Lin, W., Klein, S. A., Zelinka, M., Ma, P.-L., et al. (2019). Evaluation of clouds in version 1 of the E3SM atmosphere model with satellite simulators. *Journal of Advances in Modeling Earth Systems*, 11, 1253-1268. https://doi.org/10.1029/2018MS001562

Zhao, C., Xie, S., Klein, S. A., Protat, A., Shupe, M. D., McFarlane, S. A. et al. (2012). Toward understanding of differences in current cloud retrievals of ARM ground-based measurements, *Journal of Geophysical Research: Atmospheres*, 117, D10206. https://doi.org/10.1029/2011JD016792

Zhao, X., Lin, Y., Peng, Y., Wang, B., Morrison, H., & Gettelman A. (2017). A single ice approach using varying ice particle properties in global climate model microphysics, *Journal of Advances in Modeling Earth Systems*, 9, 2138-2157. https://doi.org/10.1002/2017MS000952